Phenotypic Models of Perfect Adaptation by $CD8^+$ T Cells



Stephanie Alana Gaglione

Sir William Dunn School of Pathology

Balliol College

University of Oxford

A thesis submitted for the degree of

Master of Science by Research

Trinity Term 2019

Acknowledgements

I would like to express my sincere gratitude to my MSc supervisor, Professor Omer Dushek, for his exceptional support in exploring a unique research project, patience while learning new concepts, and encouragement to persist. His mentorship and guidance over the past year have been invaluable. I am truly grateful for the training I have received and leave with new confidence in my ability to rigorously approach research, think critically, and consider the ethics of my work.

I would like to thank Professor Philip Maini and Professor Audrey Gerhard for their time and guidance in assessing my transfer to MSc status and providing thoughtful input on the implications of my work. I would like to sincerely thank Nicola Trendel, Philipp Kruger, and Johannes Pettmann for their kind mentorship, experimental instruction, and intellectual support over the past year, as well as all members of the Dushek and van der Merwe labs for their invaluable scientific advice and for sharing in such a supportive, fun lab community.

To my friends in Oxford, I am grateful for every moment of this Oxford university experience and could not have envisioned more supportive communities at Balliol College, the Dunn School, Rhodes House, or the climbing walls of the UK. I would not have been able to pursue this course without the generous financial support of the Rhodes Trust and feel immense gratitude for the lifelong friendship and adventures I found within the Rhodes community.

Finally, I would like to express my deepest gratitude to my parents, Norma and Greg, my sister, Alexandra, and my partner, Adam, for their unwavering support and late-night calls over the past two years. Thank you for sharing in every high and low of this adventure and for empowering me to follow this dream.

Abstract

T cells receive continuous antigenic stimulation in peripheral tolerance, cancer, and chronic infection. Persistent antigen exposure induces an initial cellular response. However, over time, T cells become unresponsive to the stimulus and cease activity, a behaviour known as adaptation. Although it is generally known that T cells adapt to persistent stimuli, the properties of this adaptation remain understudied. This thesis aims to characterize phenotypes of T cell adaptation and to suggest the possibility of relating these phenotypes to basic network models that produce adaptation.

To better understand T cell adaptive behaviour, a plate-based T cell receptor system was used to expose cells to step changes in antigen dose. In response to persistent antigen exposure, T cells can display perfect adaptation in cytokine production with incomplete TCR downregulation. Increasing the antigen dose leads to further tuning of the surface TCR level, independent of previous antigen exposure, with limited additional cytokine production. Thus, partial TCR downregulation tunes to antigen dose and perfect adaptation is observed even with partial downregulation. If T cells are exposed to gradual, incremental increases in antigen dose rather than a single dose, the cells are similarly silenced.

The experimental data was subsequently examined in the context of seven basic, preliminary models of adaptation. A model based on partial TCR downregulation with a second downstream mechanism aligns with experimental observations, suggesting the potential relevance of TCR downregulation. Clinically, T cell-modulating therapies often cause potent early cytokine production. As a proof-of-concept, I demonstrate that otelixizumab induces T cell adaptation as a non-pMHC stimulus. Further study of T cell adaptation is thus invaluable both to understanding T cell behaviour as well as therapeutic design.

Table of Contents

Abstract **2**

1 Introduction **9**

1.1 Recognition of Antigen by T Cells 9

1.2 Constant Antigen Stimulation leads to T Cell Adaptation In Vitro and In Vivo 12

1.2.1 Peripheral Tolerance 12

1.2.2 Chronic Infection 12

1.2.3 Cancer

1.3 Therapeutic Antibodies and Minimizng Cytokine Production

1.4 Mathematical Models and Molecular Mechanisms of Adaptation 16

1.4.1 Defining Adaptation 17

1.4.2 Negative Feedback Control 18

1.4.3 Incoherent Feedforward Control 21

1.5 Receptor-based Architectures for Perfect Adaptation 24

1.5.1 Complete Receptor Downregulation 24

1.5.2 Incomplete Receptor Downregulation 25

1.6 Thesis Aims 26

2 Materials and Methods **29**

2.1 Materials 29

2.2 Peptide-MHC Complex Production 31

2.3 PE-pMHC Tetramer Production 31

2.4 Isolation and Culture of Primary T Cells 32

2.5 Immobilization of pMHC to Streptavidin-coated Plates 33

2.6 Quantitative Data Collection 33

2.6.1 Flow Cytometry 33

2.6.2 Enzyme-linked Immunosorbent Assay (ELISA) 35

2.6.3 Statistical Analysis and Mathematical Model Generation 35

2.7 Experiment 1: Varying Time and Antigen Dose 36

2.8 Experiment 2: Step Changes in Antigen Dose 37

2.9 Experiment 3: Gradual Step Changes in Antigen Dose 39

2.9.1 Phase 1: Inducing Adaptation 39

2.9.2 Phase 2: Confirming Adaptation 41

2.10 Experiment 4: Adaptation by Anti-CD3Anti-CD52 Monoclonal Antibodies 42

3 Results 44
3.1 Experiment 1: Confirmation of Adaptation in Cytokine Production 45
3.1.1 Experimental Setup 45
3.1.2 Cytokine dose-response time course 45
3.1.3 CD69 data: all T cells are being activated 47
3.1.4 TCR Downregulation is Biphasic 49
3.2 Step Changes in Dose 52
3.2.1 Experimental Setup 52
3.2.2 Step Change in Dose Results 53
3.3 Incremental Step Change in Dose 58
3.3.1 Experimental Setup 58
3.3.2 Phase 1 Results 59
3.3.3 Phase 2 Results 61
3.4 NFL and IFFL Models of Adaptation 63
3.4.1 Comparison of NFL and IFFL Models 64
3.4.2 Alignment of NFL and IFFL Signatures 71
3.6 Pilot Tests of Anti-CD3 Therapeutic Antibodies 74
4 Discussion and Conclusion 77
4.1 The Role of TCR Downregulation 78
4.2 Additional Experiments and Limitations 79
4.2.1 Limitations in the Experimental Setup 79
4.2.2 Future Experiments 81
4.3 Clinical Applications 82
4.4 Conclusion 83
References 85
Appendix – Supplementary Figures 92

Table of Figures

Figure 1. TCR Downregulation and Signal Transduction post-pMHC Binding 11
Figure 2. Adaptation in Physiological Conditions 14
Figure 3. Perfect vs. Imperfect Adaptation 17
Figure 4. Negative Feedback and Incoherent Feed Forward Control 23
Figure 5. Receptor-based Models of Adaptation 25
Figure 6. Basic NFL and IFFL Network Types 26
Figure 7. Antigen Dose Escalation Experiments 27
Figure 8. Experiment 1 – General Setup 45
Figure 9. Cytokine Production vs. pMHC Dose 46
Figure 10. Cytokine Production vs. pMHC Dose: E_{max} Comparison 47
Figure 11. T Cell Activation 48
Figure 12. T Cell Downregulation 51
Figure 13. Experiment 2 – General Setup 53
Figure 14. Step Change in Dose: TCR, Activation Markers, and Cytokine Output 56
Figure 15. Maximum Values of Step Change in Dose Curves 57
Figure 16. Experiment 3 – General Setup 59
Figure 17. Phase 1 Results 60
Figure 18. Phase 2 Results and Rescue from Adaptation by CD86 62
Figure 19. Model Simulations – Step Changes in Dose for NFL Networks 66
Figure 20. Model Simulations – Step Changes in Dose for IFFL Networks 67
Figure 21. Model Simulations – Time- and Dose-Course Experiment 70
Figure 22. Adaptation in T Cells exposed to Plate-bound Otelixizumab 76
Figure 23. NFL and IFFL Ordinary Differential Equations 92
Figure 24. Purity of Isolated $CD8^+$ T Cells 99
Figure 25. T Cell Surface Marker Gating Strategy 100
Figure 26. Low-Affinity pMHC (4A8K) Time- and Dose-Course Data 101
Figure 27. High-Affinity pMHC (9V) Time- and Dose-Course Data 102
Figure 28. Phase 1: 4-1BB and PD-1 Expression 103
Figure 29. Phase 2: Supplementary Surface Markers, Cytokine Secretion, Cell Counts 103
Figure 30. Model Simulations – Time- and Dose-Course Experiment 104
Figure 31. Otelixizumab Experiment Repeat 1: Soluble Format 108
Figure 32. Otelixizumab Experiment Repeat 2: Plate-bound and Soluble Formats 109

Figure 33. Otelixizumab Experiment Repeat 3: Plate-bound Format. 110
Figure 34. Alemtuzumab Experiment: Plate-bound and Soluble Formats 111
Figure 35. Otelixizumab Data Sheet 112

Table of Tables

Table 1. 9V and 4A8K Peptide Sequences and Affinities 31
Table 2. Experiment 2 – Dose Escalation Strategy 38
Table 3. Experiment 3 – Antigen Doses 40
Table 4. Model Alignment with Experimental Phenotypes 71

Acronyms

APC	antigen-presenting cell
BiTE	bi-specific T-cell engaging antibody
CAR	chimeric antigen receptor
CRA	cytokine release assay
CRS	cytokine release syndrome
CTLA-4	cytotoxic T-lymphocyte-associated protein 4
DAG	diacylglycerol
EGF	epidermal growth factor
EGFR	epidermal growth factor receptor
ELISA	enzyme-linked immunosorbent assay
ERK	extracellular signal-regulated kinases
FSC	forward scatter
GAP	GTPase-activating protein
GDP	guanine diphosphate
GEF	guanine nucleotide exchange factor
gMFI	geometric mean fluorescence intensity
GPCR	G-protein coupled receptor
GPI	glycosylphosphatidylinositol
GTP	guanine triphosphate
HBV	hepatitis B virus
HCV	hepatitis C virus
HIV	human immunodeficiency virus
HLA	human leukocyte antigen
HRP	horseradish peroxidase
IFFL	incoherent feed forward loop
IFN-g	interferon gamma
IL-2	interleukin-2
ITAM	immunoreceptor tyrosine-based activation motif
LAG-3	lymphocyte-activation gene 3
LAT	linker for activation of T cells
LCMV	lymphocytic choriomeningitis virus
mAb	monoclonal antibody

MAP	microtubule-associated protein
MAPK	mitogen-activated protein kinase
MEK	mitogen-activated protein kinase
MHC	major histocompatibility complex
MKP	mitogen-activated protein kinase phosphatase
NFL	negative feedback loop
NY-ESO-1	New York esophageal squamous cell carcinoma 1
ODE	ordinarydifferential equation
OKT3	muromonab-CD3
PBS	phosphate-buffered saline
PBST	phosphate-buffered saline with Tween-20
PD-1	programmed cell death protein 1
PE	phycoerythrin
PFL	positive feedback loop
PLC	phospholipase C, gamma 1
pMHC	peptide-major histocompatibility complex
PTK	protein tyrosine kinase
RTK	receptor tyrosine kinase
SD	standard deviation
SEM	standard error of the mean
SHP-1	Src homology region 2 domain-containing phosphatase-1
SIV	simian immunodeficiency virus
SLE	systemic lupus erythematosus
SLP-76	lymphocyte cytosolic protein 2
SSC	side scatter
TCR	T cell receptor
TIM-3	T-cell immunoglobulin and mucin-domain containing-3
TNF-a	tumour necrosis factor alpha
ZAP70	zeta-chain-associated protein kinase 70

1 Introduction

Antigen recognition by T cells is critical to initiating and preserving adaptive immune responses to pathogens and in cancer, allergy, and autoimmune disease. Immune activation occurs when surface T cell receptors (TCRs) are ligated by antigens, typically short peptides bound to major histocompatibility complexes (MHCs) displayed by antigen-presenting cells (APCs)[1]. Recognition of peptide-MHC (pMHC) complexes results in T cell differentiation, proliferation, cytokine production, and target cell killing.

1.1 Recognition of Antigen by T Cells

The T cell signaling cascade involves several intricate branches of control. At the receptor level, the mechanisms governing pMHC triggering of the TCR are controversial. Proposed models include conformational changes to the CD3 complex, kinetic segregation, TCR aggregation or clustering, and pseudodimer formation[2]. Once triggered, the TCR complex activates Src PTKs, specifically Lck and Fyn, which phosphorylate CD3 ITAMs and recruit ZAP-70, LAT, and SLP-76 to form a proximal signaling complex that propagates the initial signal into multiple pathways[2]. The proximal signaling complex is distinct from the TCR itself. This intracellular cascade activates PLCγ1-dependent pathways (i.e. Ca^{2+}- and DAG-mediated responses), cytoskeletal rearrangements, integrin activation, and functional responses[2]. One functional response is of particular interest: cytokine production. Effector $CD8^+$ T cells, the focus of this study, generate two pro-inflammatory cytokines, TNF-α and IFN-γ. Critical to systemic inflammation, TNF-α increases vascular permeability, regulates chemokine levels to recruit neutrophils to inflammatory sites, and induces pro-coagulant proteins (i.e. tissue factor)[3,4]. IFN-γ inhibits viral replication and induces macrophages to produce chemokines and cytokines, engage in microbial killing, and function as APCs[5–7]. TCR-pMHC recognition thus activates a complex downstream network with multiple functions including cytokine production.

In addition to initiating downstream signaling, pMHC-TCR binding alters regulation and expression of the TCR itself. At rest, TCR complexes are constitutively endocytosed and recycled to the plasma membrane in continuous rapid cycles (Figure 1)[8]. pMHC engagement of the TCR disturbs the plasma membrane-endosome equilibrium, increasing endocytosis and degradation of the TCR through downregulation[8]. Downregulation of engaged TCRs is further complemented by the internalization of non-engaged 'bystander' TCRs through a different mechanism[9,10]. Although the molecular mechanisms underlying TCR downregulation are well-established, reviewed by Alcover, Alarcón, and Di Bartolo[8], the purpose of downregulation remains controversial. Nonetheless, it is generally agreed that activation-induced endocytosis and lysosomal degradation of engaged and bystander TCRs represent a critical control mechanism for moderating T cell stimulation. In summary, pMHC-TCR binding induces: (a) T cell activation and cytokine secretion via downstream signaling networks and (b) downregulation of engaged and bystander TCRs.

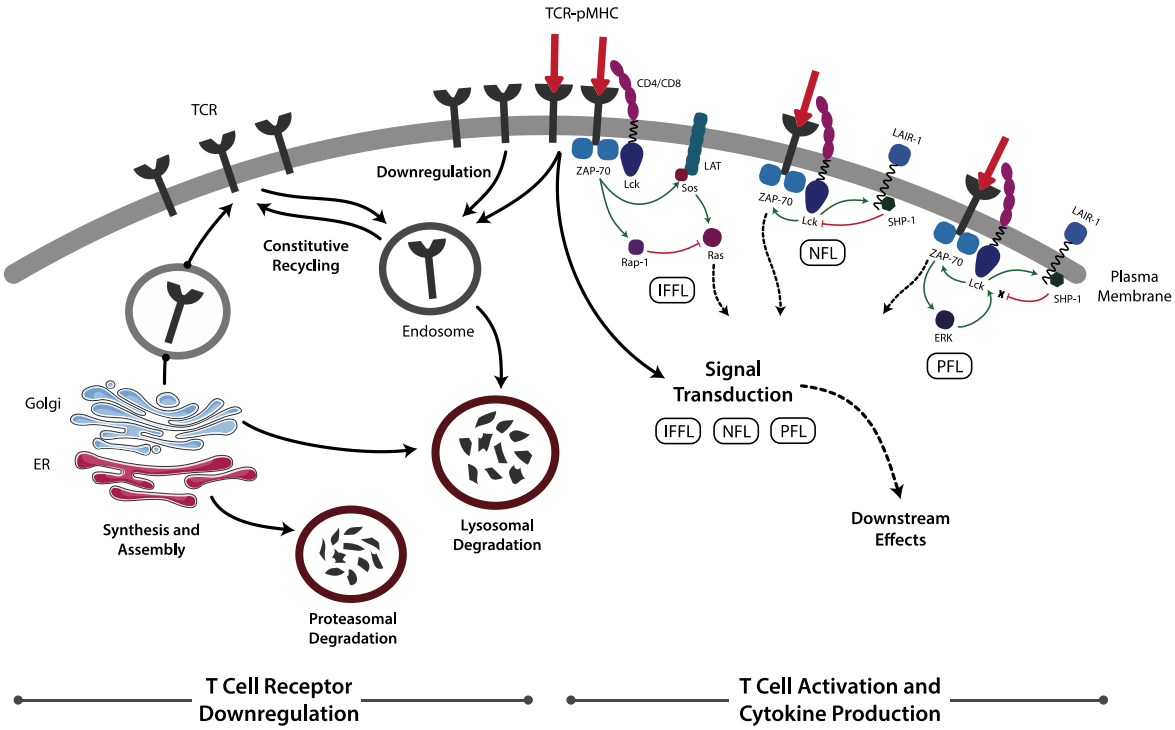


Figure 1. TCR Downregulation and Signal Transduction post-pMHC Binding. Schematic representation of TCR receptor recycling and activation. TCR-CD3 subunits are synthesized, translocated to the ER membrane, fully assembled in the Golgi apparatus, and delivered to the plasma membrane. At the membrane, TCR-CD3 complexes undergo constitutive endocytosis and recycling, some of which are degraded in lysosomes. Binding of the TCR by pMHCs causes activation which induces accelerated endocytosis and signal transduction. The downstream effects of signal transduction are mediated by incoherent feed forward loops (IFFLs), negative feedback loops (NFLs) and positive feedback loops (PFLs). Classic examples of these loops are depicted: the Ras pathway for IFFL, inhibition of Lck by SHP-1 for NFL, and ERK competing with SHP-1 for PFL[8,9,11].

1.2 Constant Antigen Stimulation leads to T Cell Adaptation *In Vitro* and *In Vivo*

If T cells are exposed to antigen continuously, the cells gradually become unresponsive to stimulation. Clinical and research literature apply a range of terms for T cell unresponsiveness following persistent antigen exposure, including anergy, exhaustion, and tolerization[12,13]. Despite varied terminology, these conditions are broad examples of a behaviour referred to as *adaptation*. Adapting cells respond transiently to an input and return their output to the pre-stimulus level despite constant input[14]. Physiologically, T cell adaptation is observed in three conditions: peripheral tolerance, cancer, and chronic infection (Figure 2).

1.2.1 Peripheral Tolerance

Upon leaving the thymus, T cells receive continuous stimulation from self-pMHC ligands. The resulting T cells are alive yet unresponsive to self-pMHCs (i.e. adapted) in a cell-intrinsic manner. Therefore, although the T cell repertoire is carefully honed in the thymus to eliminate autoreactive cells, additional tolerance in the periphery must prevent inappropriate responses to self, diet, and environmental antigens[15].

The adaptation described above represents one mechanism for inducing T cell unresponsiveness to self-pMHCs. Other mechanisms of peripheral tolerance silence T cells through (a) intrinsic control by anergy and apoptosis and (b) extrinsic control by regulatory and tolerogenic T cells[13,16]. Nonetheless, persistent antigen exposure seems to be central to inducing and maintaining T cell unresponsiveness[17–22].

1.2.2 Chronic Infection

Similarly, persistent antigen exposure during infection by chronic viruses, bacteria, and parasites induces cellular unresponsiveness, referred to as exhaustion, to limit excessive tissue damage[12,23]. T cell exhaustion is extensively documented for infections by viruses with high replication rates, including lymphocytic choriomeningitis virus

(LCMV), hepatitis C virus (HCV), hepatitis B virus (HBV), human immunodeficiency virus (HIV), and simian immunodeficiency virus (SIV)[24,25]. For example, LCMV initially stimulates virus-specific effector T cell activity[24,26]. However, sustained stimulation eventually induces exhaustion, characterized by reduced T cell proliferation, a loss of cytotoxic function, and reduced cytokine production (IL-2, IFN-γ, TNF-α)[25,27,28].

1.2.3 Cancer

Considering that tumour antigens are often self-antigens, cancer immunity recruits elements of self-tolerance in inducing T cell unresponsiveness, especially early in tumour development[24]. T cells in progressing cancers are generally assumed to be comparable to exhausted T cells in chronic infection, with high expression of inhibitory checkpoint signaling molecules (i.e. PD-1, LAG-3, TIM-3, CTLA-4), abnormally low cytokine secretion, similar changes to signaling pathways, and matched transcriptome exhaustion profiles[29–34]. T cell unresponsiveness is well-documented for a range of cancers, including melanoma[29,33,35], breast[36], prostate[37], ovarian[38], chronic lymphoid leukemia[39,40], and non-small-cell lung carcinoma[41].

Although the antigen source may differ, adaptation following persistent antigen exposure is a characteristic T cell behaviour occurring on a time scale ranging from hours to years. Further, co-stimulation (i.e. CD28 – B7-1 axis) can re-induce a response in adapted T cells, specifically in exhausted T cells for a range of cancers[42]. The potential to overcome T cell adaptation is particularly relevant for clinical applications, particularly in designing checkpoint inhibitors such as anti-PD1 and anti-CTLA-4 to rescue cancer-specific exhausted T cells[43].

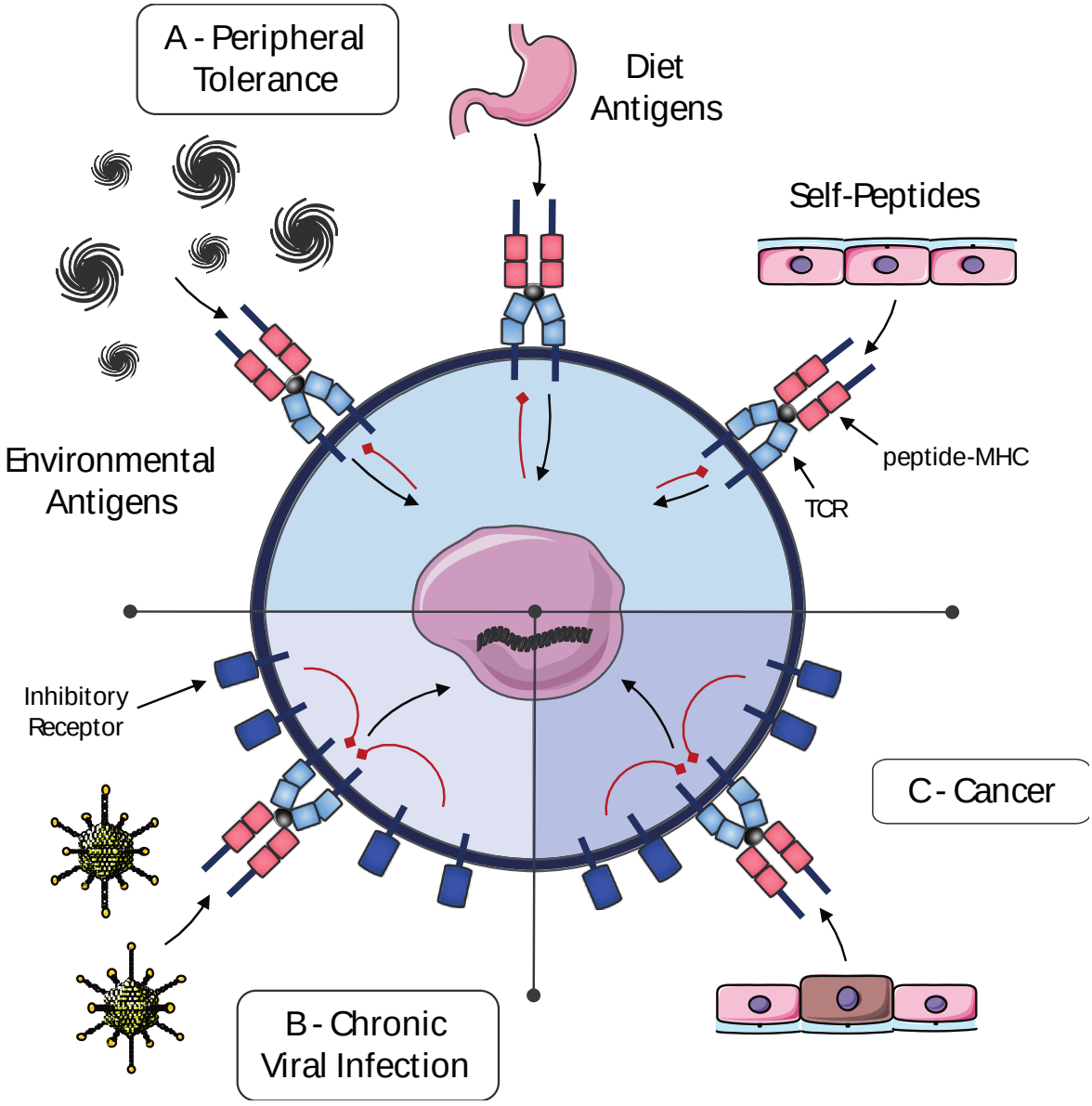


Figure 2. Adaptation in Physiological Conditions. (A) Peripheral tolerance involves adaptation induced by self or innocuous diet and environmental antigens whereas (B) chronic viral infections and (C) cancer induce exhaustion characterized by functional unresponsiveness, the expression of inhibitory receptors, and changes to cell state. (A) occurs on the scale of hours and days; (B) and (C) occur over weeks and months.

1.3 Therapeutic Antibodies and Minimizng Cytokine Production

Beyond the physiological context of self-tolerance, chronic infection, and cancer, a variety of therapeutic antibodies are specifically designed to induce T cell adaptation. Errant T cells can be silenced by two means: (a) depleting antibodies specifically eliminate cells, (b) adaptation can be induced to generate temporary unresponsiveness and therefore mitigate inflammation. Despite clinical success, both approaches elicit a serious side effect—cytokine release syndrome (CRS), a severe condition resulting in multi-organ failure[44].

As examples, I introduce two key therapeutics to treat autoimmune disease, specifically diabetes, and prevent transplant rejection—otelixizumab and alemtuzumab. First approved in the 1980s, OKT3 was the earliest anti-CD3 mAb but induced CRS[45]. To reduce toxicity, OKT3 was modified to be non-FcR-binding, yielding otelixizumab[45]. Otelixizumab (ChAglyCD3), is a humanized aglycosylated anti-CD3ε monoclonal antibody and a promising treatment for autoimmune diseases mediated by activated T cells, particularly new-onset type I diabetes, psoriasis, and rheumatoid arthritis[45]. Mechanistically, anti-CD3 antibodies bind the CD3/TCR complex and induce TCR downregulation and hyporesponsiveness[45–49]. Despite the FcR-binding design change to minimize cytokine release, toxicity remains a concern at high doses. Several studies have attempted to evaluate the efficacy of low doses of anti-CD3 mAb in murine models[50] and humans[51]. Although equally effective and less toxic in mice, lower toxicity in humans is matched by poor clinical efficacy, indicating the difficulty of designing clinically effective dosing regimens without toxic side effects[51].

Alemtuzumab (Campath-1) is a humanized monoclonal anti-CD52 antibody that binds CD52, a GPI-anchored glycoprotein expressed on malignant lymphoid cells and normal T- and B-lymphocytes[52]. Campath-1 is therefore an established therapeutic for

preventing and treating graft-versus-host disease in allogeneic stem cell transplants as well as treating T cell lymphomas and multiple sclerosis[52,53]. Similar to otelixizumab, alemtuzumab is specifically known to induce CRS, in addition to a host of other toxic side effects[54]. Founded on an understanding of T cell adaptation, an optimized regimen for T cell-modulating treatments could minimize cytokine release while maintaining efficacy. This approach is can be extended beyond type 1 diabetes and organ transplantation to treatment of other organ-specific autoimmune diseases—SLE, multiple sclerosis, rheumatoid arthritis, and psoriasis[15].

1.4 Mathematical Models and Molecular Mechanisms of Adaptation

Evidence of adaptation is conclusive in a variety of biological contexts: cell signaling[55,56], sensory systems[57,58], and during development[59,60]. Consequently, the systems biology community is interested in understanding the mechanism(s) of adaptation using mathematical models. Prior to discussing specific networks generating adaptation, it is worthwhile to discuss two broad types of mathematical models built for biological systems, molecular and phenotypic models, and the rationale of developing phenotypic models in this thesis[61].

Molecular models are high resolution and represent all interactions in a system. Despite their complexity, mechanistic models cannot effectively compute input-output relationships, are often poorly predictive, and may resemble indecipherable "hairballs" of protein-protein interactions[56,62]. Conversely, phenotypic models represent groups of species with single, representative variables[63]. Rather than account for all signaling events, these models capture high-level cell behaviour and link inputs to outputs with dominant network motifs[63]. This is particularly useful when the aim is to understand dominant mechanisms causing major functional changes rather than a detailed portrayal of phosphorylation events.

Considering that TCR signal transduction involves minimal molecular reactions following pMHC engagement, phenotypic ODE-based models are often used to represent T cell signaling in the literature[8,64–67]. Discussed below, these models can effectively represent adaptation in a range of biological and receptor-based systems. Nonetheless, phenotypic models representing T cell adaptation do not yet exist. Given that the molecular species involved in adaptation are unclear, I complete a phenotypic analysis of adaptation. I develop and compare several phenotypic models to exclude and suggest potential mechanisms of adaptation in T cells.

1.4.1 Defining Adaptation

Robust, perfect adaptation is defined as the ability of a system to respond to a stimulus and return its output to the pre-stimulus level despite persistent input (Figure 3)[14]. Adaptation can be either perfect, with the final output identical to the input level, or imperfect, with an offset between the final output and input.

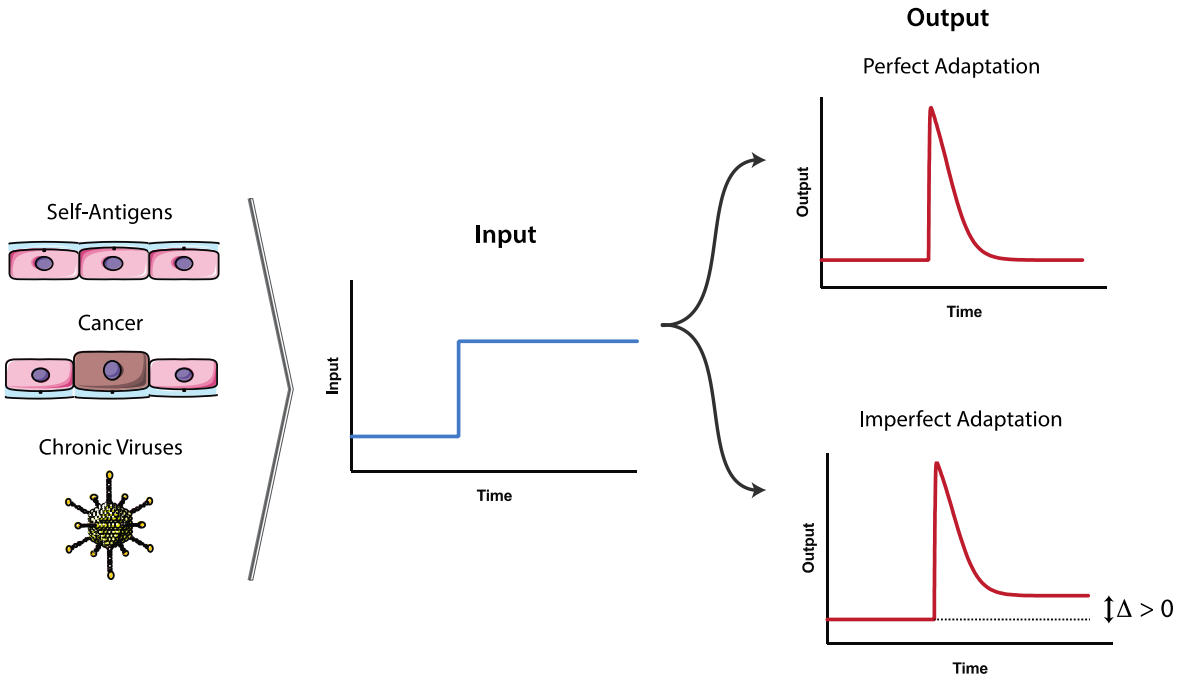


Figure 3. Perfect vs. Imperfect Adaptation. Adaptation occurs physiologically in response to self-antigens, chronic viral infection, and cancer due to persistent antigen exposure, defined as an *input*. Adaptation is defined by an initial transient response in an output followed by a return to steady-state. Perfect adaptation (upper panel) involves a perfect return to the set point whereas imperfect adaptation (lower panel) is defined by a change in the set point.

In parallel with new evidence of biological adaptation, especially in T cells, the systems biology community has identified two fundamental mechanisms that generate this effect. These two architectures, *incoherent feed forward loops (IFFLs)* and *negative feedback loops (NFLs)*, successfully produce adaptation and are overrepresented in a range of biological systems[56]. The phenotypic models that I develop and compare are based on these two motifs. In the following two sections, I explore the general architecture, unique signatures, and biological examples of IFFL and NFL motifs.

1.4.2 Negative Feedback Control

Basic Mechanism of Perfect Adaptation

Negative feedback control is output-dependent: an input signal, *A*, translates into an output, *O*, which subsequently signals to *B* to decrease the input and therefore negatively regulate *O* (Figure 4). To generate adaptation, the mediating protein, *B*, must lag behind the input, *A*, to produce a transient response and must be both precisely timed and ultrasensitive[14,68]. Negative feedback produces near-perfect adaptation under specific conditions: all enzymes acting on the mediating protein, *B*, must operate at saturation (i.e. inhibition by basal enzymes and activation by the output)[14]. This produces the necessary ultra-sensitivity for near-perfect adaptation. At saturation, the mediating protein, *B*, integrates the difference between the output and its input-independent steady-state set point, a form of integral control used in engineering[14].

The basic NFL mechanism can be implemented in a variety of different network architectures, all of which have been experimentally observed. NFLs are pervasive in signaling systems and can be designed with one of several mechanisms of control: deactivation, desensitization, sequestration, or stimulus-dependent degradation of a pathway component[69]. Deactivation involves the transformation of an active signaling species into an inactive state with the potential for reactivation (i.e. dephosphorylation of a

kinase). Desensitization involves converting a species to a form that, even when active, cannot propagate the signal. In contrast, degradation or sequestration involve the permanent elimination of an active species. These species can be either downstream of the receptor or the receptor itself. Regardless of the implementing mechanism, NFLs produce near-perfect adaptation that, in biological contexts, is indistinguishable from perfect adaptation[69].

Beyond Adaptation: Additional Phenotypes

In addition to perfect adaptation, NFLs display several additional phenotypic signatures. Depending on the parameters, negative feedback systems may generate damped oscillations as they adapt[70,71]. These systems produce strong responses for stimuli that increase quickly relative to the time scale of adaptation. In other words, step increases in the stimulus yield discrete peaks with varying amplitudes, yet slow-rising stimuli are undetectable[69]. For feedback deactivation, the duration of the response correlates with the strength of the stimulus; if degradation or sequestration is involved, high doses can completely deplete the target of the feedback, resulting in an all-or-none dose-independent response[69].

NFL systems generally produce good adaptation regardless of the stimulus strength but, once adapted, the ability of the system to recover and respond again (i.e. by re-expression or recovery of the receptor) is slow, often occurring at a rate significantly slower than the time to induce adaptation[69]. Considering that the NFL regulatory mechanism is linked to the output rather than the input, the point at which it begins to reset is independent of the stimulus duration. Once the system has adapted, lengthening the stimulus has no effect on recovery time—the refractory period is therefore stable and robust in NFLs[72]. Noting that the stimulus has no effect until the regulatory system resets, any fresh stimuli during this time have no effect. Experimentally, if a stimulus is removed

and reapplied while the reset is occurring, no response is seen for the reapplied stimulus[72]. This 'period skipping' is an exclusive characteristic of NFLs[72].

Molecular Examples

Negative feedback control occurs both at the receptor-level and in downstream signaling. The remainder of this section explores downstream signaling alone. As an example downstream of the EGF receptor, active ERK1/2 induces activation of a variety of transcription factors, one of which is the MAP kinase phosphatase MKP1[73]. MKP1 subsequently reduces phosphorylation of ERK1/2, causing its inactivation and allowing for adaptation of ERK1/2 levels[73]. Other ERK1/2 pathway proteins known to be phosphorylated in NFLs include MEK, Sos, Raf-1, LAT, and the EGF receptor itself[74].

In T cells, downstream feedback loops differentiate between the quality of pMHC-TCR engagement. Weak binding induces a negative feedback loop mediated by the tyrosine phosphatase SHP-1[11]. SHP-1 mediates the dephosphorylation of Lck and thus inactivates downstream signaling[11]. In contrast, strong binding activates a positive feedback loop, recruiting ERK to Lck and preventing SHP-1 recruitment[11]. SHP-1-mediated NFLs represent merely one of several complex feedback and feedforward mechanisms controlling the variety of signaling pathways downstream of the TCR. These downstream pathways subsequently determine cellular functional responses. Expressed in a generic form, Figure 1 displays a downstream-signaling based architecture for T cell adaptation.

1.4.3 Incoherent Feedforward Control

Basic Mechanisms of Perfect Adaptation

Incoherent feedforward control involves two stimulus-dependent pathways to an output, each exerting an opposite effect. Rather than tracking the output and feeding back to the input, feedforward loops anticipate the output directly from the input, *A*, and use a second regulatory pathway, *B*, to counteract the input's effect (Figure 4). To produce adaptation, there must be a delay between the positive and negative signals received by the output, allowing the output to rise before returning to its basal level. Two classes of incoherent feedforward loops, a total of four architectures, exist but only one class can produce perfect adaptation[14]. This class involves a regulatory protein with the opposite sign to the output as the input to the output (Figure 4). Similar to NFLs, IFFLs must operate under specific conditions to produce perfect or near-perfect adaptation. For the regulatory node to proportionally translate the input into an effect on the output, the steady-state of the regulatory node must be directly proportional to the steady-state of the input[14]. This is achieved when activation of the regulatory node operates close to saturation and the constitutive inactivation of the regulatory node operates far from saturation[14]. These conditions allow the regulatory node to repress the output proportionally to the input.

Beyond Adaptation: Additional Phenotypes

Applying the same concept of additional phenotypes to IFFLs as NFLs, IFFLs exhibit several characteristic behaviours. In contrast with NFLs, the regulatory node is linked to the input rather than output; thus, regardless of when the system adapts, the level of regulatory mechanism increases with increasing stimulus duration. The regulatory mechanism cannot recover while the stimulus is administered and begins to recover only when the stimulus is removed. The recovery time, or refractory period, therefore increases

with the stimulus duration[72]. IFFL-based systems cannot display the 'period skipping' characteristic of NFLs for this same reason—the regulatory node is linked to and responds to the input[72].

Molecular Examples

Returning to the EGF receptor example, IFFLs are essential to downstream receptor tyrosine kinase (RTK) signaling[75,76]. Activated EGFR allows a guanine nucleotide exchange factor (GEF), the Sos-Grb2 complex, to bind. Sos-Grb2 is brought into close proximity of and activates Ras, which exchanges GDP for GTP. This forms the positive pathway of the IFFL: EGFR $\rightarrow$ Sos $\rightarrow$ Ras. Activated EGFR also recruits the GTPase GAP, forming a negative pathway: EGFR $\rightarrow$ GAP $\dashv$ Ras. With a delay between the activation and inhibition pathways, a pulse of Ras is generated before levels adapt. GPCRs govern eukaryotic chemotaxis in *Dicyostelium* through an identical mechanism downstream of the receptor[77]. Two opposing enzymes, GEF and GAP, activate and deactivate Ras respectively at different rates to yield a transient response that enables chemotactic gradient sensing and motility.

In T cells, a range of downstream positive feedback mechanisms have been identified (i.e. MAPK pathway preventing Lck association with SHP-1); nonetheless, a detailed understanding of IFFLs remains elusive, especially in downstream signaling[2]. To date, mathematical models of T cell signalling have included NFLs and IFFLs but have focused on their role in T cell antigen discrimination. NFLs and IFFLs downstream of the TCR have not been evaluated in explaining T cell adaptation.

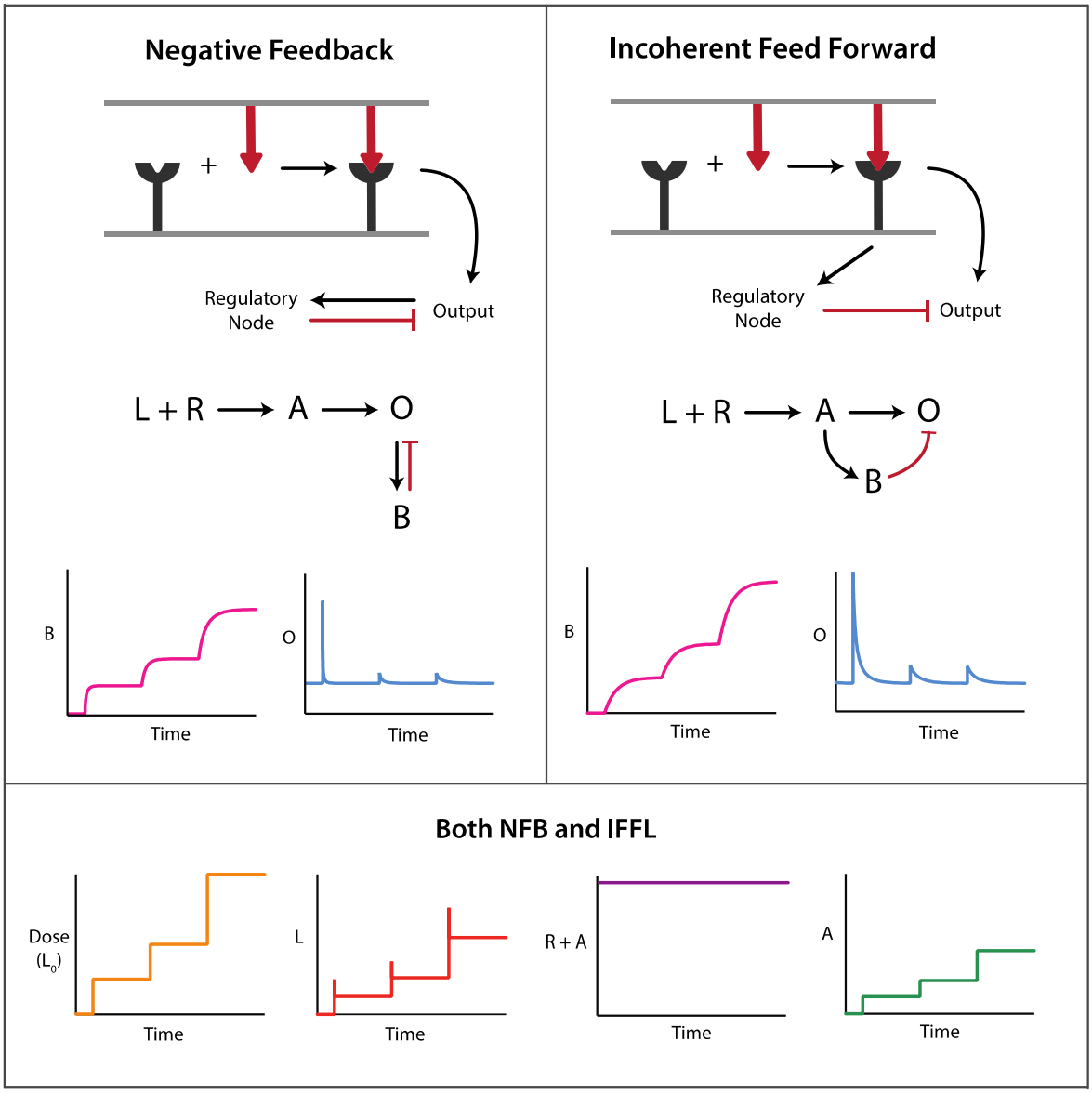


Figure 4. Negative Feedback and Incoherent Feed Forward Control. Negative feedback: an input (A) is converted into an output (O); the output level is evaluated by a regulatory node (B) and returned to a set point if the input changes. Incoherent feed forward: The input (A) influences the output through two pathways, a positive effect on the output (O) and a negative effect by activating a regulatory node (B) that suppresses the output. Simulating step changes in input dose (yellow plot), the regulatory species accumulates, resulting in transient response in the output that is returned to steady state (blue plot). L_0 – initial ligand dose, L – ligand dose, R + A – total receptor (free + bound), A – bound receptor/input, B – regulatory species, O – output.

1.5 Receptor-based Architectures for Perfect Adaptation

Although these examples suggest the importance of NFLs and IFFLs downstream of the receptor, the receptor itself can be a core component of the adaptation mechanism. Receptor-based mechanisms of adaptation involve changes in the availability or responsiveness of the receptor, impacting the functionality of the entire downstream cascade. Biologically, the downregulation and desensitization of GPCRs[78], EGFRs[75,76], and voltage-dependent ion channels[79,80] impact signaling through NFLs and IFFLs[81]. For example, EGFR stimulation by extracellular ligands greatly increases receptor endocytosis[82]. This ligand-induced endocytic downregulation directly impacts the availability of surface receptors for signaling. GPCR desensitization is similar to EGFR downregulation. The GPCR becomes desensitized to signaling when the G-protein uncouples from the receptor, forming a feedback-based system that prevents acute and chronic over-stimulation[78,81,83]. Similarly, conformational changes to ion channels obstruct pores and inhibit responses to external stimuli[79,80]. EGFR and GPCR systems in particular have been heavily studied at the receptor and downstream levels, with both experimental evidence of downregulation or desensitization and corresponding studies of receptor-mediated NFLs and IFFLs. The precise role of TCR downregulation, in contrast, has not been thoroughly studied. Here, I briefly introduce two models of TCR-mediated adaptation based on either complete or partial downregulation (Figure 5).

1.5.1 Complete Receptor Downregulation

Two potential models can be generated with total downregulation: complete receptor or complete receptor and ligand downregulation. Complete receptor downregulation occurs if ligand binding induces downregulation of all receptors with negligible receptor re-expression on the time scale of adaptation. This model assumes no change in the external ligand concentration. Alternatively, the receptor can be in excess of

the ligand or re-expressed/recycled to the surface within the time scale of adaptation, resulting in the complete removal of the ligand. A lack of ligand results in a complete abrogation of signaling. In either case, complete downregulation can be formulated as either an IFFL or a NFL.

1.5.2 Incomplete Receptor Downregulation

Incomplete receptor downregulation can be modelled identically to complete receptor downregulation with the exception that surface TCR is re-expressed. Experimental data confirms the possibility that TCR downregulation can be either complete[84–88] or incomplete[89–93]. However, partial TCR downregulation results in imperfect adaptation (Figure 5). To correct imperfect adaptation at the receptor level, an additional downstream mechanism is required. This can take the form of a switch or additional NFL or IFFL.

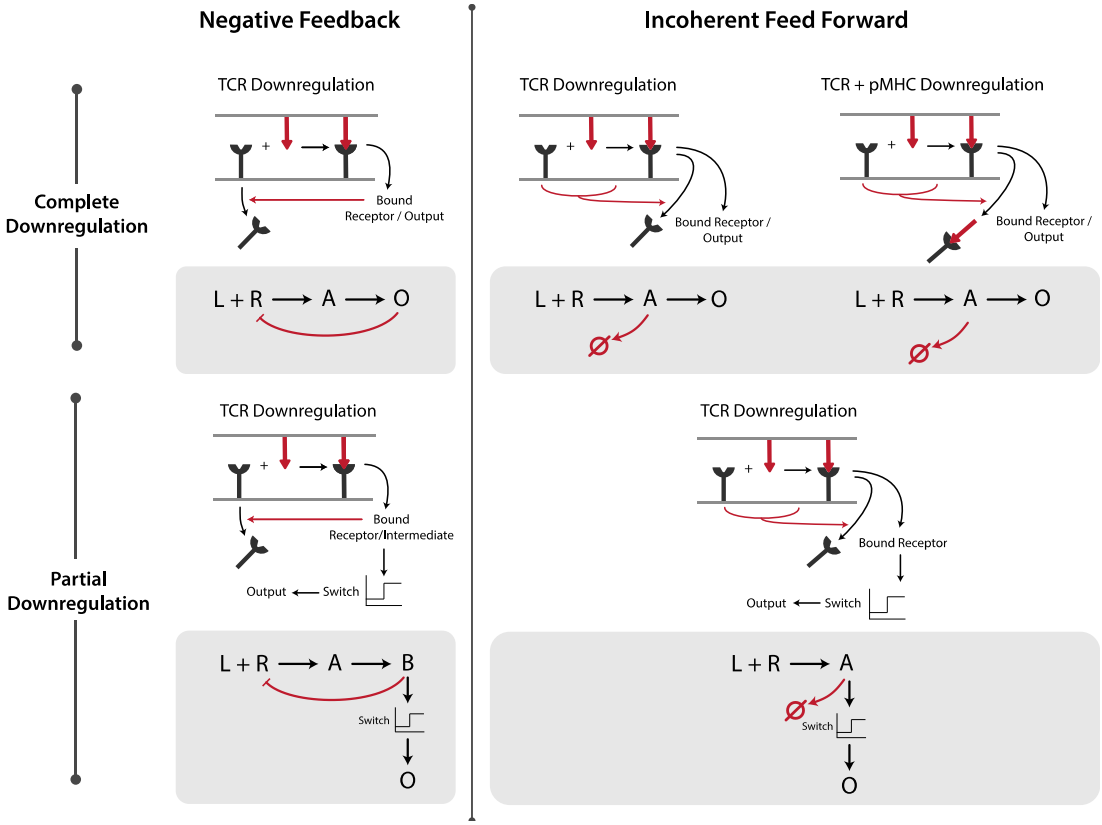


Figure 5. Receptor-based Models of Adaptation. Receptor-based models can portray downregulation as a negative feedback or incoherent feedforward loop and involve either complete or partial receptor downregulation. If receptor downregulation is partial, a second mechanism must be added; in this case, a switch is used— A must be above a threshold to generate O (i.e. a digital response). L – ligand, R – receptor, A – bound receptor, O – output.

Rather than rely on a single mechanism, biological adaptation draws on several feedback and feedforward mechanisms. Nonetheless, although multiple motifs can exist in a system, one mechanism often dominates at a given time scale[72]. Whether receptor- or downstream signaling-based and NFL- or IFFL-based, experimental data can provide powerful clues to identify potential mechanisms underlying adaptation in biological systems.

1.6 Thesis Aims

Persistent antigen exposure generates an initial transient response that leads to unresponsiveness, a behaviour defined as adaptation. Two fundamental network mechanisms can generate adaptation: incoherent feed forward and negative feedback control. Although these mechanisms are well-studied at both the receptor level and in downstream signaling for a variety of biological systems (i.e. GPCRs and EGRs), their potential role in T cell adaptation remains to be studied. This thesis aims to derive insight into T cell behaviour during adaptation by exposing cells to step changes in antigen dose. Further, it assesses the potential role of NFLs and IFFLs in T cell adaptation at the TCR or downstream of the TCR. Seven basic NFL and IFFL networks are examined, controlled by either the receptor or downstream signaling (Figure 6).

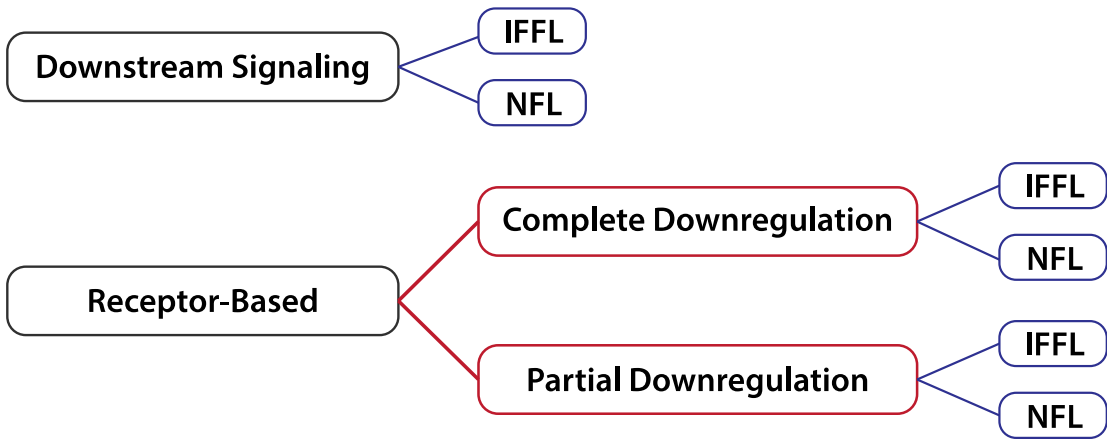


Figure 6. Basic NFL and IFFL Network Types. Seven simple IFFL or NFL models were constructed. Downstream signaling-based models involve no TCR downregulation whereas receptor-based models postulate that TCR downregulation is a mechanism of adaptation. Two IFFL models were developed, one involving complete ligand and TCR downregulation and one with TCR downregulation alone.

Motivated by the fact that T cells are continuously exposed to pMHC in peripheral tolerance, chronic infection, and cancer, a variety of experiments were designed based on step changes in dose. Three experiments were conducted (Figure 7):

- **Experiment 1: Varying time and antigen dose** – adaptation was assessed across a range of doses and time scales;
- **Experiment 2: Step changes in dose** – cells were exposed to large step changes in antigen dose, assessing the effect of previous antigen exposure on the adaptation response;
- **Experiment 3: Gradual step changes in dose** – cells were exposed to smaller step changes in antigen dose, assessing the effect of previous antigen exposure on the adaptation response if the dose change is *gradual*.

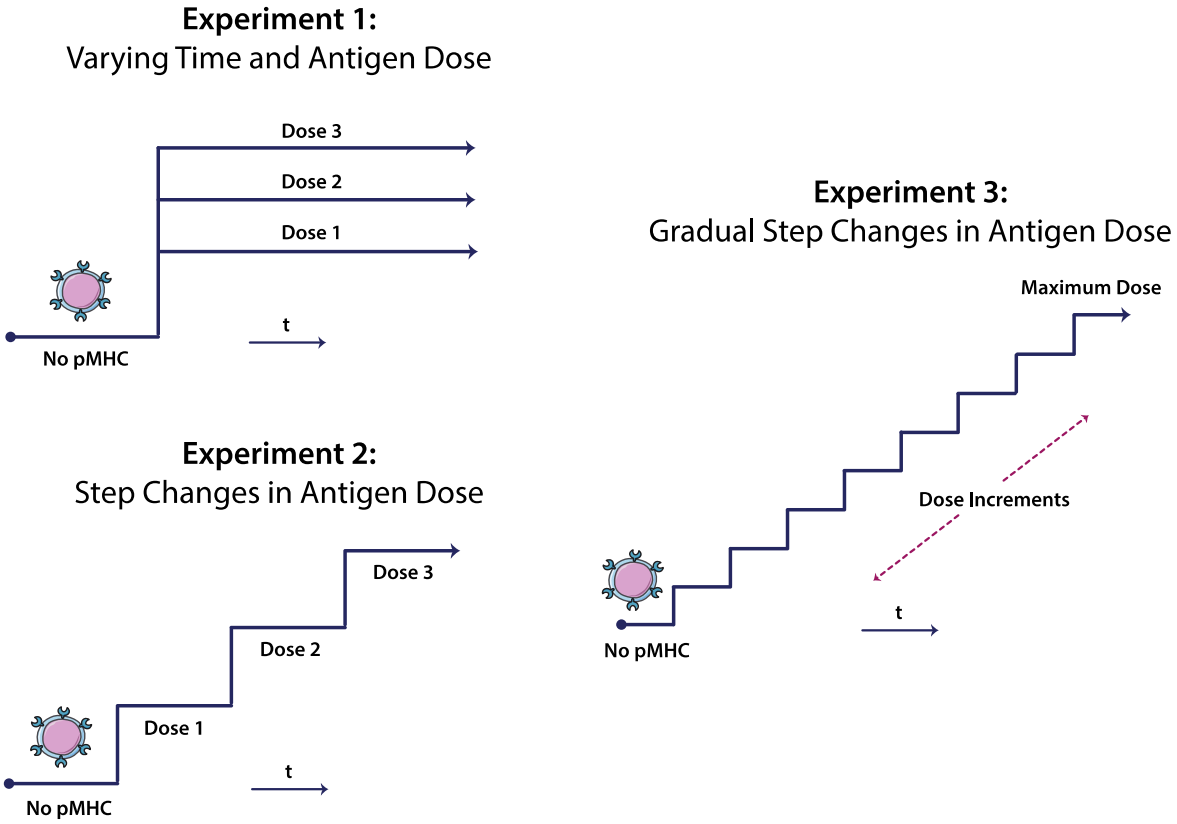


Figure 7. Antigen Dose Escalation Experiments. General experiment formats with effector $CD8^+$ T cells introduced to single, persistent antigen doses (Experiment 1), large fold-change steps in antigen dose (Experiment 2), and gradual step changes in antigen dose (Experiment 3).

The trends in T cell behaviour derived from the above experiments were used to rule out the basic NFL and IFFL networks described above and to resolve hypothetical mechanisms for T cell adaptation. To demonstrate the potential of this work beyond pMHCs, preliminary experiments exploring adaptation induced by anti-CD3 and anti-CD52 antibodies paralleled the pMHC dose- and time-course experiments.

2 Materials and Methods

2.1 Materials

Reagents and Media

Item	Cat. No.	Supplier
T Cell Isolation		
RosetteSep™ CD8⁺ T Cell Enrichment Cocktail	15063	Stem Cell Technologies
CD3/CD28-coated Human T-Activator Dynabeads	111.32D	Thermo Fisher Scientific
Ficoll® Paque Plus	17-1440-02	Amersham Biosciences
X-tremeGENE™ HP Transfection Reagent	06366546001	Sigma Aldrich
Solution 13	12604013	Gibco/Life Technologies
R10 Media		
RPMI 1640 media	R8750	Sigma Aldrich
100 U/mL Penicillin + 100 µg Streptomycin (1%)	15140122	Gibco/Life Technologies
Heat-inactivated fetal bovine serum (10%)	10500064	Gibco/Life Technologies
D10 Media		
DMEM media	D5429	Sigma Aldrich
100 U/mL Penicillin + 100 µg Streptomycin (1%)	15140122	Gibco/Life Technologies
Heat-inactivated fetal bovine serum (10%)	10500064	Gibco/Life Technologies
Recombinant Human IL-2 (100,000 U/mL)	200-02	Peprotech
Sterile PBS (pH – 7.4)	10010023	Thermo Fisher Scientific
Flow Cytometry Wash Buffer (PBS + 1% BSA)		
Bovine serum albumin (BSA)	05473	Fluka Biochemika
PBST: ELISA Wash Buffer (PBS + 0.5% Tween 20)		
Tween 20	P9416	Sigma Aldrich
Other		
Streptavidin-PE fluorophore	405204	Bio-Rad
Sulphuric acid (H_2SO_4)		Thermo Fisher Scientific

Commercial Kits

Item	Cat. No.	Supplier
Invitrogen Human IFN-γ Uncoated ELISA Kit	88-7316-77	Thermo Fisher Scientific
Invitrogen Human TNF-α Uncoated ELISA Kit	88-7346-88	Thermo Fisher Scientific
Invitrogen Human IL-2 Uncoated ELISA Kit	88-7025-77	Thermo Fisher Scientific

Equipment

Item	Supplier
BD FACSCalibur™ flow cytometer	BD Biosciences
SpectraMax M5 Gemini plate reader	Molecular Devices
Nucleocounter® NC-3000	Chemometec
ELx405 microplate washer	BioTek
Allegra X-15R centrifuge	Beckman Coulter
Megafuge 8R centrifuge	Thermo Fisher Scientific

Consumables

Item	Supplier
96-well tissue culture plates Flat-bottom Round-bottom V-bottom	Falcon®/Corning

96-well MaxiSorp™ Nunc-Immuno flat-bottom plate	Thermo Fisher Scientific
96-well Pierce™ streptavidin-coated plate	Thermo Fisher Scientific
25 cm^2 tissue culture flasks	Corning
75 cm^2 tissue culture flasks	Corning
0.45 μm Minisart® cellulose acetate syringe end filter	Minisart

Antibodies

Antigen (clone)	Conjugate	Isotype	Supplier	Cat. No.	Dil.
Human CD69 (FN50)	AlexaFluor 488®	Mouse IgG1	Biolegend	310918	1:200
Human 4-1BB/CD137 (4B4-1)	AlexaFluor 647®	Mouse IgG1	Biolegend	309824	1:200
Human PD-1	AlexaFluor 488®	Mouse IgG1	Biolegend	329936	1:200
Human TCR α/β (IP26)	PE	Mouse IgG1	BioLegend	306708	1:200
CD3 – otelixizumab	Therapeutic mAb provided by Prof. Herman Waldmann Data Sheet: Supplementary Figure 35				
CD52 – alemtuzumab	Therapeutic mAb provided by Prof. Herman Waldmann Data Sheet: Supplementary Figure 35				

2.2 Peptide-MHC Complex Production

The HLA-A*02:01 α-chain and β2-microglobulin chain, specifically extracellular residues 1-287, were expressed in *E. coli* as previously published[94]. Two variants of the NY-ESO-$1_{157-165}$ peptide were acquired from Genscript and re-folded with the HLA-A*02:01 chains to form a complete pMHC[95]. The sequences and affinities of the two protein variants, 9V and 4A8K, for the recombinant $1G4^{hi}$ TCR are in Table 1. Bold amino acids represent amino acids replaced from the higher affinity version to reduce affinity with the $1G4^{hi}$ TCR. A lab manager completed affinity measurements using surface plasmon resonance as previously published[96]. Re-folded proteins were purified with size-exclusion chromatography, biotinylated according to a published protocol, and stored at -80°C until use[96].

Table 1. 9V and 4A8K Peptide Sequences and Affinities

	Peptide	Amino Acid Sequence	$1G4^{hi}$ TCR Affinity (K_D [M])
'High affinity'	9V	SLLMWITQV	7.07×10^{-12}
'Low affinity'	4A8K	SLL**A**WIT**K**V	1.78×10^{-16}

2.3 PE-pMHC Tetramer Production

TCR cell surface levels were evaluated with flow cytometry by staining cells with 9V pMHC conjugated to a fluorophore (PE). To prepare 9V-PE tetramer, 10 μL of streptavidin-PE was added every 10 minutes for 100 minutes to 66.6 μg of 9V pMHC in a room temperature shaker. The 9V-PE tetramer stock was stored at 4°C.

2.4 Isolation and Culture of Primary T Cells

Day 0

50 mL of fresh blood was collected from a healthy HLA-A2$^-$ donor. HLA-A2$^+$ T cells are cross-reactive with the 1G4^{hi} TCR[97]. HLA-A2$^-$ donor samples were incubated with RosetteSep^{TM} CD8$^+$ T Cell Enrichment Cocktail (6 μL per mL of whole blood) for 20 minutes to allow complexes of non-CD8$^+$ T cells to form. Post-incubation, the sample was diluted 1:2 in PBS, carefully layered over 15 mL of Ficoll, and centrifuged at 1000 *g* for 30 minutes with half-acceleration and no deceleration. The visible CD8$^+$ T cell-containing layer was carefully removed, suspended to 15 mL in PBS, and centrifuged at 500 *g* for 10 minutes. The cells were washed once more with PBS. The viability and cell count of the isolated CD8$^+$ T cell population was assessed with a Nucleocounter® NC-3000^{TM}. The isolated cells were re-suspended in complete R10 media with 50 U/mL IL-2 at a concentration of 10^6 cells per mL. To activate and expand the isolated cells, CD3/CD28-coated Human T-Activator Dynabeads were added at a ratio of 0.8 beads/T cell. T cells were incubated at 37°C in 5% CO_2 for 24 hours. In conjunction with the CD8$^+$ T cell isolation process from whole blood, HEK-293T cells were transfected with three plasmids encoding the 1G4^{hi} TCR according to published protocol[95].

Day 1

24 hours post-transfection, lentivirus-containing supernatant was extracted from the transduced cells and purified using a 0.45 μm Minisart® cellulose acetate syringe end filter. The isolated and activated CD8$^+$ T cells were transduced with 1G4^{hi}-encoding lentivirus according to published protocol[95]. The transduced cells were incubated in R10 media supplemented with 50 U/mL IL-2 at 37°C in 5% CO_2. Media was replaced with fresh R10 media every 2 days.

Day 5

On the fifth day post-cell isolation, the CD3/CD28-coated activating Dynabeads were removed according to manufacturer instructions. Between days 5 and 7, expression of the transduced $1G4^{hi}$ TCR in expanded cells was determined using the 9E-PV pMHC tetramer (Section 2.3). The expanded cells were maintained at a density of 10^6 cells/mL, replacing R10 media every 2 days. Cells were suitable for experimentation at any time post-bead removal and were discarded once proliferation was no longer evident, at approximately days 15-16. This T cell isolation, transduction, and expansion protocol was completed weekly on rotation by all group members.

2.5 Immobilization of pMHC to Streptavidin-coated Plates

Aliquots of biotinylated pMHC with known concentrations were thawed to room temperature and diluted in sterile PBS as specified for each experiment. 50 μL of pMHC in PBS was added to each well of a 96-well Pierce™ streptavidin-coated plate and incubated overnight at 4°C, allowing the pMHC to immobilize to the surface of the plate through conjugation with streptavidin.

2.6 Quantitative Data Collection

Quantitative data was obtained with two techniques: flow cytometry and enzyme-linked immunosorbent assays (ELISAs).

2.6.1 Flow Cytometry

Flow cytometry was used to quantify cell surface expression of the TCR, activation markers (4-1BB, CD69), and exhaustion (PD-1). CD69 is a human transmembrane C-type lectin expressed early during lymphocyte activation[98]. As the earliest inducible cell surface glycoprotein during activation, CD69 is a classic marker of T cell activation[98]. 4-1BB (CD137) is an activation-induced co-stimulatory molecule critical for $CD8^+$ T cell proliferation, IL-2 and IFN-γ secretion, and cytolytic activity[99]. Programmed cell death

protein 1 (PD-1/CD279) is an immunoglobulin T cell surface receptor and broad negative immune regulator upregulated on T, B, and myeloid cells post-activation[100,101]. PD-1 expression correlates with reduced T cell proliferation, IL-2 and IFN-γ secretion, and effector functions[100,101]. Sustained expression of PD-1 is a classic marker of T cell exhaustion[100,101].

All stimulation assays were conducted on 96-well Pierce™ streptavidin-coated plates with different concentrations of conjugated pMHC. Cells were added to pMHC-coated plates and stimulated for varying lengths of time with or without co-stimuli. Post-stimulation, cells were removed, transferred to, and pelleted in a 96-well V-bottom plate at 500 *g* for 5 minutes. The supernatant was transferred to a 96-well U-bottom plate and stored at -20ºC for analysis by ELISAs. Cells were resuspended and stained with antibodies in PBS with 1% BSA as required for each experiment (PE-9V pMHC tetramer, anti-CD69, anti-4-1BB, anti-PD-1) for 20-30 minutes in the dark. Stained cells were washed once with PBS, pelleted at 500 *g* for 5 minutes, and resuspended in a final volume of 70 μL of PBS.

A BD FACSCalibur™ flow cytometer with high-throughput sampling and BD FACSDIVA™ software was used to analyze all flow cytometry samples. Previous lab members confirmed that the isolation process yields pure $CD8^+$ lymphocytes[95]. Analysis was completed with FlowJo v10.0.8. The following gating strategy was applied:

a) FSC/SSC: lymphocyte population
b) FSC-W/FSC-A: single cell population
c) $1G4^{hi}$ TCR^+, $CD69^+$, $4\text{-}1BB^+$, $PD\text{-}1^+$ (Supplementary Figure 25)

2.6.2 Enzyme-linked Immunosorbent Assay (ELISA)

ELISA assays were completed using Invitrogen™ uncoated ELISA kits for human IFN-γ, IL-2, and TNF-α according to manufacturer's instructions. 96-well MaxiSorp™ Nunc-Immuno plates were coated with 100 μL/well of the appropriate capture antibody diluted in coating buffer (PBS) (1:250) and incubated overnight at 4°C. Plates were washed three times with PBST using an ELx405 microplate washer. Wells were blocked with ELISA diluent (200 μL/well) for 1 hour. Post-blocking, samples were diluted between 1:3 and 1:5 in ELISA diluent and added to wells (100 μL/well). A range of standard samples were generated with known concentrations of TNF-α, IFN-γ, IL-2 to construct a standard curve. Sample-coated plates were incubated overnight at 4°C. Post-incubation, plates were washed three times with PBST and wells were coated with 100 μL/well of the appropriate detection antibody diluted in ELISA diluent (1:250) for 1 hour. Plates were washed three times with PBST. Avidin-HRP diluted in ELISA diluent (1:250) was added for 30 minutes. Plates were washed three times with PBST, soaked in PBST twice for 3-10 minutes, and washed an additional three times with PBST. Room temperature TMB solution was added (100 μL/well). The resulting colour change reaction was terminated with 2M sulphuric acid (50 μL/well) within 15 minutes. Absorbance values (A_{450nm} and A_{570nm}) were recorded with a SpectraMax M5 Gemini plate reader.

2.6.3 Statistical Analysis and Mathematical Model Generation

All data was analyzed with GraphPad Prism v7.0d. E_{max}, curve maximums, and sigmoid and bell-shaped curve fits were generated with data-fitting algorithms in MATLABR2015A and Python by Omer Dushek and Johannes Pettmann. To normalize data, the maximum surface TCR levels and cytokine levels were normalized to 1 in each repeat before averaging.

For the TCR, the total gMFI was normalized to the fraction of 1G4 TCR^{hi} -positive cells before normalizing to 1 using the control gMFI (i.e. no pMHC condition) using the following formula:

$$X_1 = \left(\frac{\bar{X}_{total}}{X_0^{(1-f)}} \right)^{1/f}$$

where X_1 represents the corrected gMFI, $\bar{X}_{total}$ represents the total average gMFI of a sample, X_0 represents the mode gMFI of the negative cell population, and f represents the fraction of $1G4^{hi}$ TCR-positive cells. Specific statistical tests are described in the Results section and figure captions where appropriate. All ODE-based models were coded in MATLAB R2015A. The ODEs for each model are presented in Supplementary Figure 23.

2.7 Experiment 1: Varying Time and Antigen Dose

Time- and dose-course data were generated for two peptide variants (9V and 4A8K) by varying both the pMHC dose and duration of stimulus. pMHC was immobilized onto streptavidin-coated plates as previously described (Section 2.5). Pre-experiment, plates were washed with 200 μL/well of PBS. At each time point (0.5, 1, 1.5, 2, 3, 4, 6, and 8 hours), 80,000 cells/well were added and the plates were centrifuged at 50 *g* to gently force the cells from suspension onto the plate surface.

At the 8 hour time point, cells were removed from each well and transferred to a 96-well V-bottom plate. The V-bottom plate was centrifuged at 500 *g* for 5 minutes and the supernatant removed and stored at -20°C for use in an ELISA (Section 2.6.2). Cells were prepared for flow cytometry as described (Section 2.6.1) using the PE-9V tetramer, anti-CD69, and anti-4-1BB antibodies. Cell supernatants were analyzed with ELISAs for TNF-α, IFN-γ, and IL-2 (Section 2.6.2).

2.8 Experiment 2: Step Changes in Antigen Dose

Steps of escalating antigen dose reveal information on cell memory of prior responses. If cells adapt at an initial dose, a step increase in dose can induce either a new transient response or continued adaptation. To select a series of escalating doses, the dose- and time-course data for 4A8K pMHC were examined. Noting that adaptation occurs within four hours for TNF-α, three doses were selected between the minimum and maximum TCR levels on the four-hour dose-response curves and the incubation time for each dose was set at four hours. The lowest dose, 150 ng/well, represents the approximate EC_{50} dose of TCR downregulation, signifying that 150 ng/well induces downregulation of approximately half of TCRs. Remaining receptors can respond to sequential changes in antigen dose, allowing the effect of previous antigen exposure on future reactions to be examined. The Results section provides further rationale for selecting doses that induce partial TCR downregulation. The three selected doses (150, 350, and 820 ng/well) are each 2.3-fold greater than the previous step.

At a high level, cells were incubated at the first dose (150 ng/well) for four hours. Every half hour, cells were sampled. After four hours, cells were transferred to the second dose (350 ng/well) and incubated for another four hours. Once again, cells were sampled every half hour. Following the second four-hour incubation, cells were transferred to wells with the third dose and incubated for a final four hours, sampling every half hour. Each four-hour incubation therefore generated eight data points.

As controls, three additional setups were generated: (a) replacing the first dose with no pMHC and transferring the cells from 0 ng/well to 350 ng/well, (b) replacing both the first and second doses with no pMHC and transferring the cells from 0 ng/well to 0 ng/well to 820 ng/well, and (c) replacing all doses with no pMHC and transferring the cells three times. The consistent number of transfers for each condition controls for cell loss. In

summary, the following conditions were prepared, with green shading indicating conditions with sampling:

Table 2. Experiment 2 – Dose Escalation Strategy

Condition	0 – 4 hours	4 – 8 hours	8 – 12 hours
Step Change	150	350	820
Control – 350	0	350	–
Control – 820	0	0	820
Control – No pMHC	0	0	0

ng/well 4A8K pMHC

4A8K pMHC was immobilized on streptavidin-coated plates as previously described (Section 2.5) and 80,000 primary $1G4^{hi}$ $CD8^{+}$ T cells were added to each well. All plates were incubated at 37ºC and 5% CO_2. Eight wells were prepared for each condition to enable sampling every half hour. For the control 350 and 820 ng/well conditions, no samples were collected during the steps with no pMHC. The shaded green cells in Table 2 therefore indicate conditions for which 30-minute sample data was collected.

At each half-hour time point, cells were collected from the appropriate wells. The only exception is the no pMHC control—eight wells were prepared and one well was sampled every two hours. Cells were transferred to a 96-well V-bottom plate, centrifuged at 500 *g* for 5 minutes, and the supernatant was removed and stored at -20ºC for ELISA analysis. The cells were resuspended in PBS with 1% BSA to prevent adhesion and stored at 4ºC until all samples were collected. All cells were prepared for flow cytometry as described (Section 2.6.1) using the PE-9V tetramer and anti-CD69 antibodies. Cell supernatants were analyzed with ELISAs for TNF-α, IFN-γ, and IL-2 (Section 2.6.2).

For three of eight experimental repeats, two identical plates were prepared using the same cells to generate two technical replicates and the time points were modified to reduce noise in later time points: sampling once at 0.5, 1, 1.5, and 2 hours and twice at 3 and 4 hours per incubation, rather than once at 0.5, 1, 1.5, 2, 2.5, 3, 3.5, and 4 hours.

2.9 Experiment 3: Gradual Step Changes in Antigen Dose

Experiment 2 transitioned cells between three escalating antigen doses with a large fold-change difference and an incubation time similar to the time scale of adaptation. If the duration of each incubation is short relative to the time scale of adaptation and the doses increase step-wise by small increments, the cumulative output can be compared to cells exposed constantly to the maximum stimulus[69]. Theoretically, the system may 'tune' to the gradually increasing stimulus and produce minimal output or the system may respond with equal or greater cumulative output[69]. Complementing experiment 2, experiment 3 examines adaptation generated by small, incremental steps in antigen dose over time scales significantly shorter than adaptation. Two key questions are addressed in two experimental phases:

(a) **Phase 1:** How does cumulative cytokine output differ between cells transitioned gradually from no pMHC to a high dose and cells exposed constantly to a high dose?

(a) **Phase 2:** Does gradually increasing dose produce a similar state of adaptation as one constant high dose?

2.9.1 Phase 1: Inducing Adaptation

To address the first question, cells were exposed to one of three conditions—increasing, constant, or no antigen. Cells were incubated for 1 hour at each dose followed by a transfer to the next dose. With 12 transfers, the total incubation time was 12 hours. Thus, cells were transitioned from 20 to 900 ng/well of pMHC with 80 ng increments for the increasing antigen condition. For the constant antigen condition, cells were transitioned from 900 ng/well to 900 ng/well for a total of 12 transfers. The no antigen condition consisted of 12 transfers between wells with no pMHC. A consistent number of transfers controls for cell loss during each transfer. Several technical repeats were carried

out for each condition: three for the increasing and constant antigen and two for no antigen. To ensure that transferring did not alter cell activation or cytokine output, a second setup of the no antigen condition was completed without transfers.

Table 3. Experiment 3 – Antigen Doses

	Dose Range	Increment Size
Increasing Antigen	20 – 900 ng/well	80 ng
Constant Antigen	900 ng/well	0 ng
No Antigen	0 ng/well	0 ng

Phase 1: Protocol Details

4A8K pMHC was immobilized on streptavidin-coated plates as previously described (Section 2.5) and 80,000 primary $1G4^{hi}$ $CD8^{+}$ T cells were added to the first set of wells (hour 1). The cells were centrifuged at 50 *g* for 2 minutes to settle the cells onto the plate surface. Sterile PBS was added to the remaining sets of wells (hours 2 to 12). All plates were incubated at 37ºC and 5% CO_2.

At each hour for 12 hours, PBS was removed from the next set of wells and the cells were transferred to the new wells. The plate was centrifuged at 50 *g* for 2 minutes as described above and returned to the incubator. This transfer process required <5 minutes in totality, ensuring that the cells were minimally impacted by the time outside the incubator. At 12 hours, cells were removed from the final set of wells, transferred to a 96-well V-bottom plate, and centrifuged at 500 *g* for 5 minutes. The supernatant was removed and stored at -20ºC for ELISA analysis. All cells were prepared for flow cytometry as described (Section 2.6.1) using the PE-9V tetramer, anti-4-1BB, and anti-CD69 antibodies. Cell supernatants were analyzed with ELISAs for TNF-α and IFN-γ (Section 2.6.2). Cumulative cytokine production over 12 hours, as well as final activation marker and TCR expression, were therefore recorded.

2.9.2 Phase 2: Confirming Adaptation

To answer the second question, cells were prepared identically as in Phase 1, exposed to increasing antigen, constant antigen, or no antigen over 12 hours. The cells were then redistributed across a full dose range of new pMHC as in Experiment 1, the dose-response experiment. The aim was to compare cells gradually exposed to antigen with cells exposed to a constant high dose to verify that both cell populations are similarly adapted.

Phase 2: Protocol Details

To generate a sufficient number of cells, eight identical wells were required for each condition (increasing antigen, constant antigen, no antigen, and no antigen + not transferred). One of the eight was processed via flow cytometry as in Phase 1 to record the activation marker and TCR levels prior to Phase 2. The remaining cells were pooled, resuspended in fresh R10 media, normalized to identical concentrations, and redistributed across a range of 4A8K pMHC doses on a new streptavidin-coated plate (Section 2.5). The plate was centrifuged at 50 *g* for 2 minutes to settle the cells and incubated overnight at 37ºC and 5% CO_2. Cells were subsequently removed from the plates, transferred to a V-bottom plate, and pelleted as previously described. The supernatant was removed and stored at -20ºC for analysis by TNF-α and IFN-γ ELISAs (Section 2.6.2). Cells were prepared for flow cytometry as described (Section 2.6.1) using the PE-9V tetramer, anti-4-1BB, and anti-CD69 antibodies.

To further verify that the cells were unresponsive and adapted, a response was re-induced with CD86 co-stimulation. The maximum dose, 900 ng/well, was supplemented with CD86 (100 ng/well) following the same PBS dilution and immobilization process as pMHC. CD86 was produced in a CHO cell line permanently expressing CD86 (amino

acids 6-247), kindly provided by Simon Davis, and purified by a senior DPhil student according to an internal lab protocol.

2.10 Experiment 4: Adaptation by Anti-CD3/Anti-CD52 Monoclonal Antibodies

As a proof of concept, primary $CD8^+$ T cells were exposed to two monoclonal antibodies to examine whether adaptation can be induced by other non-pMHC stimuli. Dose- and time-course experiments were conducted for two therapeutics: otelixizumab and alemtuzumab.

Therapeutic otelixizumab and alemtuzumab were provided by Herman Waldmann. Both antibodies were reconstituted according to the manufacturer's instructions and diluted to 100 ug/mL in PBS. A dose range was selected based on the maximum loading capacity of an ELISA plate and following consultation with the Waldmann group. Two formats were tested: a plate-bound format and soluble format. In contrast with the previously described experiment, the $1G4^{hi}$ TCR is not required. Thus, untransduced primary $CD8^+$ T cells were used.

Plate: A range of doses from 0 to 100 ug/mL were prepared in PBS and 100 μL/well was added to 96-well MaxiSorp™ Nunc-Immuno plates. Plates were incubated with mAb overnight at 4ºC and washed with 200 μL/well of PBS. 80,000 cells in 200 μL of R10 media were added to each well at the appropriate time point, described below.

Soluble: mAb antibodies were prepared in R10 media at identical concentrations as the plate format and 80,000 cells in R10 media were added for a final well volume of 200 μL at each time point, described below.

Both plate formats were incubated at 37ºC and 5% CO_2 for the duration of the experiment. At each time point (1, 2, 3, 4, 6, 8, and 15 hours), 80,000 cells/well and soluble antibody, if applicable, were added. Plates with immobilized antibody were centrifuged at 50 *g* to gently settle cells onto the plate surface.

Post-incubation, cells were removed, transferred to a 96-well V bottom plate, and centrifuged at 500 *g* for 5 min. Supernatants were collected and stored at -20ºC for analysis by ELISA for TNF-α and IFN-γ (Section 2.6.2). Cells were prepared for flow cytometry as described (Section 2.6.1) using anti- TCR α/β, anti-4-1BB, and anti-CD69 antibodies. The result is dose- and time-course data for otelixizumab and alemtuzumab. For otelixizumab, the anti-TCR α/β antibody used to evaluate TCR expression cannot bind if otelixizumab is bound to CD3ε. A duplicate setup was simultaneously prepared and incubated at 4ºC to halt cell activity and assess the effect of this binding on TCR detection.

3 Results

Four key results emerged from the project:

1) Cytokine production, specifically TNF-α, adapts in primary $CD8^+$ T cells when exposed to persistent antigen;
2) Compared with cells exposed to a single dose of antigen, escalating step changes in dose yield a unique profile: cells demonstrate limited responsiveness to further stimulation, downregulate the TCR to the same absolute level, and are uniformly activated regardless of dose;
3) Compared with cells exposed to a single high dose of antigen, gradual exposure to incremental small doses of antigen results in the same total cytokine production, TCR and activation marker expression, and unresponsiveness to further stimulation;
4) Primary $CD8^+$ T cells adapt on a longer time scale when exposed to a persistent, high dose of otelixizumab (anti-CD3) immobilized on a plate surface.

These data sets were applied to evaluate the potential role of NFLs and IFFLs in T cell adaptation. Seven basic NFL and IFFL networks were examined, controlled by either the receptor or by downstream signaling (Figure 6). Mathematical models are often applied to experimental observations. However, several different networks often fit the same experimental data. Consequently, rather than definitively selecting a motif, I applied a model invalidation-based approach to determine whether NFLs, IFFLs, or a combination could mechanistically link TCR downregulation and adaptation. This section discusses the experimental results of Experiments 1-3 exploring adaptation behaviour, their alignment with models of adaptation, and a proof-of-concept experiment of otelixizumab- and alemtuzumab-induced adaptation (Experiment 4).

3.1 Experiment 1: Confirmation of Adaptation in Cytokine Production

3.1.1 Experimental Setup

T cell adaptation is characterized by reduced cytokine secretion despite continuous pMHC exposure. Time- and dose-course data indicate that T cells adapt when exposed to persistent low- and high-affinity pMHC stimuli (4A8K and 9V). Figure 8 below depicts the general experimental setup. T cells were exposed to a range of pMHC doses for various lengths of time and data on surface marker expression and secreted cytokines were collected.

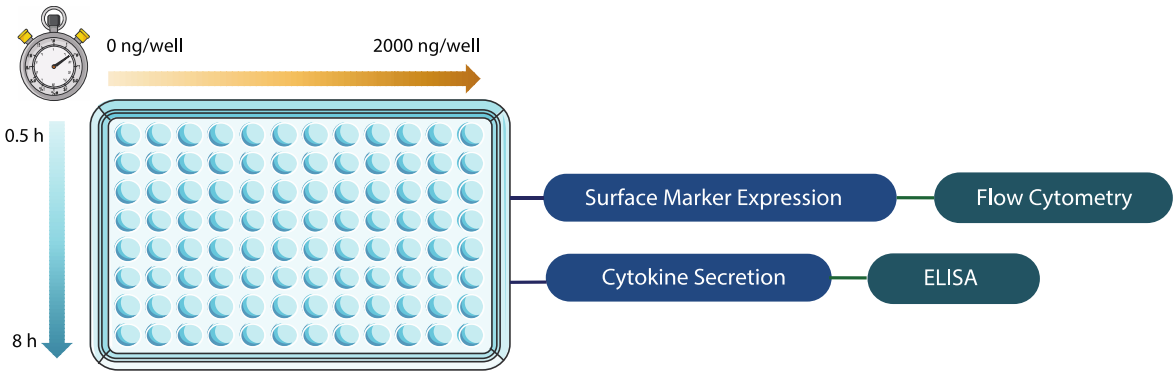


Figure 8. Experiment 1 – General Setup. Primary human $CD8^+$ effector T cells expressing the $1G4^{hi}$ TCR were stimulated using two recombinant peptides (high-affinity: 9V, low-affinity: 4A8K) immobilized on plates. Cells were exposed to a range of antigen doses (0 – 2000 ng/well) and sampled at a series of time points (0.5 – 8 hours). Surface marker expression (CD69, TCR, 4-1BB) was assessed via flow cytometry and cytokine secretion (TNF-α, IFN-γ, and IL-2) was assessed via ELISA.

3.1.2 Cytokine dose-response time course

Figure 9 plots *cumulative* secreted TNF-α, IFN-γ, and IL-2 following exposure to a range of pMHC doses over 8 hours. The *production rate* of cytokine adapts rather than the cumulative cytokine itself (i.e. the production rate increases upon stimulation and returns to zero over time), resulting in overlapping curves when adaptation occurs.

Examining Figure 9**, TNF-α** secretion adapts at approximately 4 hours for both 4A8K and 9V. By fitting sigmoidal or bell-shaped dose-response curves, the maximum values for each experiment at each time point can be used to confirm adaptation (Figure 10). A two-way ANOVA with multiple comparisons corrected by Tukey's test can then

be applied to compare whether the time points are significantly different from each other. For example, for TNF-α secreted by 9V-stimulated cells, the differences between 1 and 2 hours and 2 to 3 hours are significant but 3 to 4, 4 to 5, and 5 to 6 hours are not significant. Thus, the difference in maximum secreted TNF-α between successive time points becomes insignificant post-3 hours for 9V-treated cells. The difference between time points becomes insignificant post-2 hours for 4A8K-treated cells. A lack of difference between time points can be roughly abstracted as a representation of adaptation. Similarly, **IL-2** production seems to adapt post-5 hours for both peptides. Nonetheless, the difference between consecutive time points is insignificant and variability between experimental repeats is high. The data for **IFN-γ** suggests that adaptation does not occur within 8 hours. It can therefore be concluded that adaptation occurs at approximately 4 hours for **TNF-α** and 5 hours for **IL-2** secretion. Supplementary Figure 26 and Figure 27 present single-experiment data for all cytokines.

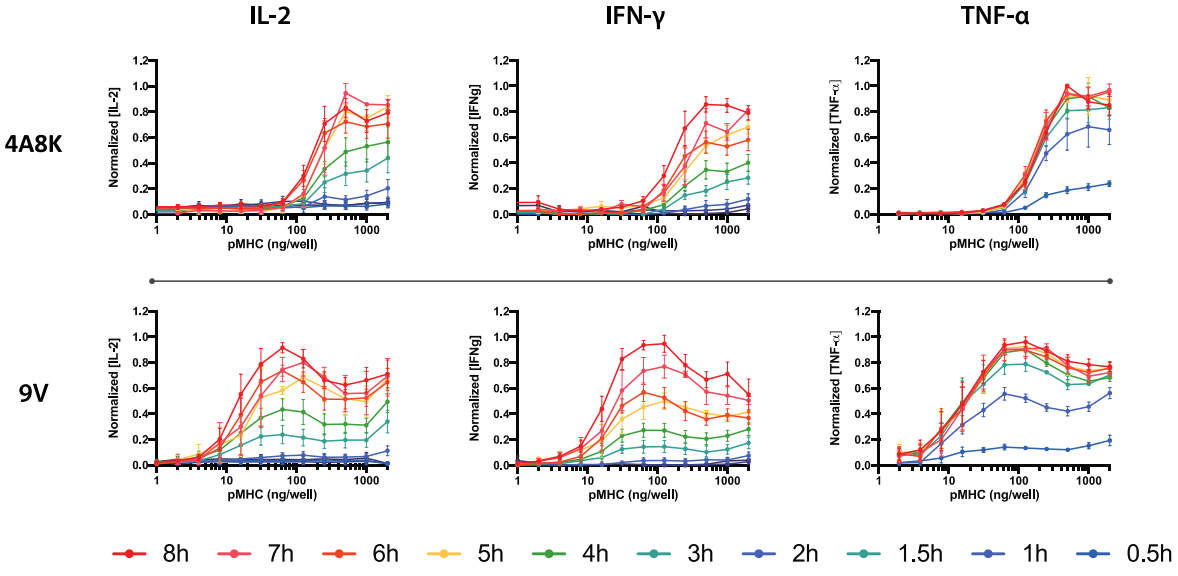


Figure 9. Cytokine Production vs. pMHC Dose. Cumulative cytokine secretion (TNF-α, IFN-γ, and IL-2) by T cells exposed to a range of pMHC doses over time for both high-affinity (9V) and low-affinity (4A8K) pMHC. Due to poor ELISA data quality, likely a result of freezing and thawing supernatants, the TNF-α data is sourced from earlier experiments by Nicola Trendel (n = 3). All other cytokine data was combined Nicola's earlier collected data (n = 6). Mean and SD with n = 6 for IFN-γ and IL-2 and n = 3 for TNF-α.

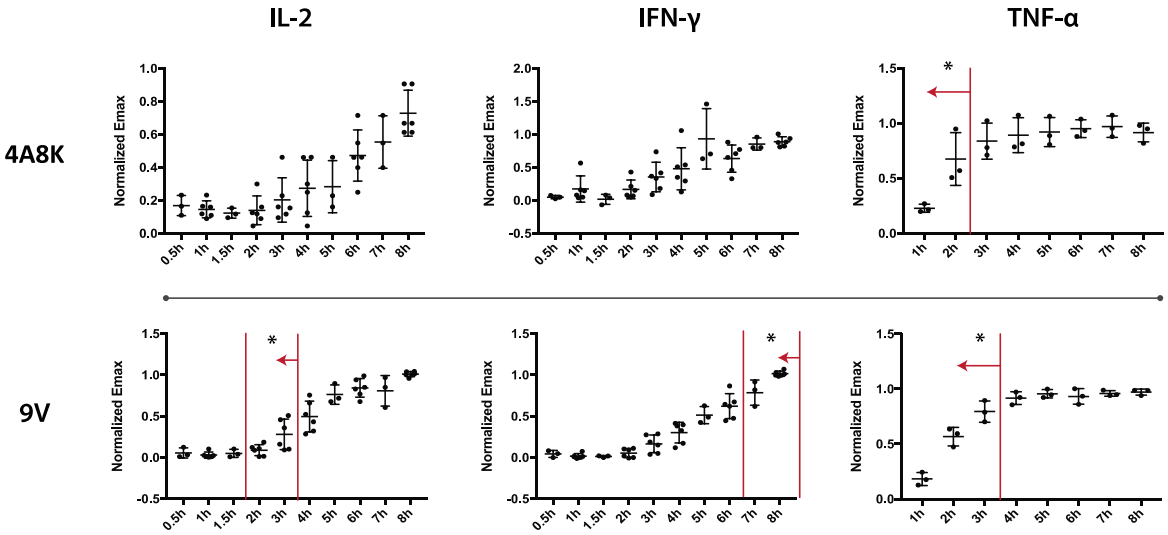


Figure 10. Cytokine Production vs. pMHC Dose: E_{max} Comparison. Sigmoidal (4A8K) or bell-shaped (9V) dose-response curves were fit to all time points for each repeat (normalized to 1). The E_{max} values were extracted and plotted. Bars represent mean and SD. Mean and SD with n = 6 for IFN-γ and IL-2 and n = 3 for TNF-α. Time points for TNF-α and 3 repeats for IFN-γ and IL-2 (Nicola Trendel's data): 1, 2, 3, 4, 5, 6, 7, 8 h; time points for 3 repeats of IFN-γ and IL-2: 0.5, 1, 1.5, 2, 3, 4, 6, 8 h. The statistical significance of differences between each pair of successive time points was assessed using a two-way ANOVA with a multiple comparisons test comparing the mean of all E_{max} values for each time point. Time points between the red bars or below single red bars are statistically significant. IL-2, 9V: p = 0.0035, IFN-γ, 9V: p = 0.0096, TNF-α, 4A8K: p = 0.0003, TNF-α, 9V: p = < 0.0001.

3.1.3 CD69 data: all T cells are being activated

CD69 is the earliest inducible cell surface glycoprotein expressed during activation and is therefore a classic marker of T cell activation[98]. Figure 11A depicts CD69 expression over time as mean fluorescence for 9V and 4A8K. Complementing this, Figure 11B plots the E_{max} values of the curves for each individual experimental repeat. Previous work and Figure 14 demonstrate that the proportion of CD69-positive cells achieves a maximum within 4 hours. Nonetheless, Figure 11 indicates that gMFI increases continuously past 4 hours. Drawing a conclusion, all cells become activated and express CD69 uniformly within 4 hours. Past this time, all cells express CD69 further. Activation does not occur in distinct cell populations at different times.

At high doses (> 200 ng/well), CD69 expression is independent of dose for both 4A8K and 9V (i.e. identical for all doses above a threshold). Further, the 9V curve is uniquely bell shaped. Considering that CD69 is induced by activation[98,102], reduced TCR downregulation at intermediate doses allows for greater activation. High antigen doses induce stronger downregulation that limits overall activation signaling, resulting in a bell-shaped CD69 activation marker curve. Overall, all cells exposed to pMHC experience some degree of activation.

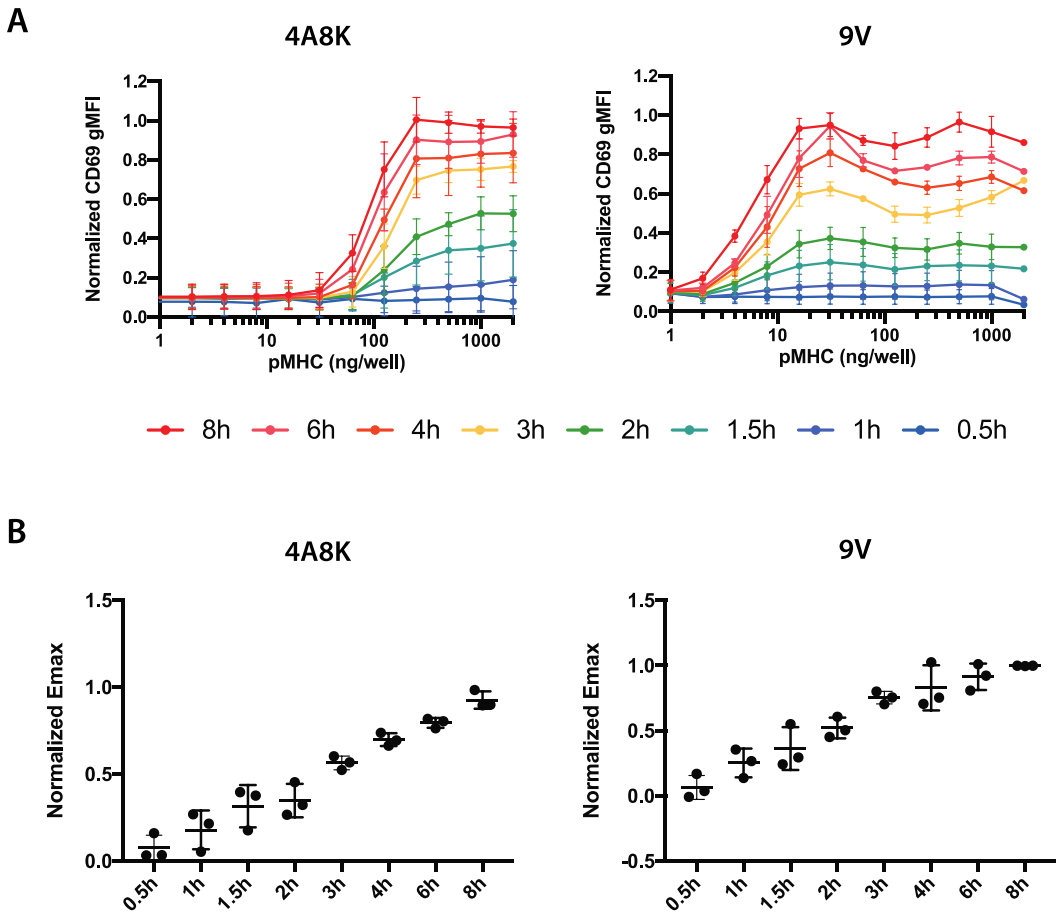


Figure 11. T Cell Activation. (A) Surface CD69 expression (mean CD69 gMFI) of T cells exposed to a range of pMHC doses over time for both high-affinity (9V) and low-affinity (4A8K) pMHC for a range of time points. Mean and SEM with n = 3. (B) Sigmoidal (4A8K) or bell-shaped (9V) dose-response curves were fit to all time points for each repeat (normalized to 1). The E_{max} values were extracted and plotted. Bars represent mean and SD. Mean and SD with n = 3. Statistical significance between successive time points was assessed using a two-way ANOVA with a multiple comparisons test comparing the means of the E_{max} values for each time point. No differences are statistically significant except 2h vs. 3h for 4A8K: p = 0.0198.

3.1.4 TCR Downregulation is Biphasic

TCR downregulation is dose-dependent and continues for several hours following pMHC exposure. Figure 12A shows aggregate data of TCR downregulation over 8 hours for both 4A8K and 9V. Data for both peptides suggests that TCR downregulation is biphasic: large amounts of TCR are downregulated between 0 and 30 minutes, followed by slower downregulation until approximately 4 hours at which point TCR surface levels stabilize. For both 4A8K and 9V, this relationship is most pronounced for doses near the EC_{50} of the TCR downregulation curves (i.e. ~200 ng/well for both).

To resolved the statistical difference between the time points, I compare each time point to the final time point (8 hours). A two-way ANOVA with multiple comparisons corrected by Dunnett's test was applied to compare the overall mean of each time point against the mean for 8 hours. For 4A8K, the 8 hour mean is significantly different than the 0.5 to 4 hour conditions, confirming that the TCR level reaches a steady-state after 4 hours (8 h vs. 4 h: $p = 0.0077$). For 9V, the 8 hour condition is significantly different than the 0.5 to 3 hour conditions (8 h vs. 3 h: $p = 0.0906$), suggesting that TCR levels stabilize at a slightly earlier time point. Figure 12B is a representative histogram displaying the decreasing TCR expression on TCR-positive cells for one dose of 4A8K.

An unexpected result, the 9V TCR curve takes the form of an inverted bell-shape. Higher doses of pMHC correlate with decreased downregulation and resolution of the slower downregulation phase is lost. Nonetheless, the data on this part of the curve is high in error and the shape thus requires further investigation beyond the scope of this thesis.

Figure 12C plots time against TCR levels rather than dose. This figure confirms biphasic downregulation, particularly for 4A8K. A majority of downregulation occurs within the first half hour followed by slower downregulation. Several high doses (>250 ng/well) are plotted for 9V, displaying the high degree of uncertainty for this increasing

part of the dose-response curve. For the purpose of this thesis, 4A8K is the ideal variant to study with both a physiological affinity and a well-characterized TCR downregulation curve.

A former DPhil student, Nicola Trendel, initially completed this experiment but lacked the capacity to detect a TCR-time relationship due to less sensitive 9V-PE tetramers. Considering my interest in TCR downregulation as a potential mechanism of NFL- or IFFL-mediated downregulation, I repeated the time- and dose-course experiments with more sensitive TCR tetramers to supplement Nicola's data.

Time- and dose-course data yielded two key conclusions relevant to the design of Experiments 2 and 3: (a) TNF-α secretion adapts on a time scale of 4 hours and can serve as a proxy for output cytokine production and (b) the kinetics of cytokine secretion differ for TNF-α, IFN-γ, and IL-2. Additional repeats of this experiment would be worthwhile to generate high quality TNF-α, IFN-γ, and IL-2 data confirming adaptation on different time scales.

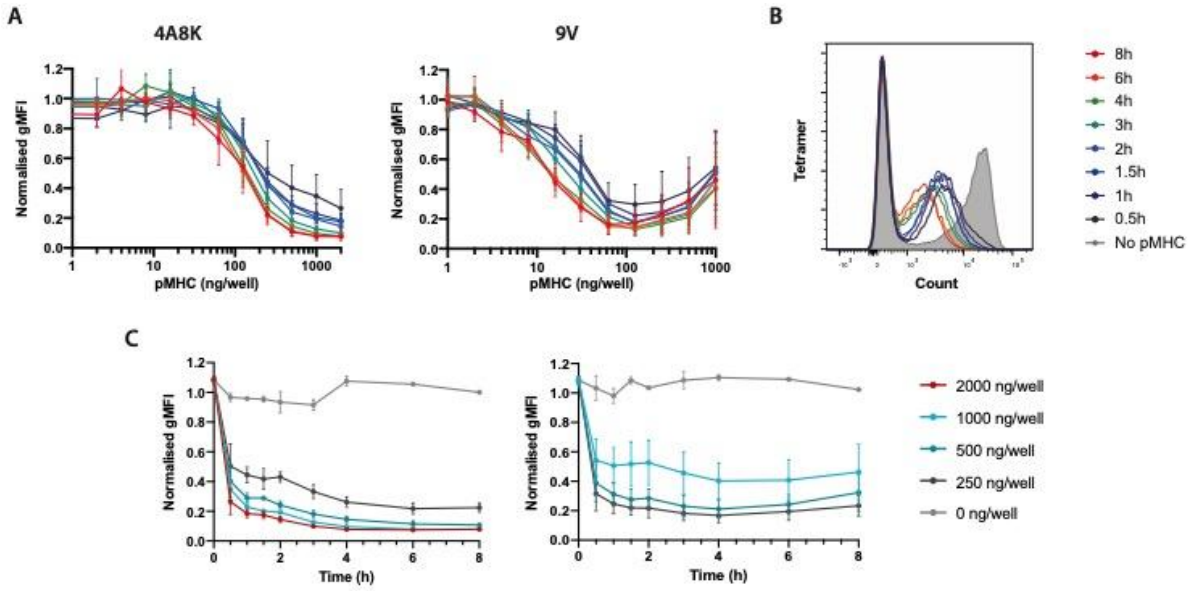


Figure 12. T Cell Downregulation. (A) Surface TCR expression of T cells exposed to a range of pMHC doses over time for both high-affinity (9V) and low-affinity (4A8K) pMHC for a range of time points. Mean gMFI and SD with n = 3. TCR values for each repeat were normalized to the fraction of $1G4^{hi}$-expressing T cells (Section 2.6.3). A two-way ANOVA and multiple Dunnett's comparison test were applied to compare the overall mean of each time point against the mean for 8 hours. *4A8K*: 8 h vs. 4 h: $p = 0.0077$, 8 h vs. 3 h: $p = 0.0087$, 8 h vs. 2 h/1.5 h/1 h: $p < 0.0001$; *9V*: 8 h vs. 3 h: $p = 0.0906$, 8 h vs. 2 h: $p = 0.0116$, 8 h vs. 1.5h: $p = 0.0005$, 8 h vs. 1 h/0.5 h: $p < 0.0001$. (B) Representative histogram of surface TCR expression measurement using flow cytometry with pMHC tetramers. The lower peak represents the cell population with no $1G4^{hi}$ TCR while the upper peak represents cells successfully transduced with the $1G4^{hi}$ TCR. Note that the upper peak shifts toward the lower peak with increasing time (see legend), indicating downregulation of surface TCR. (C) Surface TCR expression of T cells in (A) presented as expression versus time for select doses on the dose-response curve. Mean gMFI and SEM with n = 3.

3.2 Step Changes in Dose

Considering that T cells continuously contact antigen *in vivo*, fluctuations in local antigen concentrations can impact adaptation. To develop mathematical models and understand T cell adaptation, it is crucial to determine how cells respond to higher antigen doses once adapted at lower doses. Steps of escalating antigen dose reveal information on the cells' memory of prior responses. If cells adapt at an initial dose, a step increase in dose can induce either a new transient response or continued adaptation.

3.2.1 Experimental Setup

Cells were exposed to three escalating doses of antigen, adapting at each step (Figure 13). The 4A8K peptide, a ligand with lower affinity for the $1G4^{hi}$ TCR than 9V, was selected considering its physiological affinity and well-defined TCR downregulation and cytokine dose-response relationships.

The minimum and maximum doses were selected to span the range of TCR downregulation with two steps in dose: 150, 350, and 820 ng/well. The three selected doses are each 2.3-fold greater than the previous step. Fold changes in dose permit the study of fold change detection in T cell adaptation. Fold change detection describes a system in which output amplitude and response time are determined only by the relative change in signal—scaling the input by a multiplicative factor generates the same output[103]. Noting that adaptation of TNF-α occurs within four hours and to complete the experiment in a reasonable length of time, I incubated cells at each dose for four hours (4 hour incubations × 3 dose steps = 12 hours total) and collected samples every 30 minutes. As controls, three additional setups were generated, replacing all doses before each step with no pMHC (Table 2).

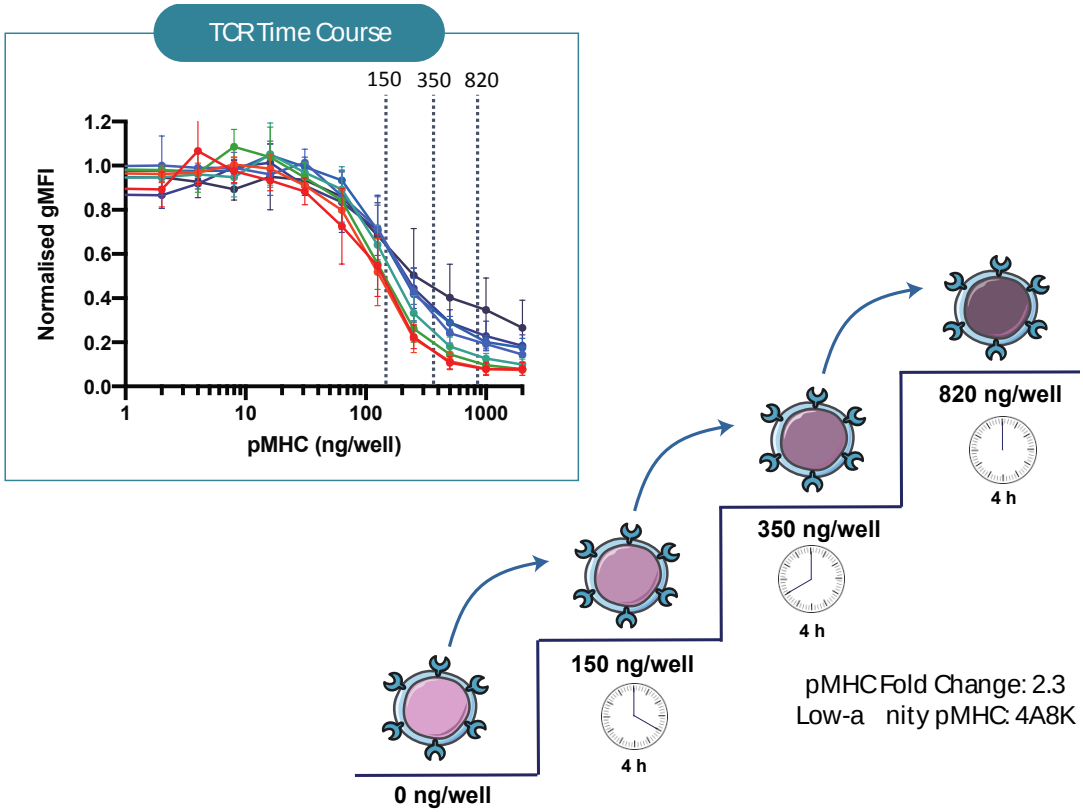


Figure 13. Experiment 2 – General Setup. Primary human CD8^{+} T cells expressing the 1G4^{hi} TCR were exposed to three sequential doses (150, 350, 820 ng/well) of 4A8K that induce partial downregulation and complete adaptation in cytokine production (upper panel displays TCR downregulation dose-response curves). Doses are 2.3-fold different from one another. Cells were incubated for 4 hours at each dose, sampled every half hour, and then transferred to a higher dose. Two transfers were completed for a total of 12 hours. Surface marker expression (CD69, TCR) and cytokine secretion (IFN-γ and TNF-α) were measured every half hour using flow cytometry and ELISAs.

3.2.2 Step Change in Dose Results

Figure 14 depicts the aggregate results of six experimental repeats. CD69 is rapidly-expressed on the surface during activation. For the first dose (150 ng/well), nearly all T cells were activated. Subsequent increases to 350 and 820 ng/well resulting in only a minor further increase. This highlights that all T cells have recognized the antigen and are uniformly activated.

TCR Downregulation

Supporting Experiment 1, TCR downregulation is biphasic. Figure 14 depicts a sharp initial decrease in surface TCR expression in the first half hour followed by a gradual, linear decline, primarily occurring in the first two hours of each step. This observation is supported by the literature[66,67]. Sequential antigen doses yield the same

absolute TCR level as an identical dose introduced without any prior exposure. Cells therefore exhibit no memory of prior pMHC stimuli, tuning their TCR levels to the current antigen concentration regardless of previous exposure. Further, TCR downregulation is biphasic regardless of prior antigen exposure.

Cytokine Production

TCR downregulation data is complemented with cumulative cytokine data. Despite limitations in collecting and interpreting data (see Discussion), overall trends in cumulative TNF-α production suggest that the change in cytokine is not proportional to fold changes in dose (Figure 14). The increase in cumulative TNF-α between 4 and 8 hours following prior antigen exposure is lower than the increase for unstimulated cells. Similarly, the change between 8 and 12 hours is far greater if cells are unstimulated than if cells have memory of antigen exposure. If T cells exhibit fold change detection, scaling the input by a multiplicative factor should generate the same output[103]. Although inconclusive, the variation in output amplitude suggests that T cells do not exhibit fold change detection.

IFN-γ production does not adapt within 4 hours. Thus, increased IFN-γ production in one step cannot be isolated from the effect of antigen in the previous step. Nonetheless, Figure 14 displays three notable results. IFN-γ production is delayed; production does not occur until cells have been exposed to pMHC for ~2 hours. However, if previously exposed to antigen, IFN-γ production increases without a delay, observed as an immediate increase within 30 minutes when cells are transferred (4 h and 8 h). Second, the absolute increase in IFN-γ production following pMHC exposure is higher in cells that have not previously seen antigen. Thus, the difference between the minimum and maximum for both blue curves, representing 0 ng/well → 350 or 820 ng/well, is greater than for cells that had previously seen antigen. Third, the red curve, depicting the step change condition,

suggests a large increase in IFN-γ production within the first two hours of incubation followed by adaptation for the second two hours; the misalignment with Experiment 1 warrants further investigation. The most plausible hypothesis is that the apparent adaptation is an artifact falling within the bounds of error for this assay, especially considering the relatively low quantity of IFN-γ secreted.

Comparison of Maximum Values for each Step

In an attempt to derive deeper insight despite data limitations and to depict the variability between repeats, I generated approximate maximum values for each step (Figure 15). This can be approximated as the average of the final 2 hours of each step (i.e. time points 2.5, 3, 3.5, 4 h). Although it would be preferable to determine maximum values by fitting a sigmoidal, bell-shaped, or spline curve to the data, the high degree of error limits the value of this approach. My approach prevents an analysis of variability in the final section of the red curve. However, it fixes the maximum and allows the relative variability in other curves to be studied. Two comparisons can be made:

(a) Cells exposed to previous antigen versus no pMHC at each step:

- The lack of significant difference between transferred and unstimulated cells for both CD69 and the TCR confirms that neither have a memory of prior antigen exposure (Figure 15(a))). In contrast, final TNF-α and IFN-γ levels differ for the highest dose depending on whether cells were previously stimulated (Figure 15(a))).

(b) The change between each step (i.e. each part of the red curve):

- Complementing earlier conclusions, step changes in dose result in no significant change in CD69 (Figure 15(b)). The significant change in maximum TNF-α and IFN-γ between each step is expected but reveals limited information (Figure 15(b)).

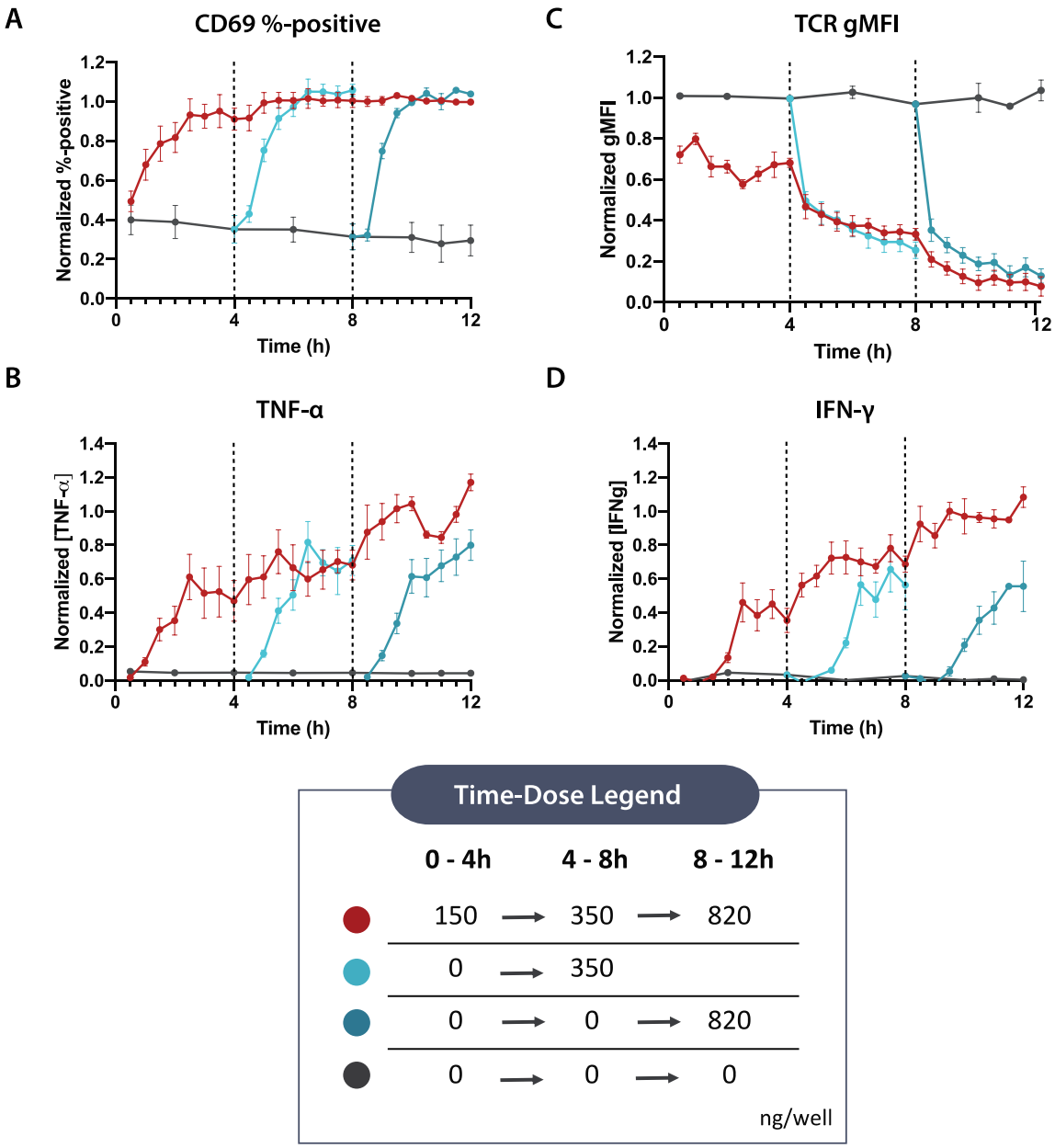


Figure 14. Step Change in Dose: TCR, Activation Markers, and Cytokine Output. Surface marker expression and cytokine production over time with two step changes in dose at 4 hours and 8 hours, indicated by two dotted lines. The time-dose legend indicates the 4A8K pMHC dose for each time range. (A) Surface expression of CD69 on T cells (percentage of CD69-positive cells) over time. Mean and SEM, n = 5, normalized to the final three data points of the red plot (i.e. fixing the maximum to 1.0). (B) Surface expression of the TCR on T cells (gMFI) over time. Mean and SEM, n = 5, normalized to the percentage of $1G4^{hi}$-positive cells and to the zero control (dark grey) as described in Section 2.6.3. (C) Cumulative TNF-α secreted over time. Mean and SEM, n = 6, normalized to the final three data points of the red plot. (D) Cumulative IFN-γ secreted over time. Mean and SEM, n = 3, normalized to the final three data points of the red plot.

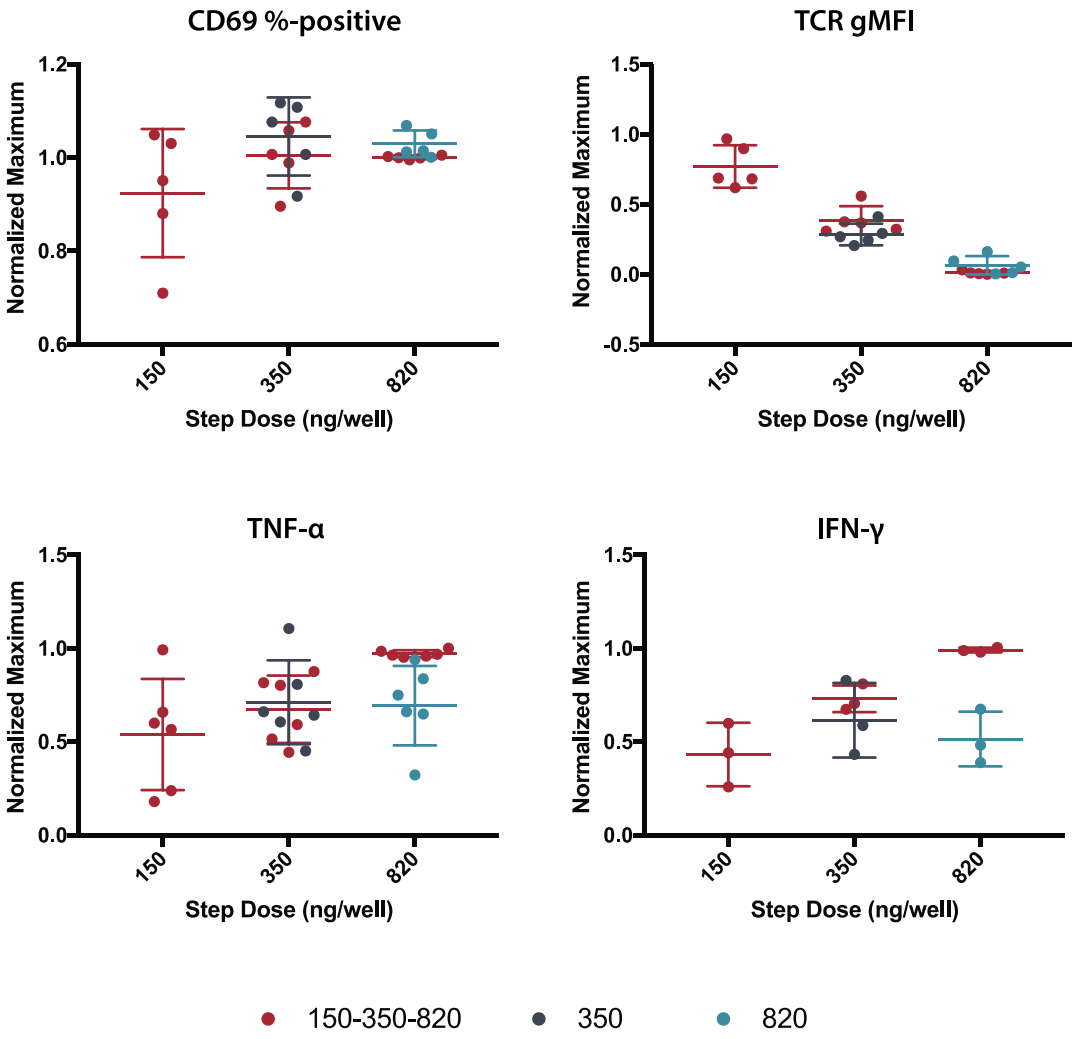


Figure 15. Maximum Values of Step Change in Dose Curves. Mean of the normalized values for the second half of each incubation (i.e. 2.5, 3, 3.5, and 4 hour time points) for each repeat and each step (*x*-axis). The bar represents mean with SD; number of repeats corresponds with the previous figure. The legend represents the condition (i.e. red represents cells transferred from 150 → 350 → 820 ng/well, grey represents cells transferred from 0 → 350 ng/well, and blue represents cells transferred from 0 → 820 ng/well). The *x* axis represents the step (150 = first four hour step, 350 = second four hour step, 820 = third four hour step). The statistical significance of differences between conditions was assessed with a two-way ANOVA: *p* values are listed in tables below.

(a) A comparison of cells in the 150 → 350 → 820 ng/well condition with unstimulated cells transferred to the same dose. Values in brackets represent *p* values;

Comparison	CD69	TCR	TNF-α	IFN-γ
350 ng/well (red vs. light blue)	N (0.7505)	N (0.1300)	N (0.9570)	N (0.4340)
820 ng/well (red vs. dark blue)	N (0.8862)	N (0.6430)	*Y (0.0031)	*Y (< 0.0001)

(b) For the 150 → 350 → 820 ng/well condition, each section can be compared to the other (i.e. comparing the maximums of each section). Values in brackets represent *p* values:

Comparison	CD69	TCR	TNF-α	IFN-γ
150 ng/well vs. 350 ng/well	N (0.2011)	*Y (< 0.0001)	N (0.1999)	*Y (0.0012)
350 ng/well vs. 820 ng/well	N (0.2396)	*Y (< 0.0001)	*Y (< 0.0001)	*Y (< 0.0001)
150 ng/well vs. 820 ng/well	N (0.9944)	*Y (< 0.0001)	*Y (0.0009)	*Y (0.0041)

3.3 Incremental Step Change in Dose

Experiment 2 transferred cells between three doses with a fold-change difference and an incubation time that allowed cells to adapt at each step. If the incubation time is shorter than the time scale of adaptation and the doses increase step-wise gradually, the cumulative output can be compared with the output of cells exposed constantly to the maximum stimulus alone[69]. The total cytokine output can be greater than, equal to, or less than the output of cells exposed to a constant, high antigen dose[69]. Complementing Experiment 2, Experiment 3 addresses two key questions in two experimental phases:

(a) **Phase 1:** How does cumulative cytokine output differ between cells transitioned gradually to a high dose and cells exposed constantly to a high dose?

(b) **Phase 2:** Do gradually increasing doses produce a similar state of adaptation as a single persistent high dose?

3.3.1 Experimental Setup

Phase 1 involved transferring cells from a low dose to a high dose over small increments or exposing cells to one high dose. Phase 2 involved exposing both cells from Phase 1 to a range of pMHC doses and comparing their final adapted states (Figure 16).

Once again, 4A8K was selected over 9V due to its physiological affinity and to allow for easy removal of cells from the plate surface when transferring them to higher doses. TCR downregulation and cytokine data from Experiment 1 was examined to select an appropriate dose range. No cytokine production or TCR downregulation was observed at the lowest dose (20 ng/well) whereas the highest dose (900 ng/well) induces maximum cytokine production and TCR downregulation. This range (20 to 900 ng/well) was split into 12 steps of 80 ng each with a 1 hour incubation for each step (Table 3). Several optimization experiments were completed to address the significant loss of cells between transfers and to ensure a sufficient number of replicates.

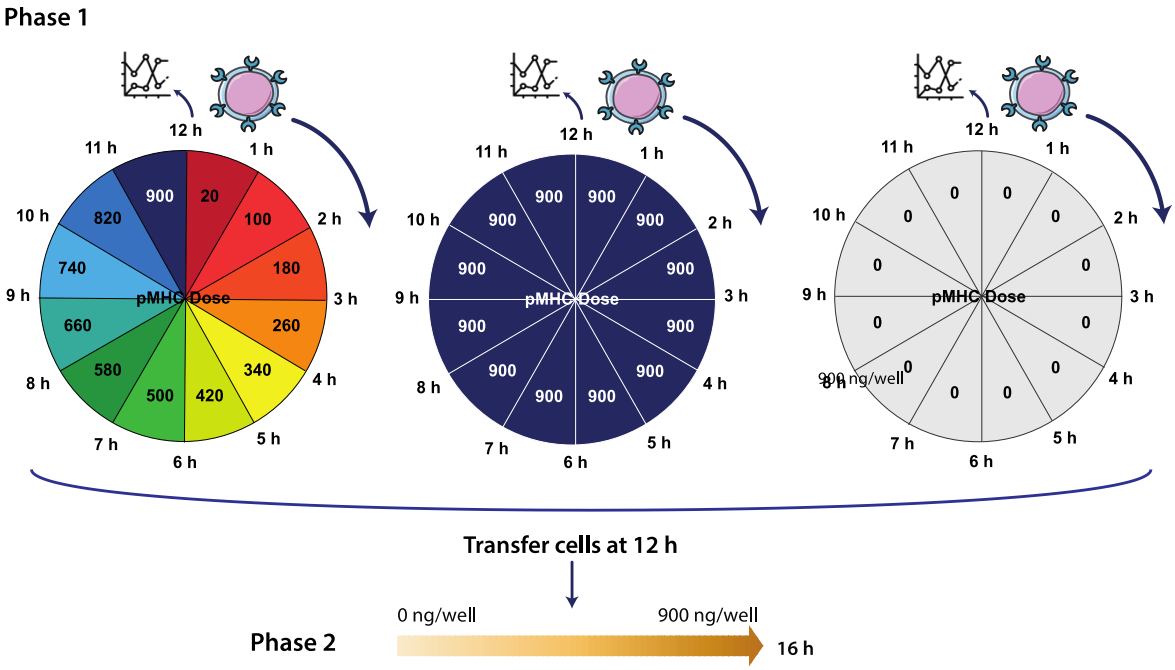


Figure 16. Experiment 3 – General Setup. *Phase 1*: Primary human $CD8^+$ T cells expressing the $1G4^{hi}$ TCR were exposed to three conditions: (1) increasing antigen – 20 ng/well for 1 hour, followed by an increase of 80 ng each hour for 12 hours until the dose is 900 ng/well, (2) constant antigen – 900 ng/well for 12 hours, transferred hourly, and (3) no antigen – 0 ng/well for 12 hours, transferred hourly. A second version of (3) did not transfer the cells hourly to assess whether the transfer process impacts the results. *Phase 2*: The cells from Phase 1 were transferred to a fresh plate with a range of antigen doses (0 to 900 ng/well) for 16 hours to assess whether the cells were identically adapted. Surface marker expression and cumulative cytokine production were measured at the end of both phases.

3.3.2 Phase 1 Results

Figure 17 depicts the aggregate Phase 1 results. Increasing antigen generates a similar CD69 phenotype as cells exposed to a constant high dose of antigen ($p = 0.2632$). Supplementary Figure 28 presents data confirming a similar 4-1BB phenotype ($p = 0.9559$) and PD-1 expression ($p = 0.8315$) as well. Considering data from Experiment 2, this result is expected. Once activated at a lower dose, the proportion of activated cells remains relatively unchanged. Similarly, final TCR levels are comparable between the constant and increasing antigen conditions. This conclusion is consistent with Experiment 2, indicating that TCR expression at a given dose is independent of previous antigen exposure. Cells exposed to gradually increasing doses secrete similar levels of TNF-α and IFN-γ compared with cells exposed to constant antigen ($p = 0.7557$ for TNF-α; $p = 0.4899$ for IFN-γ, two-way ANOVA with multiple comparisons corrected by Tukey's test).

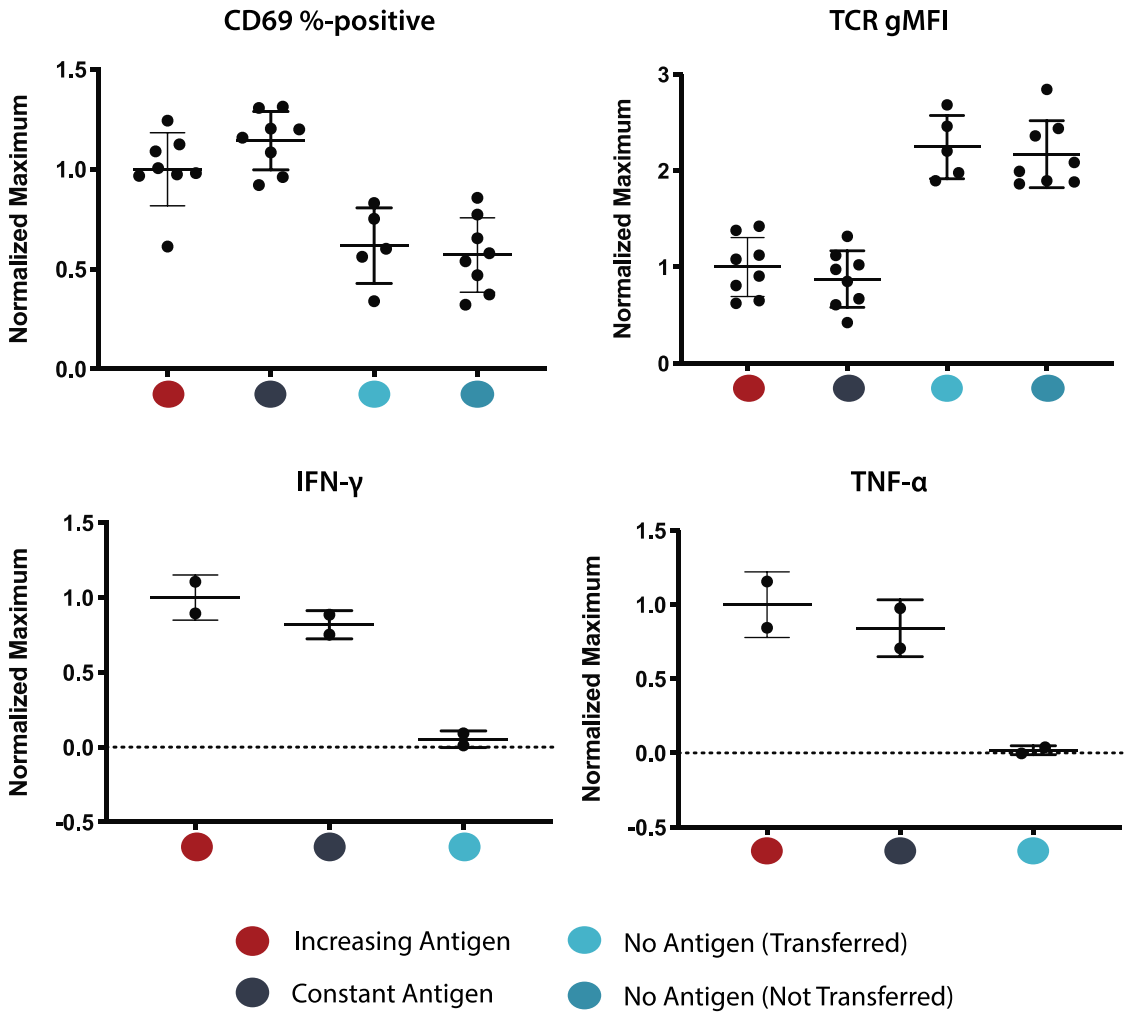


Figure 17. Phase 1 Results. Surface expression of CD69 (%-positive) and the TCR (gMFI), and cumulative TNF-α and IFN-γ secreted during Phase 1. Mean with SD, CD69: n = 8, TCR: n = 8, TNF-α: n = 2, IFN-γ: n = 2. Normalization: (a) The mean of all conditions (increasing antigen, constant antigen, and no antigen) was calculated for each experimental repeat. Each repeat was normalized to its mean value. (b) The mean of the increasing antigen condition across all experiments was calculated. All values from (a) were normalized to this value. Each experiment was therefore normalized to 1 in itself before normalization to the increasing antigen condition. Statistical analysis was completed using two-way ANOVAs with multiple comparisons tests.

For the above figure, values in brackets represent *p* values:

	CD69	TCR	TNF-α	IFN-γ
Increasing Antigen vs. Constant Antigen	N	N	N	N
Increasing Antigen vs. No Antigen*	Y (0.0006)	Y (< 0.0001)	N	Y (0.0341)
Constant Antigen vs. No Antigen*	Y (< 0.0001)	Y (< 0.0001)	N	N

*transferred condition only

3.3.3 Phase 2 Results

Phase 2 examined whether cells exposed gradually or suddenly to antigen are identically adapted by transferring the cells from Phase 1 to a fresh plate with a range of pMHC doses. Figure 18A and Supplementary Figure 29 present the normalized surface marker expression and cytokine secretion of six experimental repeats. Unstimulated cells responded as in Experiment 1, downregulating their TCRs, upregulating CD69 and 4-1BB, and producing both TNF-α and IFN-γ in a dose-dependent manner (both blue curves). The identical response of the unstimulated controls confirms that the transfer process did not impact adaptation. As anticipated, cells exposed to a high, constant dose of antigen over 12 hours were fully adapted. I observed no further TCR downregulation, significant CD69 or 4-1BB expression, or cytokine production. The increased cytokine produced for the 900 ng/well dose is unexpected, likely resulting from the transfer of pMHC with cells from Phase 1, yielding a dose higher than 900 ng/well.

Contrasted against these controls, cells exposed to gradually increasing antigen are indeed fully adapted. Cytokine secretion does not change appreciably over the full dose range. Surface levels of CD69, 4-1BB, and PD-1 remain unchanged from their post-Phase 1 state. The phenotypes of cells exposed to increasing and constant antigen were indistinguishable. Taken together with the Phase 1 results, both populations of cells release cytokine over the duration of exposure before adapting and displaying unresponsiveness to further stimulation. To refine this conclusion, information on the kinetics of cytokine production, TCR downregulation, and activation over Phase 1 would be beneficial.

Adapted T cells can be rescued from unresponsiveness with co-stimulation via the CD28-CD86 axis[94,104]. To confirm that cells exposed to increasing or constant antigen are similarly adapted, I assessed whether exposure to the maximum dose supplemented with

CD86 could re-induce a response in Phase 2 (Figure 18B). Compared with the maximum dose alone, the addition of CD86 generated 20+ fold greater TNF-α and IFN-γ production by all cells, particularly by the two adapted cell populations. Alternatively, a response could be re-induced with exposed to the higher-affinity 9V peptide[94].

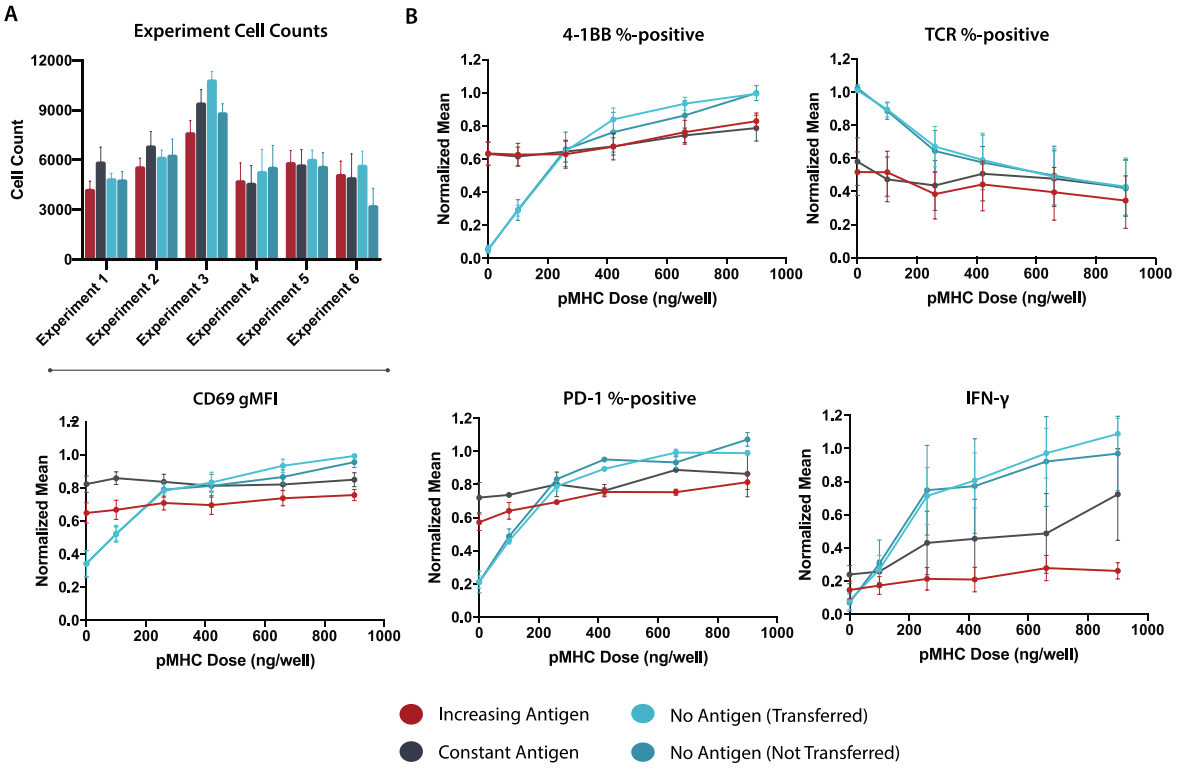


Figure 18. Phase 2 Results and Rescue from Adaptation by CD86. (A) Surface marker expression (CD69 %-positive and TCR gMFI) and TNF-α dose response curves for cells exposed to increasing, constant, or no antigen in Phase 1. Mean with SEM, CD69: n = 6, TCR: n = 6, TNF-α: n = 5, IFN-γ: n = 5. Normalization: All experiments normalized to the E_{max} of the control/no antigen condition. (B) Cumulative TNF-α and IFN-γ cytokine secretion for cells from Phase 1 exposed to either 900 ng/well 4A8K pMHC or 900 ng/well 4A8K pMHC + CD86 as a co-stimulus. Values normalized to the increasing antigen condition. Mean with SD, n = 3. Applying a two-way ANOVA corrected for multiple comparisons by Sidak test: $p < 0.0001$ for pMHC vs. pMHC + CD86 for all conditions.

3.4 NFL and IFFL Models of Adaptation

Experiments 1 to 3 reveal general signatures of T cell adaptation following persistent antigen exposure. Five phenotypes of T cell adaptation can be derived from the above data:

- **Phenotype 1:** T cell cytokine production displays perfect adaptation (Experiment 1);
- **Phenotype 2:** Partial TCR downregulation tunes to antigen strength and perfect adaptation is observed even with partial downregulation (Experiment 1);
- **Phenotype 3:** Increasing antigen dose leads to further tuning of the TCR level, independent of previous exposure, with limited further cytokine production; therefore, cells display memory in cytokine production but not TCR levels (Experiment 2);
- **Phenotype 4:** The dose-response curve of cytokine production following persistent pMHC exposure is bell-shaped (Experiment 1);
- **Phenotype 5:** Gradual exposure to incremental antigen doses yields the same cumulative cytokine secretion, TCR and CD69 expression, and unresponsiveness to further stimulation as a constant high dose of antigen (Experiment 3);

Linking these phenotypes to mathematical models, I can explore the role of TCR downregulation in adaptation and derive potential NFL- and IFFL-based mechanisms using a model invalidation approach. Phenotypes 1 to 4 are useful for this aim. The next section introduces an array of the simplest NFL- and IFFL-based models that theoretically generate adaptation. These models involve the TCR or downstream signaling as the regulatory mechanism.

3.4.1 Comparison of NFL and IFFL Models

As described in the Introduction, the seven basic networks include two NFL- and IFFL-based signaling-mediated models, three NFL- and IFFL-based models with complete TCR downregulation, and two NFL- and IFFL-based models with partial TCR downregulation and an additional downstream mechanism. The project aim was to resolve a hypothetical mechanism explaining adaptation in T cells by ruling out the above mechanisms with a model invalidation approach.

Interpreting the above phenotypes of T cell adaptation does not require each data set to be fit with a model. In fact, comparing models by fitting the experimental data is difficult—several mathematical models often fit data equally well. To assess the potential of NFL- and IFFL-based models, toy models allow for a broader study of adaptation signatures. Prior to assessing the alignment of the seven models with phenotypes, it is worth noting a key limitation. Depending on the parameter regime, several phases are possible for NFL- and IFFL-based networks[69,105]. As an example, NFL-based systems can generate oscillatory or non-oscillatory responses depending on the parameter set. Thus, the parameters selected to model adaptation carry an inherent risk of reflecting only one phase. The trends derived from studying toy models must be supplemented with literature and rigorous future study. The ODEs and parameters for each of the seven models can be found in Supplementary Figure 23.

Two experiments were simulated for each model: step changes in dose (i.e. Experiment 2) and a dose- and time-course experiment (i.e. Experiment 1).

Step Changes in Dose – Experiment 2

Figure 19 compares the kinetics of a dose step change simulation for all models. Both non-receptor mediated NFL and IFFL models (A and B) display perfect or near perfect adaptation, returning to a parameter-defined steady-state with no downregulation and an accumulating regulatory species. With similar parameter values, the output curves of both signaling-mediated models are similar—the first dose yields a large peak and each subsequent dose generates smaller peaks due to the accumulating regulatory species. Likewise, receptor-mediated NFL and IFFL models (C, D, E) generate adaptation when the TCR is completely downregulated.

In contrast with the two signaling-mediated models, once either receptor-based system (D and E) is exposed to antigen and adapts completely, it becomes unresponsive until the TCR is replenished on the surface. If the ligand is consumed with the TCR (C), perfect adaptation is possible without complete TCR downregulation. Rather, TCR is downregulated proportionally with the ligand until the ligand is completely consumed. Cells adapt perfectly at each step until the TCR is completely downregulated, at which point the ligand is no longer consumed and the system becomes unresponsive until the TCR is replenished.

NFL- and IFFL-based models of partial receptor downregulation (F and G) are comparable. The initial peak has a relatively large amplitude and declines to a parameter-defined steady state value. Each sequential peak decreases as the TCR is downregulated and perfect adaptation is not achieved. A downstream mechanism (i.e. switch, hill function, further NFL/IFFL) is required to convert imperfect to perfect adaptation.

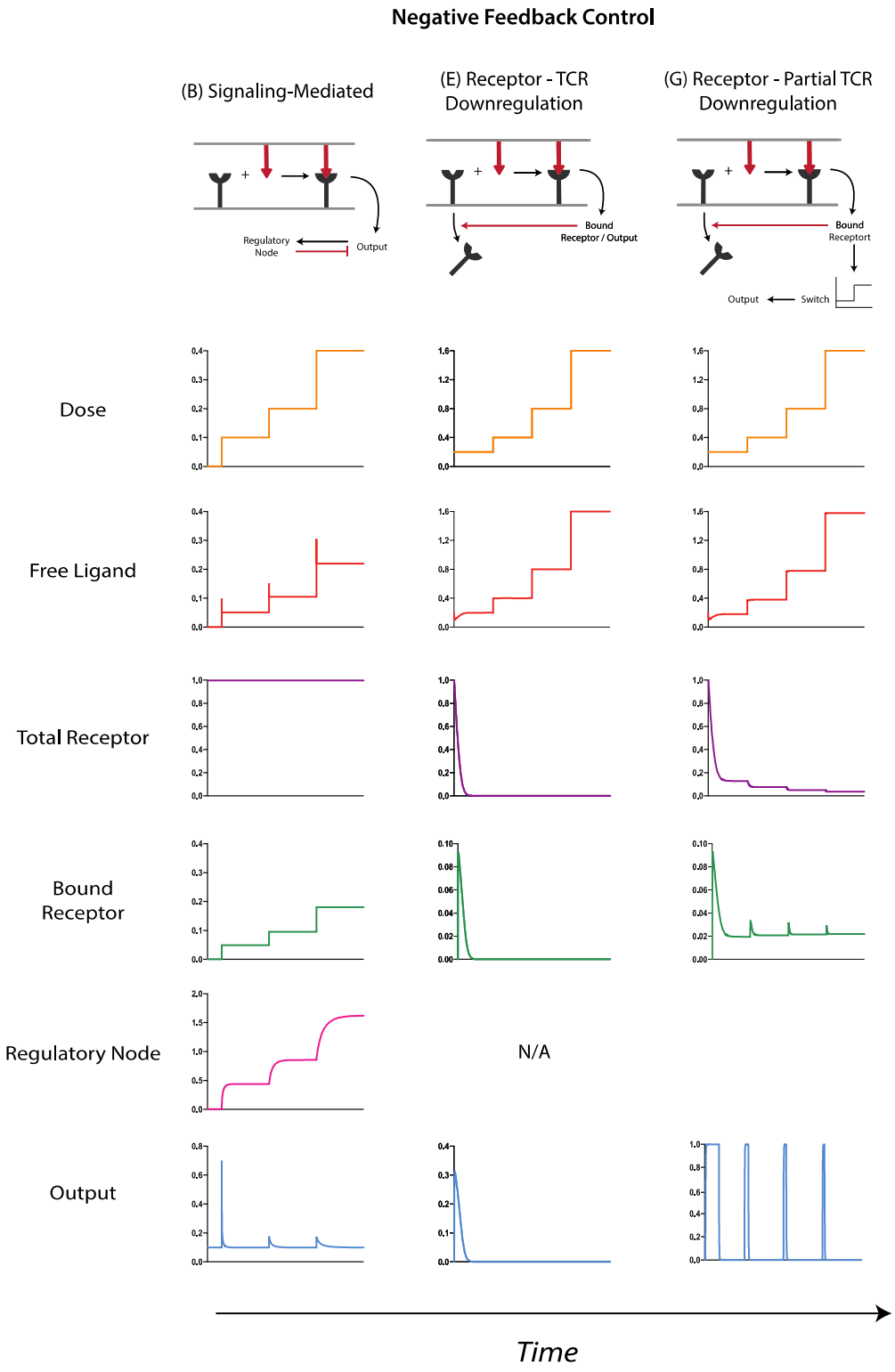


Figure 19. Model Simulations – Step Changes in Dose for NFL Networks. Model simulations for three negative feedback models with the receptor or downstream signaling as the control mechanism for adaptation. Dose represents the input ligand and is increased fold-wise. Parameters and ODEs can be found in Supplementary Figure 23.

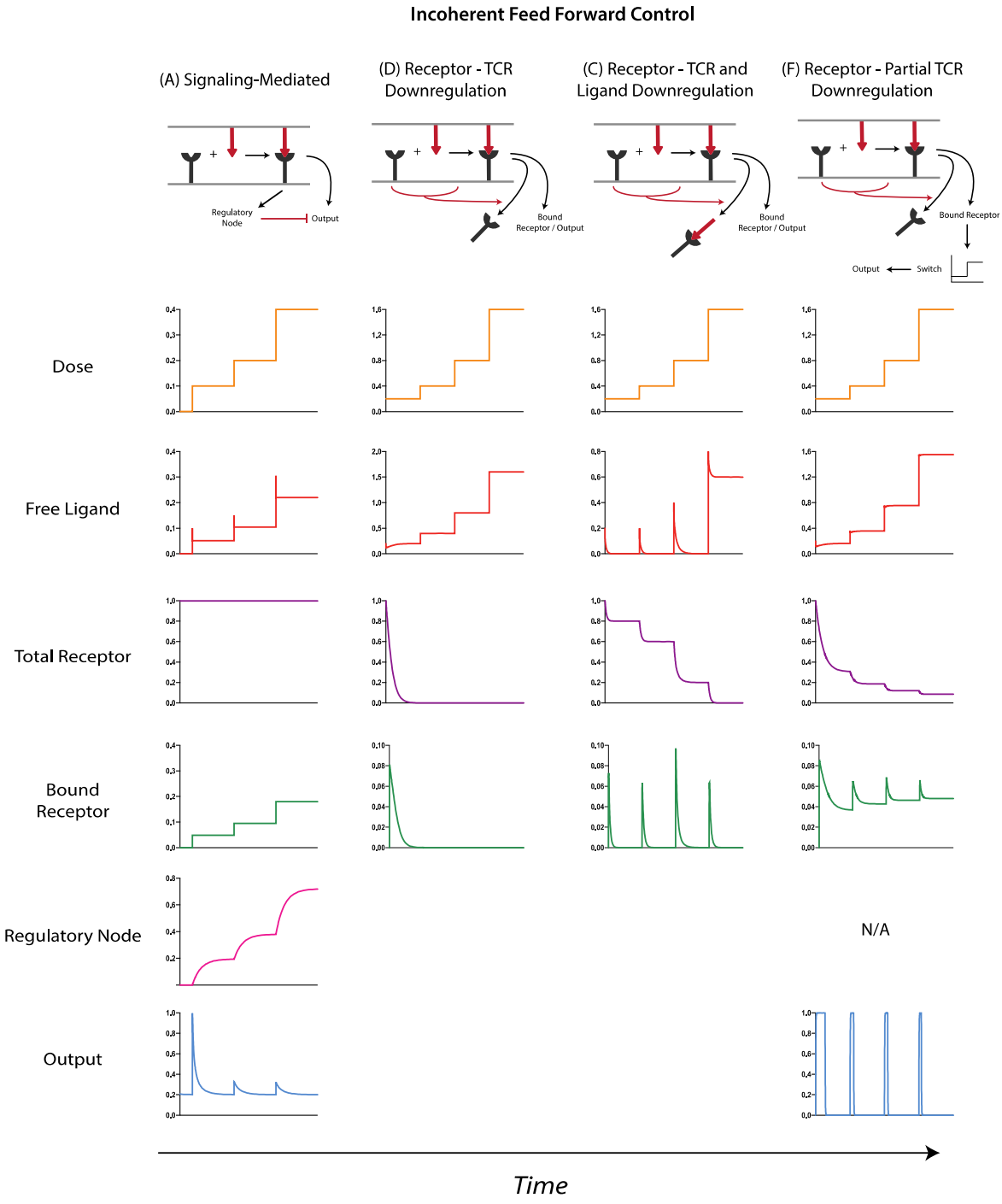


Figure 20. Model Simulations – Step Changes in Dose for IFFL Networks. Model simulations for four incoherent feed forward models with the receptor or downstream signaling as the control mechanism for adaptation. Dose represents the input ligand and is increased fold-wise. Parameters and ODEs can be found in Supplementary Figure 23.

Time- and Dose-Course Experiment – Experiment 1

Time- and dose-course simulations supplement this initial experiment to study the kinetics of each model. The 'output' of the model systems (*O*) in Figure 21 represents the *production rate* of cytokine. Thus, the production rate must return to zero in order for *cumulative* cytokine production to halt. For both the NFL- and IFFL-based signaling-mediated systems (Figure 21A and B), the production rate adapts but the rate is a non-zero value (*O*). Thus, the cumulative cytokine does not adapt, instead increasing at a constant, steady-state rate determined by the parameters. For an IFFL system, the production rate steady state (*O*) can only be zero if k_1 is zero (Supplementary Figure 23). The NFL system steady-state can approach but never equal zero. Unless the cytokine is consumed or degraded at an equivalent rate to the steady-state production rate, these models suggest infinite cytokine secretion.

In contrast, both NFL- and IFFL-based receptor-mediated systems with complete TCR downregulation (Figure 21D and E) involve perfect adaptation in cytokine production. The dose positively correlates with the rate of initial cytokine production and converges to a maximum cumulative level more quickly at higher than lower doses. Adaptation occurs when the TCR is completely downregulated, consistent with Figure 21. At high doses, the cumulative cytokine output is independent of dose. This relationship is similarly true for IFFL-based systems with complete receptor and ligand downregulation (Figure 21C). In this model, complete downregulation is not required for perfect adaptation. The receptor level *R* converges to a steady-state value for each dose. Above a threshold dose, the TCR is completely downregulated and cumulative output becomes independent of antigen dose, as described above.

The two models of partial TCR downregulation with a downstream switch, Figure 21F and G, generate a response with several notable features: the final receptor level *R*

correlates with dose, even at high doses and the cumulative output curve displays a bell-shape due to the more rapid deterioration of signal at high doses. With similar parameters, the NFL-based curve is a more pronounced bell shape. Supplementary Figure 30 displays plots for all intermediate species for each model (i.e. R, L, total R, A, etc.).

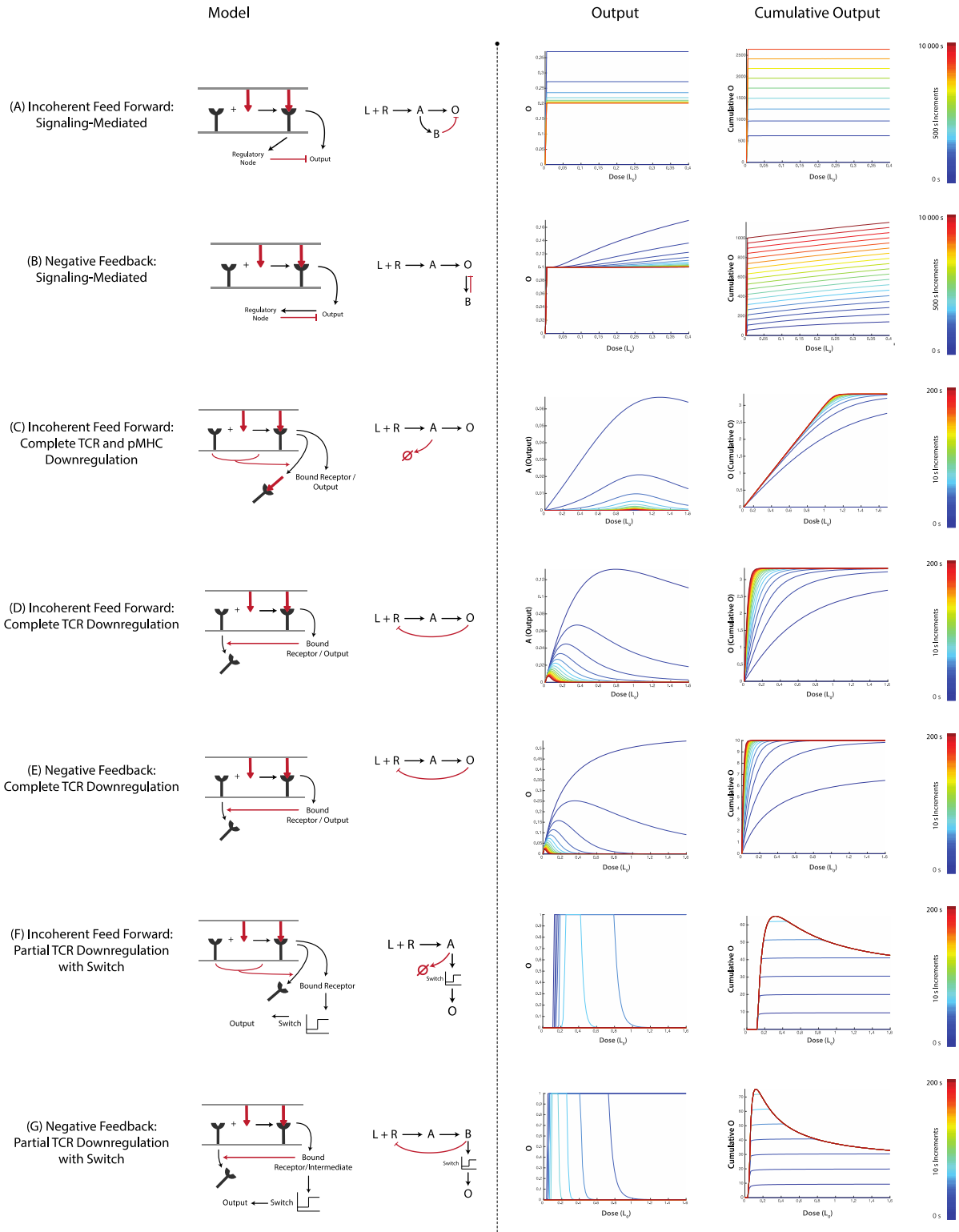


Figure 21. Model Simulations – Time- and Dose-Course Experiment. Model simulations for the seven NFL- and IFFL-based models with the receptor or downstream signaling as the control mechanism for adaptation. Parameters and ODEs can be found in Supplementary Figure 23.

3.4.2 Alignment of NFL and IFFL Signatures

Aligning the above models with the experimental phenotypes at the start of section 3.4, I can apply a model invalidation approach. Phenotypes 1 to 4 are useful for this purpose. Table 4 summarizes whether each model produces the experimental phenotypes. The sections below discuss the alignment of the models in greater detail according to their regulatory mechanism: downstream signaling (A and B), complete TCR downregulation (C, D, and E), and partial TCR downregulation (F and G).

Table 4. Model Alignment with Experimental Phenotypes

Model	A	B	C	D	E	F	G
Phenotype 1	✓	✓	✓	✓	✓	✓	✓
Phenotype 2	–	–	✓	–	–	✓	✓
Phenotype 3	✓*	✓*	–	–	–	✓	✓
Phenotype 4	–	–	–	–	–	✓	✓

*Cytokine data only

Signaling-Mediated Models (A and B)

Both signaling-based NFL and IFFL models generate perfect adaptation in cytokine production given a constant dose, aligning with *Phenotype 1*. Examining *Phenotype 3*, both models generate a large cytokine output with the first dose, followed by smaller peaks if the dose is increased step-wise. As constructed, however, both models have significant, disqualifying limitations. Both imply that the *production rate* of cytokine returns to a steady-state, non-zero value. Cytokine must be degraded or consumed at a corresponding rate in order for cumulative cytokine to adapt. This is observed in both Figure 19A/B and Figure 21A/B.

In isolation, a downstream signaling-mediated model alone is unlikely due to the lack of involvement of TCR downregulation. It is possible that TCR downregulation is a by-product or consequence of the activation process rather than an integral part of

controlling the response. In this case, the second part of *Phenotype 3*, tuning of the TCR to step changes in dose, and *Phenotype 2*, perfect adaptation with partial downregulation, may not be relevant to the adaptation process. As outlined in the Introduction, however, the critical role of the TCR in initiating signaling renders this an unlikely hypothesis.

Further, models A and B cannot reproduce *Phenotype 4*, the bell-shaped dose response curve. Research literature suggests a potential reason for the lack of bell shape in these models. Exploring the dynamics of the IFFL motif, two types of responses are possible—a time-dependent biphasic response and dose-dependent biphasic response[105]. The time-dependent biphasic response is essentially adaptation over time (i.e. *Phenotype 1*). The dose-dependent biphasic response is the bell shape of *Phenotype 4*. In other words, a dose-dependent biphasic response involves output increasing over a specific input range and decreasing if the input increases further. However, these two responses occur in different parameter spaces and seem to be mutually exclusive[105]. Applying this conclusion to the thesis, perfect adaptation over time (*Phenotype 1*) and a bell-shaped dose-response curve (*Phenotype 4*) are unlikely to co-exist based on one mechanism alone. The combined effect of these limitations rule out signaling-mediated NFLs and IFFLs, implying that an additional control mechanism is necessary.

Complete TCR Downregulation (C, D, and E)

Models based on complete NFL- and IFFL-mediated TCR downregulation successfully reproduce *Phenotype 1*, generating perfect adaptation in cytokine production. However, in models D and E, the TCR must be completely downregulated to do so. This caveat contradicts *Phenotype 2*: perfect adaptation is possible even with partial TCR downregulation. Model C, based on complete downregulation of both the TCR and ligand, can produce complete adaptation with partial TCR downregulation. However, the partial downregulation is directly linked to ligand availability. Complete adaptation therefore

depends on the ligand being completely consumed. Experiment 3 definitively rules out this possibility. Transferring adapted cells to plates with fresh ligand does not induce cytokine production, disqualifying Model C.

Examining *Phenotype 3*, models D and E cannot produce adaptation to multiple dose steps and tune the TCR level to each antigen dose. In order to adapt to the first dose, the TCR must be completely downregulated, preventing future responses. Model C can produce pulsatile responses to step changes in dose and tune the TCR level to each antigen dose. However, the TCR level and adaptation are directly determined by the removal of ligand. As discussed above, this does not align with experimental data. Similar to the signaling-mediated models (A and B), the models based on complete downregulation (C, D, and E) cannot produce a bell-shaped dose-response curve, *Phenotype 4*. TCR downregulation alone is therefore unlikely to account for adaptation but seems to contribute to adaptation on some level.

Partial TCR Downregulation (F and G)

A more complex, higher-dimensional model, either NFL- or IFFL-based, is therefore required to generate all phenotypes. In this case, two models (F and G) were constructed with an IFFL or NFL receptor-based control mechanism and a downstream switch. Based on the experimental data, neither model can be invalidated. Both produce perfect adaptation with partial TCR downregulation (*Phenotypes 1 and 2*), decreasing pulses of output with step changes in input (*Phenotype 3*), and a bell-shaped dose response curve *(Phenotype 4*). It can be broadly concluded that the TCR cannot be eliminated as a potential mechanism of cell control and that both NFLs and IFFLs can produce the experimental phenotypes observed in this project. A hybrid model successfully predicts complete adaptation in cytokine production while allowing for residual TCR signaling.

These remaining receptors are crucial in allowing co-stimulation or a higher-affinity ligand to rescue cells, as demonstrated in Experiment 2[42,106].

Both hybrid NFL and IFFL systems can reproduce the effect observed in the gradual dose change experiment (*Phenotype 5*). However, resolution of the cytokine amount produced at each step is necessary for this data to be useful in a model invalidation approach. Thus, although the experimental data generated contributes to the body of literature on T cell adaptation, improved data quality and further experimentation are required to distinguish between NFL- and IFFL-based models.

3.6 Pilot Tests of Anti-CD3 Therapeutic Antibodies

As discussed in the Introduction, a range of immune cell-mediating therapeutics, specifically otelixizumab and alemtuzumab, aim to induce unresponsiveness in aberrant T cells[45,52]. Models explaining and predicting adaptation in primary effector T cells are thus invaluable to the design and implementation of clinical interventions. Inducing adaptation in T cells without transient cytokine production is the ultimate goal. Clinically, this translates to silencing T cells without the side effect of cytokine release syndrome.

As a proof of concept, I modified our reductionist assay by replacing the pMHC stimulus with otelixizumab and alemtuzumab and piloted two forms of mAb presentation. Pre-clinical safety testing of new therapeutic antibodies involves cytokine release assays (CRAs) to assess the risk of cytokine release syndrome[107]. Although incubation of therapeutic mAbs in whole blood is the most common CRA, its ability to stimulate cytokine release depends on the therapeutic mAb tested. Alternative CRA methods offer improved predictivity including: PBMCs incubated with mAbs coated on tissue culture plates, whole blood incubated with mAbs coated on protein A capture beads, PBMCs incubated with soluble mAb, whole blood or diluted whole blood incubated with soluble mAb, and co-culture of PBMCs with soluble mAb on human umbilical vein endothelial

cells[107]. To investigate the potential of manipulating adaptation induced by therapeutic mAbs, I assessed two forms of CRA, plate-bound and aqueous formats, for otelixizumab and alemtuzumab (Section 2.11). Otelixizumab exhibited adaptation in cytokine production in dose- and time-course experiments.

Otelixizumab

Figure 22 shows surface marker expression and cytokine secretion by primary $CD8^+$ T cells exposed to plate-bound otelixizumab. Adaptation occurs on a time scale of ~15 hours for both activation and cytokine secretion. The soluble form of otelixizumab did not elicit cytokine production or surface marker expression (Supplementary Figure 31). This data is representative of one experiment; Supplementary Figure 32 and Figure 33 display the results of two additional repeats with a maximum time point of 8 hours. Noting that adaptation is observed post-8 hours, additional repeats of longer time-course assays are required to confirm this conclusion. Further, otelixizumab is an aglycosylated anti-CD3 mAb. It is therefore unsurprising that the antibody binds the TCR receptor and interferes with binding by an anti-TCR α/β flow cytometry antibody. The apparent TCR downregulation depicted by the figure may simply indicate competitive binding of otelixizumab. An alternative method is required to resolve the role of downregulation in otelixizumab-induced adaptation.

Alemtuzumab

Alemtuzumab did not stimulate cytokine production or TCR downregulation in either the plate-bound or soluble form (Supplementary Figure 34). Vessillier et al. reported similar results for alemtuzumab in several CRAs, the most comparable of which is PBMC incubation in plate form[107]. However, Vessillier reported significant cytokine release in whole blood form, indicating that the form of mAb presentation or cell type may be limiting the detection of adaptation (i.e. NK cells may produce cytokines in

alemtuzumab-induced CRS rather than T cells). In a whole blood CRA, isolating T cells as the source of cytokine production would be challenging. Further study of adaptation in cytokine production by T cells in whole blood is required.

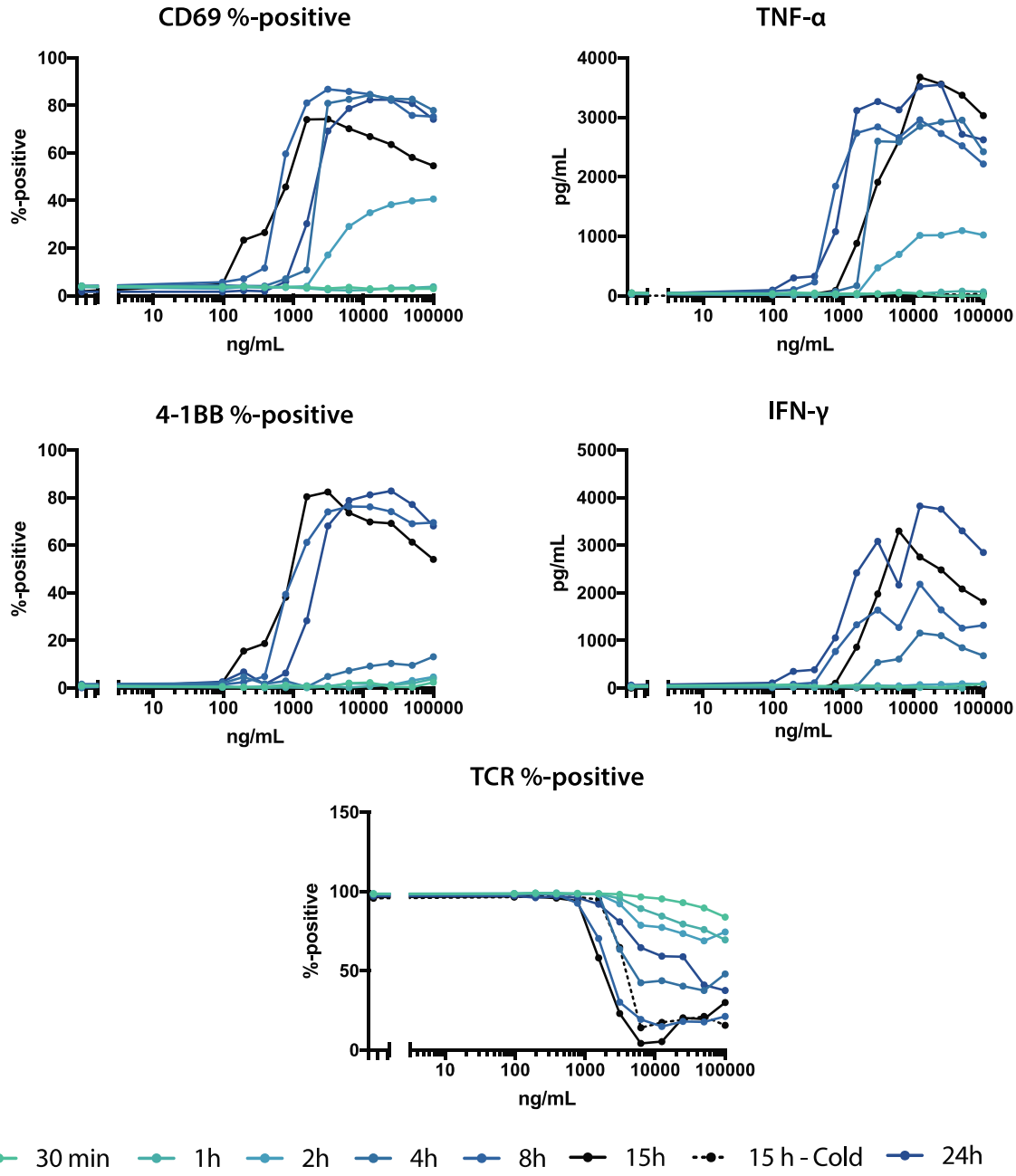


Figure 22. Adaptation in T Cells exposed to Plate-bound Otelixizumab. Cumulative cytokine secretion (TNF-α, IFN-γ) and surface marker expression (CD69, 4-1BB, TCR %-positive) by T cells exposed to a range of otelixizumab doses immobilized to a plate over time. 'Cold' indicates incubation at 4°C. n = 1.

4 Discussion and Conclusion

T cells receive continuous pMHC ligand stimulation in self-tolerance, chronic viral infections, and cancer. This persistent antigen exposure generates an initial transient response that leads to unresponsiveness known as adaptation. A variety of experiments were designed based on step changes in dose with the aim of linking experimental data to mathematical models of adaptation. Three experiments were conducted: dose- and time-course, step changes in dose, and incremental step changes in dose. Five phenotypes were observed:

- **Phenotype 1:** T cell cytokine production displays perfect adaptation (Experiment 1);
- **Phenotype 2:** Partial TCR downregulation tunes to antigen strength and perfect adaptation is observed even with partial downregulation (Experiment 1);
- **Phenotype 3:** Increasing antigen dose leads to further tuning of the TCR level, independent of previous exposure, with limited further cytokine production; therefore, cells display memory in cytokine production but not TCR levels (Experiment 2);
- **Phenotype 4:** The dose-response curve of cytokine production following persistent pMHC exposure is bell-shaped (Experiment 1);
- **Phenotype 5:** Gradual exposure to incremental antigen doses yields the same cumulative cytokine secretion, TCR and CD69 expression, and unresponsiveness to further stimulation as a constant high dose of antigen (Experiment 3);

Two fundamental network mechanisms generate adaptation: incoherent feed forward and negative feedback control. Although these mechanisms are well-studied at both the receptor level and in downstream signaling in other biological systems, their potential role in T cell biology remains to be critically examined. Seven models based on IFFLs and NFLs downstream or at the receptor level were constructed. A model invalidation

approach was applied, excluding models based on the above phenotypes. As an example, this approach has been successfully applied to identify incoherent feed forward control as a dominant network motif in eukaryotic chemotaxis[77].

A model based on partial TCR downregulation with a second downstream mechanism, either NFL- or IFFL-based, best reproduces the above phenotypes. This section explores the implications of the relevance of TCR downregulation to adaptation, limitations of experiments in this thesis, suggestions for future experiments, and the clinical relevance of mathematical models explaining T cell adaptation.

4.1 The Role of TCR Downregulation

Understanding TCR downregulation as a mechanism of imperfect adaptation has several important implications. Imperfect adaptation allows for extrinsic regulation in a pMHC-dependent manner. Remaining receptors can respond to higher affinity pMHCs or co-stimuli (ex. CD28 – B7-1 and B7-2)[42]. For example, naïve T cells require two signals for activation, both pMHC-TCR signaling and co-stimulatory signaling, primarily mediated by CD28[2,42]. In the absence of co-stimulation, the TCR can be downregulated following pMHC engagement but naïve T cell priming and activation cannot occur. Viewing TCR downregulation as a mechanism of imperfect adaptation therefore allows for co-stimulation to activate naïve T cells or sustain effector T cell activation.

The surface TCR level is often regarded as a controversial marker. Noting that perfect adaptation can be produced with partial TCR downregulation, the absolute TCR level itself is not meaningful without considering the antigen strength that induced activation. pMHCs with different affinities induce different levels of TCR downregulation but similar adaptation[94]. Nonetheless, if the stimulus is sufficiently high, cells adapt perfectly regardless of pMHC affinity and dose. This implies that perfect adaptation becomes affinity- and dose-independent once complete downregulation occurs.

Physiologically, this phenomenon may be relevant for peripheral tolerance and chronic infections. Persistent antigen exposure involves a wide range of antigens with variable affinities and inconsistent concentrations. Regardless of this variation and the antigen source, constant ligand stimulation must induce an identical functional response. Complete downregulation corrects for chance differences in affinity and dose for self and pathogenic antigens. The exact functional significance of TCR downregulation remains to be fully elucidated. Further, mechanistic studies are required to rule out TCR downregulation being a consequence rather than cause of adaptation.

4.2 Additional Experiments and Limitations

4.2.1 Limitations in the Experimental Setup

Despite its limitations, the experimental setup used in the thesis offers the significant advantage of studying primary human effector $CD8^+$ T cells rather than Jurkat or murine T cells. Further, a reductionist 2D plate-based assay enables a quantitative, reproducible evaluation of cell signaling with precise control over dose. However, immobilization on a 2D surface differs significantly from presentation by APCs or a 3D setup. Both *in vivo* and *ex vivo*, pMHC turnover on the APC surface results in changing antigen density, a contrast to the static antigen density on a plate[108]. Immobilization of pMHC on a 2D surface facilitates significantly greater TCR clustering not possible on APCs[108]. Further, the 2D environment does not allow for TCR-pMHC catch bonds possible in a 3D environment with pervasive mechanical forces[109]. Although a 3D environment enables more predictive models, the increased complexity would require substantial optimization.

Despite the benefits of a 2D assay, my conclusions were severely limited by the poor sensitivity of output measurements for the experiment introducing step changes in dose (Experiment 2). The intended result of Experiment 2 was a TNF-α output curve with

consistent, well-defined time points, the derivative of which would represent the production rate of TNF-α. As step changes in dose stimulate further cytokine production, the production rate would increase; as cells adapt, the rate would decline to zero. The resulting peaks would therefore differ in amplitude and period. Experimentally, individual replicates demonstrated promise in tracking TNF-α output over time. However, two key issues emerged: (a) poor ELISA sensitivity in detecting cumulative cytokine production for each half-hour time point and (b) donor heterogeneity. To address the first issue, I introduced technical replicates for all wells (i.e. two separate plates) and sampled twice for each time point in the second half of the incubation for each step (i.e. 2 of the 4 hours) to reduce noise. A large number of repeats with 8+ donors aimed to mitigate the second. Nonetheless, the cumulative error introduced by distinct sample wells for each half-hour time point, cytokine degradation due to the supernatant freeze-thaw process, limited ELISA sensitivity, and donor heterogeneity preclude detailed quantitative conclusions on changes in cytokine output. My original aim of linking NFL- and IFFL-based models to experimental cytokine data with a parameter-fitting algorithm was inappropriate considering the quality of the quantitative TNF-α data. Nonetheless, the ELISA data exhibited useful general trends in cytokine production.

Considering the sensitivity and consistency of flow cytometry, intracellular staining is a viable alternative for Experiment 2. The secretion of cytokines can be blocked with brefeldin A, an inhibitor of intracellular protein transport to the Golgi complex[110]. Changes in cytokine production over time can be quantified by fixing the cells and intracellularly staining TNF-α and IFN-γ. A flow cytometry-based assay with improved sensitivity would complement ELISAs well in generating quantitative cytokine data.

4.2.2 Future Experiments

Single on-off stimulus pulses (i.e. Experiment 1) are insufficient to discriminate between adaptation motifs. Both NFLs and IFFLs fit the same time- and dose-course data equally well. Although step- and ramp-like dynamic inputs are traditionally applied to distinguish between NFL and IFFL mechanisms, Cross and Sontag propose two input formats that would allow for more effective model invalidation[72]:

(1) **Two or more pulses of stimulus**: In an IFFL, the regulatory node increases independently of the response. Removing the stimulus initiates a reset process for the regulatory node. In an NFL, the regulatory node is entrained to the output rather than the stimulus. Regardless of the stimulus length, the regulatory node begins to reset as the output adapts. Thus, the reset time or refractory period increases with stimulus duration for IFFLs but remains constant for NFLs. A second stimulus pulse after a long first pulse would result in a smaller output for an IFFL and an identical output to the first pulse for an NFL.

(2) **Multiple short pulses**: With the regulatory node linked to the output rather than input, NFL-based systems become insulated to stimuli once adapted. Until the regulatory node resets, the NFL 'skips' stimuli. In contrast, IFFLs cannot skip stimuli, discussed further in the Introduction.

Both experiments would complement step-based approaches and provide the additional information required to discriminate between NFLs and IFFLs in T cells. However, the ability to manipulate primary $CD8^+$ T cells using our reductionist 2D assay is limited. The significant cell loss introduced by the experimental design would confound analysis. Techniques in synthetic biology offer a potential robust solution. Optogenetics allow for light-gated inputs and facilitate precise, dynamic control of stimuli dose and duration[111,112]. Lim et al. have proposed optogenetic strategies for investigating

sophisticated signaling behaviour including adaptation by precisely controlling the input and mapping component nodes based on the output[111,112]. Optogenetic chimeric antigen T (CAR-T) cell receptors are a potential option for investigating T cell adaptation with improved quantitative resolution.

Beyond alterations to the experimental design and additional experiments, further analytical study of the basic 3-node networks and the design of higher-dimensional systems would be beneficial. In particular, an analysis of models with parameter combinations that yield bell-shaped dose response curves should be further studied. With improved data quality, fitting algorithms can be applied to align NFL- and IFFL-based models with experimental data.

4.3 Clinical Applications

Modelling T cell adaptation and understanding the mechanistic role of TCR downregulation are highly relevant to explaining T cell unresponsiveness in peripheral tolerance and chronic immune responses. Clinically, T cell adaptation is a desirable response induced in treating of autoimmune disease and preventing transplant rejection with otelixizumab and alemtuzumab. Discussed in the Introduction, otelixizumab and other anti-CD3 antibodies primarily modulate the CD3/TCR complex, inducing TCR downregulation and cellular hyporesponsiveness[45–49]. However, the transient release of cytokines before adaptation is a serious side effect. Cytokine release syndrome (CRS) frequently accompanies antibody-mediated T cell-targeting therapies and causes multi-organ failure[44]. The *in vitro* CRA assay developed for this project (Section 3.5) confirms both an initial cytokine release and subsequent T cell unresponsiveness for otelixizumab. Extending the core project aim, a predictive NFL- or IFFL-based model of T cell adaptation may be useful in designing antibodies and dosing regimens that minimize cytokine release during the adaptation process. Experiments in whole blood and

optimization of the dose range and increments in Experiment 4 would be useful toward this goal. CRS is not isolated to monoclonal antibody therapies. Severe cytokine responses frequently accompany the administration CAR-T cells and bi-specific T-cell engaging (BiTE) antibodies such as blinatumomab[44,113].

Beyond CRS, knowledge on the relevance of TCR downregulation in adaptation would be beneficial to re-activating exhausted effector T cells in cancer and designing new therapeutics[114]. Both BiTE antibodies and CAR-T cells would especially benefit. BiTE antibodies simultaneously bind CD3 on T cells and specific tumour cell antigens. The availability of TCRs on the cell surface is therefore critical to the therapeutic effectiveness of BiTEs[115]. The modular design of synthetic receptors, particularly CARs[116], could benefit from models that enable a custom-engineered downregulation response to improve efficacy or safety. Gradual adaptation may allow for partial desensitization of therapeutic T cells to preserve an appropriate amount of function while minimizing initial cytokine release. Cumulatively, models of adaptation incorporating T cell downregulation are invaluable both in understanding T cell signaling and disease pathology as well as the rational design of therapeutics to foster or avoid adaptation in T cells.

4.4 Conclusion

Conclusively, this thesis identifies general phenotypes of T cell adaptation in response to varied steps in antigen dose and suggests partial TCR downregulation, either NFL- or IFFL-mediated, with additional downstream control as a potential control mechanism. I anticipate that these results will serve as a promising foundation for understanding and modelling mechanisms of T cell adaptation and in resolving the precise role of TCR downregulation.

Statement of Authorship

This thesis is wholly my own work with the exception of the following:

- Figure 9, Supplementary Figure 26, and Supplementary Figure 27: TNF-α data and three repeats of IL-2 and IFN-γ data were collected by Nicola Trendel (Donors 1 to 3 in Figures 26 and 27), Johannes Pettmann and I jointly collected data for the time points of Donors 4 to 6.
- Figure 12: As above, Johannes Pettmann and I jointly collected time-course data.
- Figure 10, Figure 11B: Algorithms for sigmoidal and bell-shaped curve-fitting and E_{max} extraction are credited to Johannes Pettmann.

Statement of Previous Acceptance or Concurrent Submission of Thesis for Degree

- Experiment 3: I presented three repeats of raw unanalyzed data for Phase 1 (surface markers only) and Phase 2 in a thesis for the MSc in Integrated Immunology. Following the 3-month research project for this MSc, I joined the Omer Dushek group for the MSc(Res.) in Molecular Cell Biology in Health and Disease and included these repeats in my aggregate analysis as a part of this project.
- Supplementary Figures 24 and 25: I presented the purity and gating strategy in the MSc in Integrated Immunology thesis.

References

1. Waldmann, H. & Munro, A. B Cell Activation. *Immunol. Rev.* **23**, 213–222 (1975).
2. Smith-Garvin, J. E., Koretzky, G. A. & Jordan, M. S. T Cell Activation. *Annu. Rev. Immunol.* **27**, 591–619 (2009).
3. Griffin, G. K. *et al.* IL-17 and TNF- Sustain Neutrophil Recruitment during Inflammation through Synergistic Effects on Endothelial Activation. *J. Immunol.* **188**, 6287–6299 (2012).
4. Li, M. *et al.* An Essential Role of the NF- B/Toll-Like Receptor Pathway in Induction of Inflammatory and Tissue-Repair Gene Expression by Necrotic Cells. *J. Immunol.* **166**, 7128–7135 (2001).
5. Nathan, C. F. Identification of interferon-gamma as the lymphokine that activates human macrophage oxidative metabolism and antimicrobial activity. *J. Exp. Med.* **158**, 670–689 (1983).
6. Su, X. *et al.* Interferon-γ regulates cellular metabolism and mRNA translation to potentiate macrophage activation. *Nat. Immunol.* **16**, 838–849 (2015).
7. Karupiah, G. *et al.* Inhibition of viral replication by interferon-γ-induced nitric oxide synthase. *Science (80-.).* (1993). doi:10.1126/science.7690156
8. Alcover, A., Alarcón, B. & Di Bartolo, V. Cell Biology of T Cell Receptor Expression and Regulation. *Annu. Rev. Immunol.* **36**, 103–125 (2018).
9. San Jose, E., Borroto, A., Niedergang, F., Alcover, A. & Alarcón, B. Triggering the TCR complex causes the downregulation of nonengaged receptors by a signal transduction-dependent mechanism. *Immunity* **12**, 161–170 (2000).
10. Monjas, A., Alcover, A. & Alarcón, B. Engaged and bystander T cell receptors are down-modulated by different endocytotic pathways. *J. Biol. Chem.* **279**, 55376–55384 (2004).
11. Štefanová, I. *et al.* TCR ligand discrimination is enforced by competing ERK positive and SHP-I negative feedback pathways. *Nat. Immunol.* (2003). doi:10.1038/ni895
12. Crawford, A. *et al.* Molecular and Transcriptional Basis of CD4+ T Cell Dysfunction during Chronic Infection. *Immunity* **40**, 289–302 (2014).
13. Choi, S. & Schwartz, R. H. Molecular mechanisms for adaptive tolerance and other T cell anergy models. *Seminars in Immunology* **19**, 140–152 (2007).
14. Ma, W., Trusina, A., El-Samad, H., Lim, W. A. & Tang, C. Defining Network Topologies that Can Achieve Biochemical Adaptation. *Cell* **138**, 760–773 (2009).
15. Redmond, W. L. & Sherman, L. A. Peripheral tolerance of CD8 T lymphocytes. *Immunity* **22**, 275–284 (2005).
16. Mueller, D. L. Mechanisms maintaining peripheral tolerance. *Nature Immunology* (2010). doi:10.1038/ni.1817
17. Ferber, I. *et al.* Levels of peripheral T cell tolerance induced by different doses of tolerogen. *Science* **263**, 674–6 (1994).
18. Teague, R. M. *et al.* Peripheral CD8+T Cell Tolerance to Self-Proteins Is Regulated Proximally at the T Cell Receptor. *Immunity* **28**, 662–674 (2008).
19. Chiodetti, L., Choi, S., Barber, D. L. & Schwartz, R. H. Adaptive Tolerance and Clonal Anergy Are Distinct Biochemical States. *J. Immunol.* **176**, 2279–2291 (2006).
20. Tanchot, C., Barber, D. L., Chiodetti, L. & Schwartz, R. H. Adaptive tolerance of CD4+ T cells in vivo: multiple thresholds in response to a constant level of antigen presentation. *J Immunol* **167**, 2030–2039 (2001).

21. Chuang, E., Augustine, M., Jung, M., Schwartz, R. H. & Singh, N. J. Density dependent re-tuning of autoreactive T cells alleviates their pathogenicity in a lymphopenic environment. *Immunol. Lett.* **192**, 61–71 (2017).
22. Grossman, Z. & Paul, W. E. Dynamic Tuning of Lymphocytes: Physiological Basis, Mechanisms, and Function. *Annu. Rev. Immunol.* **33**, 677–713 (2015).
23. Schietinger, A. & Greenberg, P. D. Tolerance and exhaustion: Defining mechanisms of T cell dysfunction. *Trends in Immunology* (2014). doi:10.1016/j.it.2013.10.001
24. Schietinger, A. & Greenberg, P. D. Tolerance and exhaustion: Defining mechanisms of T cell dysfunction. *Trends in Immunology* **35**, 51–60 (2014).
25. Wherry, E. J. *et al.* Molecular Signature of CD8+ T Cell Exhaustion during Chronic Viral Infection. *Immunity* **27**, 670–684 (2007).
26. Wherry, E. J. T cell exhaustion. *Nature Immunology* (2011). doi:10.1038/ni.2035
27. Zajac, A. J. *et al.* Viral Immune Evasion Due to Persistence of Activated T Cells Without Effector Function. *J. Exp. Med.* **188**, 2205–2213 (1998).
28. Bucks, C. M., Norton, J. A., Boesteanu, A. C., Mueller, Y. M. & Katsikis, P. D. Chronic Antigen Stimulation Alone Is Sufficient to Drive CD8+ T Cell Exhaustion. *J. Immunol.* **182**, 6697–6708 (2009).
29. Zippelius, A. *et al.* Effector Function of Human Tumor-Specific CD8 T Cells in Melanoma Lesions: A State of Local Functional Tolerance. *Cancer Res.* **64**, 2865–2873 (2004).
30. Wherry, E. J. T cell exhaustion. *Nature Immunology* **12**, 492–499 (2011).
31. Fourcade, J. *et al.* CD8 + T cells specific for tumor antigens can be rendered dysfunctional by the tumor microenvironment through upregulation of the inhibitory receptors BTLA and PD-1. *Cancer Res.* **72**, 887–896 (2012).
32. Fourcade, J. *et al.* Upregulation of Tim-3 and PD-1 expression is associated with tumor antigen–specific CD8 $^{+}$ T cell dysfunction in melanoma patients. *J. Exp. Med.* **207**, 2175–2186 (2010).
33. Baitsch, L. *et al.* Exhaustion of tumor-specific CD8+T cells in metastases from melanoma patients. *J. Clin. Invest.* **121**, 2350–2360 (2011).
34. Woo, S. R. *et al.* Immune inhibitory molecules LAG-3 and PD-1 synergistically regulate T-cell function to promote tumoral immune escape. *Cancer Res.* **72**, 917–927 (2012).
35. Ahmadzadeh, M. *et al.* Tumor antigen-specific CD8 T cells infiltrating the tumor express high levels of PD-1 and are functionally impaired. *Blood* **114**, 1537–1544 (2009).
36. Muenst, S. *et al.* Expression of programmed death ligand 1 (PD-L1) is associated with poor prognosis in human breast cancer. *Breast Cancer Res. Treat.* **146**, 15–24 (2014).
37. Sfanos, K. S. *et al.* Human prostate-infiltrating CD8+ T lymphocytes are oligoclonal and PD-1+. *Prostate* **69**, 1694–1703 (2009).
38. Matsuzaki, J. *et al.* Tumor-infiltrating NY-ESO-1–specific CD8 $^{+}$ T cells are negatively regulated by LAG-3 and PD-1 in human ovarian cancer. *Proc. Natl. Acad. Sci.* **107**, 7875–7880 (2010).
39. Riches, J. C. *et al.* T cells from CLLpatients exhibit features of T-cell exhaustion but retain capacity for cytokine production. *Blood* **121**, 1612–1621 (2013).
40. Zenz, T. Exhausting T cells in CLL. *Blood* **121**, 1485–1486 (2013).

41. Zhang, Y., Huang, S., Gong, D., Qin, Y. & Shen, Q. Programmed death-1 upregulation is correlated with dysfunction of tumor-infiltrating CD8+ T lymphocytes in human non-small cell lung cancer. *Cell. Mol. Immunol.* **7**, 389–395 (2010).
42. Chen, L. & Flies, D. B. Molecular mechanisms of T cell co-stimulation and co-inhibition. *Nature Reviews Immunology* (2013). doi:10.1038/nri3405
43. Muenst, S. *et al.* The immune system and cancer evasion strategies: Therapeutic concepts. *Journal of Internal Medicine* **279**, 541–562 (2016).
44. Barrett, D. M., Teachey, D. T. & Grupp, S. A. Toxicity management for patients receiving novel T-cell engaging therapies. *Current Opinion in Pediatrics* **26**, 43–49 (2014).
45. Wiczling, P., Rosenzweig, M., Vaickus, L. & Jusko, W. J. Pharmacokinetics and pharmacodynamics of a chimeric/humanized anti-CD3 monoclonal antibody, otelixizumab (TRX4), in subjects with psoriasis and with type 1 diabetes mellitus. *J. Clin. Pharmacol.* **50**, 494–506 (2010).
46. Anasetti, C., Tan, P., Hansen, J. A. & Martin, P. J. Induction of specific nonresponsiveness in unprimed human T cells by anti-CD3 antibody and alloantigen. *J. Exp. Med.* **172**, 1691–700 (1990).
47. Smith, J. A., Tso, J. Y., Clark, M. R., Cole, M. S. & Bluestone, J. A. Nonmitogenic anti-CD3 monoclonal antibodies deliver a partial T cell receptor signal and induce clonal anergy. *J. Exp. Med.* **185**, 1413–22 (1997).
48. Woodle, E. S., Hussein, S. & Bluestone, J. A. In vivo administration of anti-murine CD3 monoclonal antibody induces selective, long-term anergy in CD8+ T cells. *Transplantation* **61**, 798–803 (1996).
49. Chau, L. A., Tso, J. Y., Melrose, J. & Madrenas, J. HuM291(nuvion), a humanized Fc receptor-nonbinding antibody against CD3, anergizes peripheral blood T cells as partial agonist of the T cell receptor. *Transplantation* **71**, 941–950 (2001).
50. Mehta, D. S., Christmas, R. A., Waldmann, H. & Rosenzweig, M. Partial and transient modulation of the CD3-T-cell receptor complex, elicited by low-dose regimens of monoclonal anti-CD3, is sufficient to induce disease remission in non-obese diabetic mice. *Immunology* **130**, 103–113 (2010).
51. Aronson, R. *et al.* Low-dose otelixizumab anti-CD3 monoclonal antibody DEFEND-1 study: Results of the randomized phase III study in recent-onset human type 1 diabetes. *Diabetes Care* **37**, 2746–2754 (2014).
52. Ravandi, F. & O'Brien, S. Alemtuzumab in CLL and other lymphoid neoplasms. *Cancer Investigation* (2006). doi:10.1080/07357900600981414
53. Waldmann, H. & Hale, G. CAMPATH: From concept to clinic. *Philosophical Transactions of the Royal Society B: Biological Sciences* (2005). doi:10.1098/rstb.2005.1702
54. Hansel, T. T., Kropshofer, H., Singer, T., Mitchell, J. A. & George, A. J. T. The safety and side effects of monoclonal antibodies. *Nature Reviews Drug Discovery* (2010). doi:10.1038/nrd3003
55. Yi, T. M., Huang, Y., Simon, M. I. & Doyle, J. Robust perfect adaptation in bacterial chemotaxis through integral feedback control. *Proc. Natl. Acad. Sci. U. S. A.* (2000).
56. Alon, U. An Introduction to Systems Biology: Design Principles of Biological Circuits. *Chapman HallCRC mathematical and computational biology series* **10**, 301 (2007).
57. Kaupp, U. B. Olfactory signalling in vertebrates and insects: Differences and commonalities. *Nature Reviews Neuroscience* **11**, 188–200 (2010).

58. Yau, K. W. & Hardie, R. C. Phototransduction Motifs and Variations. *Cell* **139**, 246–264 (2009).
59. Ben-Zvi, D. & Barkai, N. Scaling of morphogen gradients by an expansion-repression integral feedback control. *Proc. Natl. Acad. Sci.* **107**, 6924–6929 (2010).
60. Eldar, A. *et al.* Robustness of the BMP morphogen gradient in Drosophila embryonic patterning. *Nature* **419**, 304–308 (2002).
61. Morris, M. K., Saez-Rodriguez, J., Sorger, P. K. & Lauffenburger, D. A. Logic-based models for the analysis of cell signaling networks. *Biochemistry* **49**, 3216–3224 (2010).
62. Yan, K. K. *et al.* Cross-Disciplinary Network Comparison: Matchmaking between Hairballs. *Cell Systems* **2**, 147–157 (2016).
63. Lever, M., Maini, P. K., Van Der Merwe, P. A. & Dushek, O. Phenotypic models of T cell activation. *Nat. Rev. Immunol.* **14**, 619–629 (2014).
64. Altan-Bonnet, G. & Germain, R. N. Modeling T cell antigen discrimination based on feedback control of digital ERK responses. *PLoS Biol.* **3**, 1925–1938 (2005).
65. Coward, J., Germain, R. N. & Altan-Bonnet, G. Perspectives for computer modeling in the study of T cell activation. *Cold Spring Harbor perspectives in biology* (2010). doi:10.1101/cshperspect.a005538
66. Sousa, J. & Carneiro, J. A mathematical analysis of TCR serial triggering and down-regulation. *Eur. J. Immunol.* (2000). doi:10.1002/1521-4141(200011)30:11<3219::AID-IMMU3219>3.0.CO;2-7
67. Utzny, C., Coombs, D., Müller, S. & Valitutti, S. Analysis of peptide/MHC-induced TCR downregulation. *Cell Biochem. Biophys.* (2006). doi:10.1385/CBB:46:2:101
68. Ferrell, J. E. Perfect and near-perfect adaptation in cell signaling. *Cell Systems* (2016). doi:10.1016/j.cels.2016.02.006
69. Behar, M., Hao, N., Dohlman, H. G. & Elstonz, T. C. Mathematical and computational analysis of adaptation via feedback inhibition in signal transduction pathways. *Biophys. J.* (2007). doi:10.1529/biophysj.107.107516
70. Tyson, J. J., Chen, K. C. & Novak, B. Sniffers, buzzers, toggles and blinkers: Dynamics of regulatory and signaling pathways in the cell. *Current Opinion in Cell Biology* (2003). doi:10.1016/S0955-0674(03)00017-6
71. Kholodenko, B. N. Negative feedback and ultrasensitivity can bring about oscillations in the mitogen-activated protein kinase cascades. *Eur. J. Biochem.* (2000). doi:10.1046/j.1432-1327.2000.01197.x
72. Rahi, S. J. *et al.* Oscillatory stimuli differentiate adapting circuit topologies. *Nat. Methods* (2017). doi:10.1038/nmeth.4408
73. Sun, H., Charles, C. H., Lau, L. F. & Tonks, N. K. MKP-1 (3CH134), an immediate early gene product, is a dual specificity phosphatase that dephosphorylates MAP kinase in vivo. *Cell* (1993). doi:10.1016/0092-8674(93)90383-2
74. Lake, D., Corrêa, S. A. L. & Müller, J. Negative feedback regulation of the ERK1/2 MAPK pathway. *Cellular and Molecular Life Sciences* (2016). doi:10.1007/s00018-016-2297-8
75. Sasagawa, S., Ozaki, Y. I., Fujita, K. & Kuroda, S. Prediction and validation of the distinct dynamics of transient and sustained ERK activation. *Nat. Cell Biol.* (2005). doi:10.1038/ncb1233
76. Avraham, R. & Yarden, Y. Feedback regulation of EGFR signalling: Decision making by early and delayed loops. *Nature Reviews Molecular Cell Biology* (2011). doi:10.1038/nrm3048

77. Takeda, K. *et al.* Cell biology: Incoherent feedforward control governs adaptation of activated ras in a eukaryotic chemotaxis pathway. *Sci. Signal.* (2012). doi:10.1126/scisignal.2002413
78. Ferguson, S. S. G. & Caron, M. G. G protein-coupled receptor adaptation mechanisms. *Semin. Cell Dev. Biol.* (1998). doi:10.1006/scdb.1997.0216
79. Marom, S. & Levitan, I. B. State-dependent inactivation of the Kv3 potassium channel. *Biophys. J.* (1994). doi:10.1016/S0006-3495(94)80517-X
80. Marom, S. Slow changes in the availability of voltage-gated ion channels: Effects on the dynamics of excitable membranes. *Journal of Membrane Biology* (1998). doi:10.1007/s002329900318
81. Shankaran, H., Steven, H. S. & Resat, H. Receptor downregulation and desensitization enhance the information processing ability of signalling receptors. *BMC Syst. Biol.* (2007). doi:10.1186/1752-0509-1-48
82. Wiley, H. S. *et al.* The role of tyrosine kinase activity in endocytosis, compartmentation, and down-regulation of the epidermal growth factor receptor. *J. Biol. Chem.* (1991).
83. Ferguson, S. S. Evolving concepts in G protein-coupled receptor endocytosis: the role in receptor desensitization and signaling. *Pharmacol. Rev.* (2001).
84. Schönrich, G. *et al.* Down-regulation of T cell receptors on self-reactive T cells as a novel mechanism for extrathymic tolerance induction. *Cell* **65**, 293–304 (1991).
85. Ferber, I. *et al.* Levels of peripheral T cell tolerance induced by different doses of tolerogen. *Science (80-.).* **263**, 674–676 (1994).
86. Tafuri, A., Alferink, J., Möller, P., Hämmerling, G. J. & Arnold, B. T cell awareness of paternal alloantigens during pregnancy. *Science (80-.).* **270**, 630–633 (1995).
87. Martin, S. & Bevan, M. J. Transient alteration of T cell fine specificity by a strong primary stimulus correlates with T cell receptor down-regulation. *Eur. J. Immunol.* **28**, 2991–3002 (1998).
88. Stamou, P. *et al.* Chronic Exposure to Low Levels of Antigen in the Periphery Causes Reversible Functional Impairment Correlating with Changes in CD5 Levels in Monoclonal CD8 T Cells. *J. Immunol.* **171**, 1278–1284 (2003).
89. Singh, N. J. & Schwartz, R. H. The Strength of Persistent Antigenic Stimulation Modulates Adaptive Tolerance in Peripheral CD4 $^{+}$ T Cells. *J. Exp. Med.* **198**, 1107–1117 (2003).
90. Hawiger, D., Masilamani, R. F., Bettelli, E., Kuchroo, V. K. & Nussenzweig, M. C. Immunological unresponsiveness characterized by increased expression of CD5 on peripheral T cells induced by dendritic cells in vivo. *Immunity* **20**, 695–705 (2004).
91. Ryan, K. R. Fas-mediated death and sensory adaptation limit the pathogenic potential of autoreactive T cells after strong antigenic stimulation. *J. Leukoc. Biol.* **78**, 43–50 (2005).
92. Lees, J. R. *et al.* Deletion is neither sufficient nor necessary for the induction of peripheral tolerance in mature CD8+T cells. *Immunology* **117**, 248–261 (2006).
93. Han, S., Asoyan, A., Rabenstein, H., Nakano, N. & Obst, R. Role of antigen persistence and dose for CD4+ T-cell exhaustion and recovery. *Proc. Natl. Acad. Sci.* **107**, 20453–20458 (2010).
94. Trendel, N., Kruger, P., Nguyen, J., Gaglione, S. & Dushek, O. Perfect adaptation of CD8+ T cell responses to constant antigen input over a wide range of affinity is overcome by costimulation. *Biorxiv* (2019). doi:10.1101/535385

95. Lever, M. *et al.* Architecture of a minimal signaling pathway explains the T-cell response to a 1 million-fold variation in antigen affinity and dose. *Proc. Natl. Acad. Sci.* **113**, E6630–E6638 (2016).
96. Aleksic, M. *et al.* Dependence of T Cell Antigen Recognition on T Cell Receptor-Peptide MHC Confinement Time. *Immunity* **32**, 163–174 (2010).
97. Maus, M. V. *et al.* An MHC-restricted antibody-based chimeric antigen receptor requires TCR-like affinity to maintain antigen specificity. *Mol. Ther. - Oncolytics* (2016). doi:10.1038/mto.2016.23
98. Cibrián, D. & Sánchez-Madrid, F. CD69: from activation marker to metabolic gatekeeper. *European Journal of Immunology* **47**, 946–953 (2017).
99. Vinay, D. S. & Kwon, B. S. 4-1BB (CD137), an inducible costimulatory receptor, as a specific target for cancer therapy. *BMB Reports* **47**, 122–129 (2014).
100. Butte, M. J., Keir, M. E., Phamduy, T. B., Sharpe, A. H. & Freeman, G. J. Programmed death-1 ligand 1 interacts specifically with the B7-1 costimulatory molecule to inhibit T cell responses. *Immunity* **27**, 111–122 (2007).
101. Thommen, D. S. & Schumacher, T. N. T Cell Dysfunction in Cancer. *Cancer Cell* (2018). doi:10.1016/j.ccell.2018.03.012
102. Wyzgol, A. *et al.* Trimer stabilization, oligomerization, and antibody-mediated cell surface immobilization improve the activity of soluble trimers of CD27L, CD40L, 41BBL, and glucocorticoid-induced TNF receptor ligand. *J. Immunol.* **183**, 1851–1861 (2009).
103. Adler, M. & Alon, U. Fold-change detection in biological systems. *Current Opinion in Systems Biology* (2018). doi:10.1016/j.coisb.2017.12.005
104. Lanier, L. L. *et al.* CD80 (B7) and CD86 (B70) provide similar costimulatory signals for T cell proliferation, cytokine production, and generation of CTL. *J. Immunol.* (1995).
105. Kim, D., Kwon, Y. K. & Cho, K. H. The biphasic behavior of incoherent feed-forward loops in biomolecular regulatory networks. *BioEssays* (2008). doi:10.1002/bies.20839
106. Trendel, N., Kruger, P., Nguyen, J., Gaglione, S. & Dushek, O. Perfect adaptation of CD8+ T cell responses to constant antigen input over a wide range of affinity is overcome by costimulation. *bioRxiv* (2019).
107. Vessillier, S. *et al.* Cytokine release assays for the prediction of therapeutic mAb safety in first-in man trials - Whole blood cytokine release assays are poorly predictive for TGN1412 cytokine storm. *J. Immunol. Methods* (2015). doi:10.1016/j.jim.2015.04.020
108. Chervin, A. S. *et al.* The Impact of TCR-Binding Properties and Antigen Presentation Format on T Cell Responsiveness. *J. Immunol.* **183**, 1166–1178 (2009).
109. Liu, B. *et al.* The cellular environment regulates in situ kinetics of T-cell receptor interaction with peptide major histocompatibility complex. *Eur. J. Immunol.* **45**, 2099–2110 (2015).
110. Letsch, A. & Scheibenbogen, C. Quantification and characterization of specific T-cells by antigen-specific cytokine production using ELISPOT assay or intracellular cytokine staining. *Methods* **31**, 143–149 (2003).
111. Toettcher, J. E., Voigt, C. A., Weiner, O. D. & Lim, W. A. The promise of optogenetics in cell biology: interrogating molecular circuits in space and time. *Nat. Methods* (2011). doi:10.1038/nmeth.f.326

112. Bugaj, L. J., O'Donoghue, G. P. & Lim, W. A. Interrogating cellular perception and decision making with optogenetic tools. *J. Cell Biol.* (2017). doi:10.1083/jcb.201612094
113. Teachey, D. T. *et al.* Identification of predictive biomarkers for cytokine release syndrome after chimeric antigen receptor T-cell therapy for acute lymphoblastic leukemia. *Cancer Discov.* **6**, 664–679 (2016).
114. Chen, D. S. & Mellman, I. Elements of cancer immunity and the cancer–immune set point. *Nature* **541**, 321–330 (2017).
115. Osada, T. *et al.* CEA/CD3-bispecific T cell-engaging (BiTE) antibody-mediated T lymphocyte cytotoxicity maximized by inhibition of both PD1 and PD-L1. *Cancer Immunol. Immunother.* **64**, 677–688 (2015).
116. Barrett, D. M., Singh, N., Porter, D. L., Grupp, S. A. & June, C. H. Chimeric Antigen Receptor Therapy for Cancer. *Annu. Rev. Med.* (2014). doi:10.1146/annurev-med-060512-150254

Appendix – Mathematical Models and Supplementary Figures

Notes:

- All models are non-dimensional.
- Variable definitions:

L	ligand	P	total product (i.e. cytokine)
R	receptor	k_x	rate
A	bound ligand-receptor complex	t	time
O / O_1 / O_2	outputs / intermediate species	*	threshold value
B	regulatory species / 'node'		

- Serious concern: models B, E, and G can generate negative values for variables, as evidenced by Figure 30, (2) (variables B and O). Future work should refine these models to ensure physiological relevance and correct this issue. Negative values of species are not possible.
- For all models, the on- and off-rates of receptor binding the ligand are considered to be approximately equal, aligning with previous models generated by the Dushek group. Other parameter values are generally motivated for each model below.
- Adaptation is observed on two different time scales generated by the models, one with a basis of 10 000 units and one with 500 units (see scales on figures below). Neither is physiologically relevant in seconds or hours. Time would be ideally measured in units of hours – the parameter values should be adjusted to reflect the occurrence of adaptation within ~4-8 hours.
- A sample MATLAB ODE function and script are provided for model C. Both are presented at the end of the thesis.

Figure 23. NFL and IFFL Ordinary Differential Equations

(A) Incoherent Feed Forward – Signaling-Mediated

$$\frac{dL}{dt} = -k_{on}RL + k_{off}A$$

$$\frac{dR}{dt} = -k_{on}RL + k_{off}A$$

$$\frac{dA}{dt} = k_{on}RL - k_{off}A$$

$$\frac{dO}{dt} = k_1A(1 - O) - k_2BO$$

$$\frac{dB}{dt} = k_3A - k_4B$$

$$\frac{dP}{dt} = O$$

$$k_{on} = 1$$
$$k_{off} = 1$$
$$k_1 = 100$$
$$k_2 = 100$$
$$k_3 = 0.002$$
$$k_4 = 0.0005$$

Initial Conditions

$L_0 = 1$
$R_0 = 1$
$A_0 = 0$
$O_0 = 0$
$B_0 = 0$
$P_0 = 0$

Parameter Values

- Regulatory species B is generated at a considerably slower rate (k_3) and degraded at a slower rate than it is generated (k_4). The rate of generation and consumption of the output species O, representing the production rate of cytokines, are approximated as equal and high (100). The basis for the values chosen for these parameters and range in which the adaptation phenotype is observed should be further investigated.

(B) Negative Feedback – Signaling-Mediated

$$\frac{dL}{dt} = -k_{on}RL + k_{off}A$$

$$\frac{dR}{dt} = -k_{on}RL + k_{off}A$$

$$\frac{dA}{dt} = k_{on}RL - k_{off}A$$

$$\frac{dO}{dt} = k_1A(1 - O) - k_2BO$$

$$\frac{dB}{dt} = k_3O - k_4$$

$$\frac{dP}{dt} = O$$

$k_{on} = 1$
$k_{off} = 1$
$k_1 = 10$
$k_2 = 10$
$k_3 = 0.01$
$k_4 = 0.001$

Initial Conditions

$L_0 = 1$
$R_0 = 1$
$A_0 = 0$
$O_0 = 0$
$B_0 = 0$
$P_0 = 0$

Parameter Values

- Regulatory species B is generated at a considerably slower rate (k_3) and degraded at a slower rate than it is generated (k_4). The rate of generation and consumption of the output species O, representing the production rate of cytokines, are approximated as equal and high (10). The basis for the values chosen for these parameters and range in which the adaptation phenotype is observed should be

further investigated.

(C) Incoherent Feed Forward – Complete Receptor Downregulation

$$\frac{dL}{dt} = -k_{on}RL + (k_{off} + k_1)A \qquad k_{on} = 1,\ k_{off} = 1,\ k_1 = 0.3$$

$$\frac{dR}{dt} = -k_{on}RL + k_{off}A$$

$$\frac{dA}{dt} = k_{on}RL - (k_{off} + k_1)A$$

$$\frac{dP}{dt} = A$$

Initial Conditions

$L_0 = 1$
$R_0 = 1$
$A_0 = 0$
$P_0 = 0$

Parameter Values

- The rate of receptor downregulation relative to the binding on- and off-rates is derived from literature (see references in Introduction) and experimental observations by the Dushek group. The rate is generally considered to be on the same order of magnitude as the on- and off-rates. The basis for the values chosen for these parameters and range in which the adaptation phenotype is observed should be further investigated.

(D) Incoherent Feed Forward – Complete Receptor and Ligand Downregulation

$$\frac{dL}{dt} = -k_{on}RL + k_{off}A \qquad k_{on} = 1,\ k_{off} = 1,\ k_1 = 0.3$$

$$\frac{dR}{dt} = -k_{on}RL + k_{off}A$$

$$\frac{dA}{dt} = k_{on}RL - (k_{off} + k_1)A$$

$$\frac{dP}{dt} = A$$

Initial Conditions

$L_0 = 1$
$R_0 = 1$
$A_0 = 0$
$P_0 = 0$

Parameter Values

- The rate of receptor downregulation relative to the binding on- and off-rates is derived from literature (see references in Introduction) and experimental observations by the Dushek group. The rate is generally considered to be on the same order of magnitude as the on- and off-rates. The basis for the values chosen for these parameters and range in which the adaptation phenotype is observed should be further investigated.

(E) Negative Feedback – Complete Receptor Downregulation

$$\frac{dL}{dt} = -k_{on}RL + k_{off}A$$

$$\frac{dR}{dt} = -k_{on}RL + k_{off}A - k_1O$$

$$\frac{dA}{dt} = k_{on}RL - k_{off}A$$

$$\frac{dO}{dt} = k_2A(1 - O) - k_3A$$

$$\frac{dP}{dt} = O$$

$k_{on} = 1$
$k_{off} = 1$
$k_1 = 0.1$
$k_2 = 5$
$k_3 = 1$

Initial Conditions

$L_0 = 1$
$R_0 = 1$
$A_0 = 0$
$O_0 = 0$
$P_0 = 0$

Parameter Values

- The rate of receptor downregulation relative to the binding on- and off-rates is derived from literature (see references in Introduction) and experimental observations by the Dushek group. The rate k_1 is generally considered to be on the same order of magnitude as the on- and off-rates. Similarly, the values of k_2 and k_3 are on the same order of magnitude as well. Values were selected to be 1 initially and altered manually to exaggerate or tweak the observed phenotype. The basis for the values chosen for these parameters and range in which the adaptation phenotype is observed should be further investigated.

(F) Incoherent Feed Forward – Partial Receptor Downregulation

$$\frac{dL}{dt} = -k_{on}RL + (k_{off} + k_1)A$$

$$\frac{dR}{dt} = k_{syn} - k_{on}RL + k_{off}A - k_{int}R$$

$$\frac{dA}{dt} = k_{on}RL - (k_{off} + k_1)A$$

$$\frac{dO}{dt} = H(A - A^*) - k_{deg}O$$

$$\frac{dP}{dt} = O$$

$$k_{on} = 1$$
$$k_{off} = 1$$
$$k_1 = 0.3$$
$$k_{syn} = 0.01$$
$$k_{int} = 0.01$$
$$k_{deg} = 1$$
$$A^* = 0.052$$

Initial Conditions

$L_0 = 1$
$R_0 = 1$
$A_0 = 0$
$O_0 = 0$
$P_0 = 0$

Parameter Values

- The rate of receptor downregulation relative to the binding on- and off-rates is derived from literature (see references in Introduction) and experimental observations by the Dushek group. The rate k_1 is generally considered to be on the same order of magnitude as the on- and off-rates. k_{syn} represents the synthesis rate of the receptor, R, while k_{int} represents the basal internalization rate of the receptor. Low values were selected following consultation with Nicola Trendel and Omer Dushek – these values are considered to be at least an order of magnitude lower than the downregulation rate of the TCR following binding by ligand. k_{deg} represents the degradation of the output signal that links to product production, P. The value was initially and arbitrarily set to 1. The threshold value was manually selected to generate an observable adaptation phenotype. The basis for the values chosen for these parameters and range in which the adaptation phenotype is observed should be further investigated.

(G) Negative Feedback – Partial Receptor Downregulation

$$\frac{dL}{dt} = -k_{on}RL + k_{off}A$$

$$\frac{dR}{dt} = k_{syn} - k_{on}RL + k_{off}A - k_{int}R - k_1O_1$$

$$\frac{dA}{dt} = k_{on}RL - k_{off}A$$

$$\frac{dO_1}{dt} = k_2A(1 - O_1) - k_3O_1$$

$$\frac{dO_2}{dt} = H(O_1 - O_1{}^*) - k_{deg}O_2$$

$$\frac{dP}{dt} = O_2$$

$k_{on} = 1$
$k_{off} = 1$
$k_1 = 0.1$
$k_2 = 5$
$k_3 = 1$
$k_{syn} = 0.01$
$k_{int} = 0.01$
$k_{deg} = 1$
$O_1{}^* = 0.1$

Initial Conditions

$L_0 = 1$
$R_0 = 1$
$A_0 = 0$
$O_{1,0} = 0$
$O_{2,0} = 0$
$P_0 = 0$

Parameter Values

- The rate of receptor downregulation relative to the binding on- and off-rates is derived from literature (see references in Introduction) and experimental observations by the Dushek group. The rate k_1 is generally considered to be on the same order of magnitude as the on- and off-rates. k_{syn} represents the synthesis rate of the receptor, R, while k_{int} represents the basal internalization rate of the receptor. Low values were selected following consultation with Nicola Trendel and Omer Dushek – these values are considered to be at least an order of magnitude lower than the downregulation rate of the TCR following binding by ligand. k_{deg} represents the degradation of the output signal that links to product production, P. The value was initially and arbitrarily set to 1. Other rate values were selected to be on the same order of magnitude as the on- and off-rates. The threshold value was manually selected to generate an observable adaptation phenotype. The basis for the values chosen for these parameters and range in which the adaptation phenotype is observed should be further investigated.

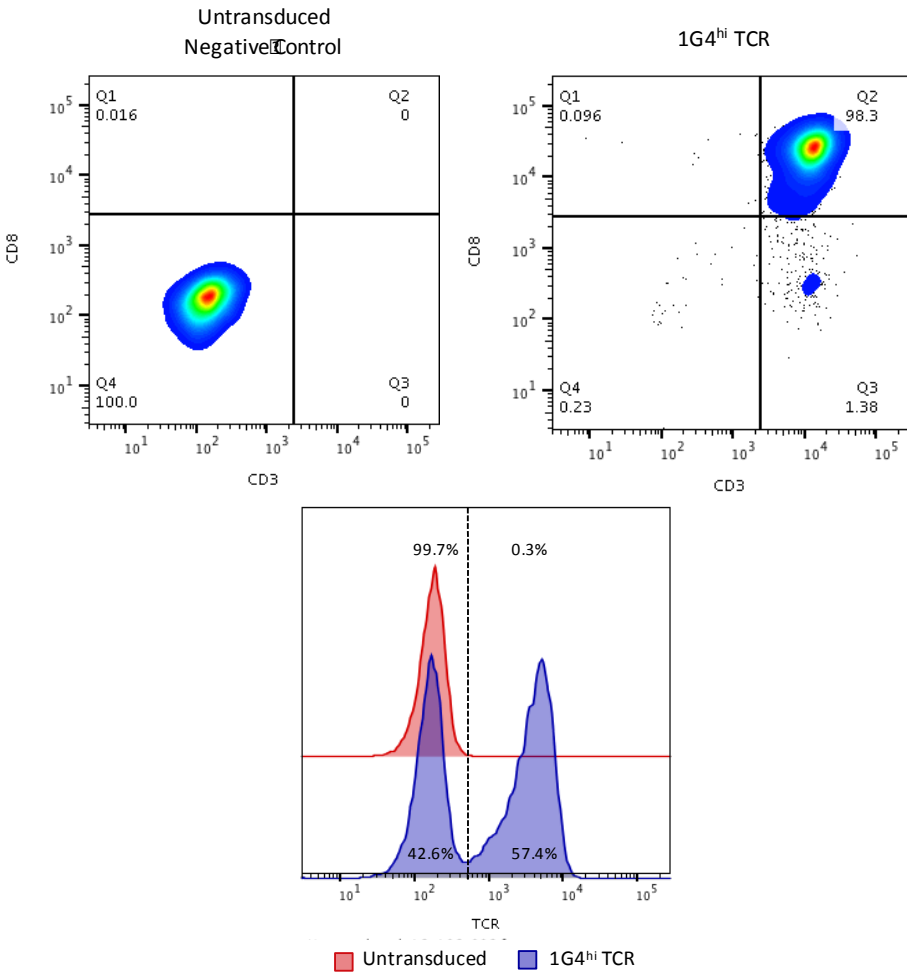


Figure 24. Purity of Isolated CD8$^+$ T Cells. Untransduced cells not treated with anti-CD3 or anti-CD8 antibodies display no fluorescence and serve as a negative control. 1G4^{hi} TCR-positive cells are CD3$^+$CD8$^+$ with a purity of 98.3%. The lower panel is a representative histogram of cells stained with 9V-PE tetramer (i.e. 57.3% TCR expression level).

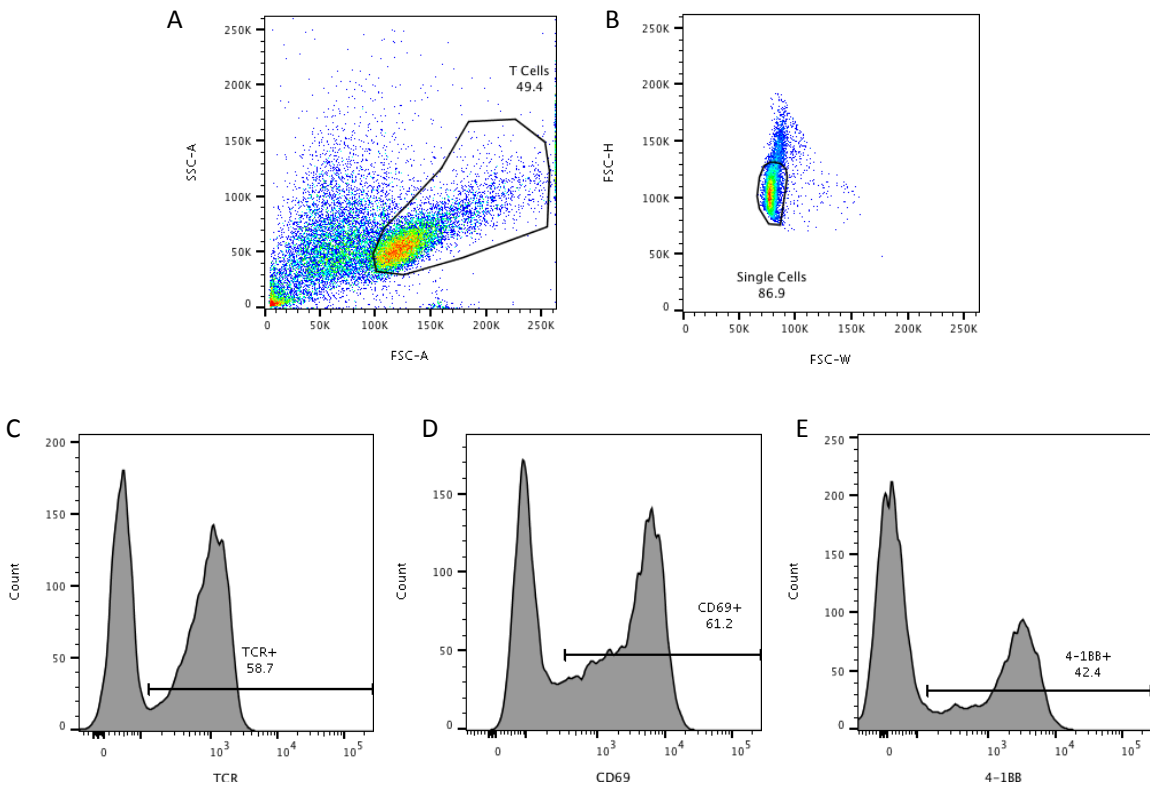


Figure 25. T Cell Surface Marker Gating Strategy – (A) Gating of the T cell population, (B) single cells, (C) $1G4^{hi}$ TCR^{+} population, (D) $CD69^{+}$ population, and (E) $4\text{-}1BB^{+}$ population. Adapted from Stephanie Gaglione, MSc in Integrated Immunology (thesis).

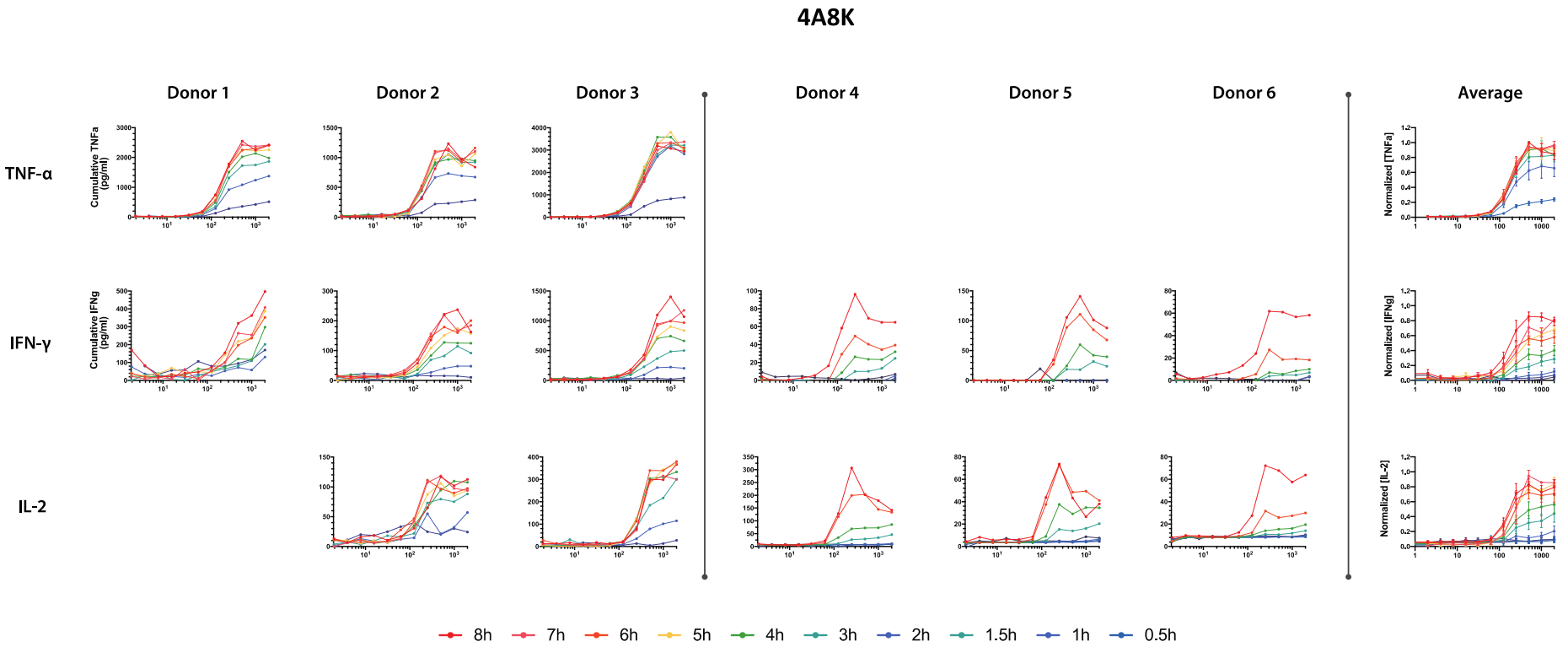


Figure 26. Low-Affinity pMHC (4A8K) Time- and Dose-Course Data. Cumulative. TNF-α, IFN-γ, and IL-2 secretion for individual repeats (Donors 1 to 3 – Nicola Trendel) and averaged data (right column). Error bars represent SD.

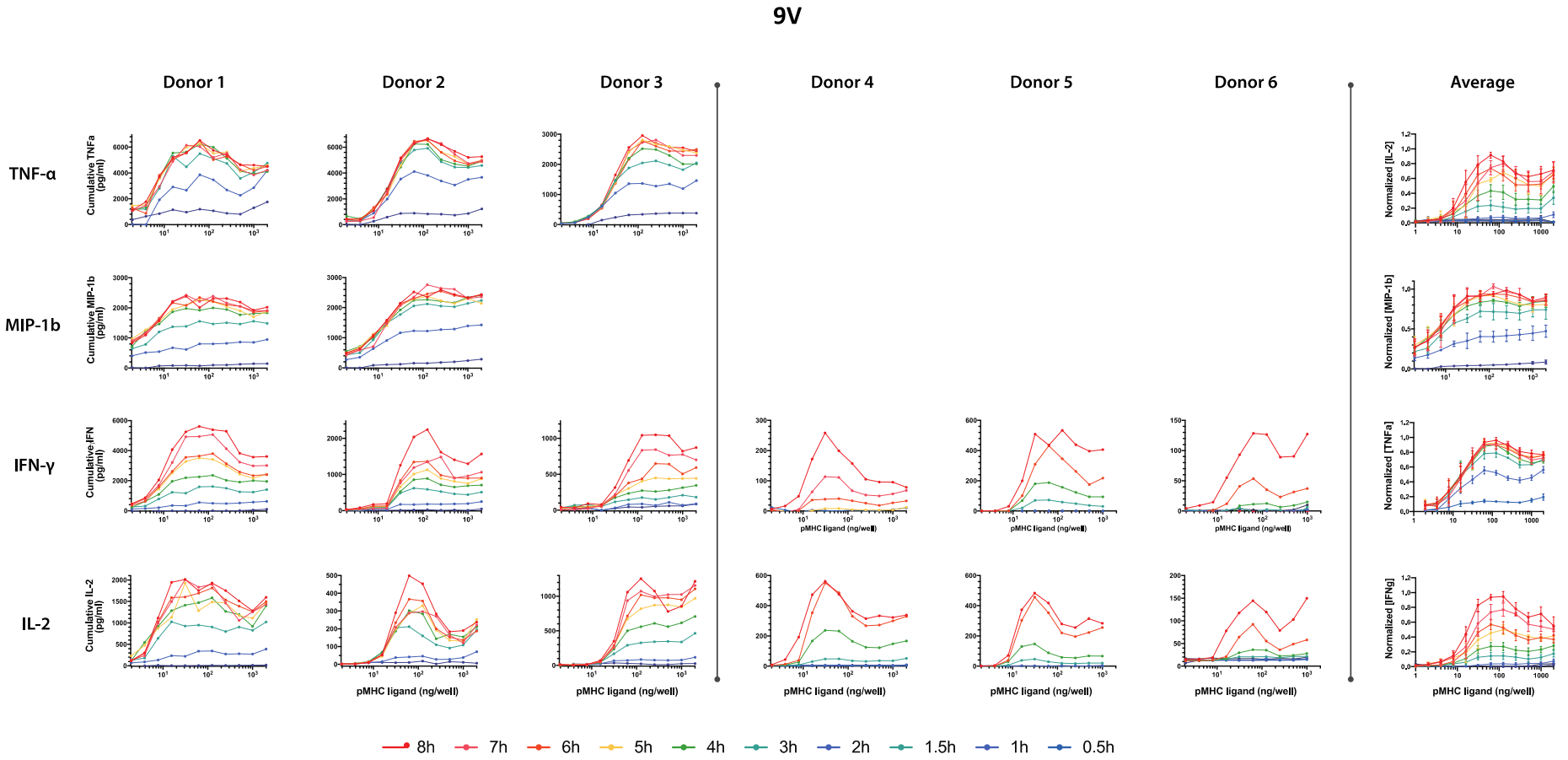


Figure 27. High-Affinity pMHC (9V) Time- and Dose-Course Data. TNF-α, IFN-γ, MIP-1β, and IL-2 secretion for individual repeats (Donors 1 to 3 – Nicola Trendel) and averaged data (right column). Error bars represent SD.

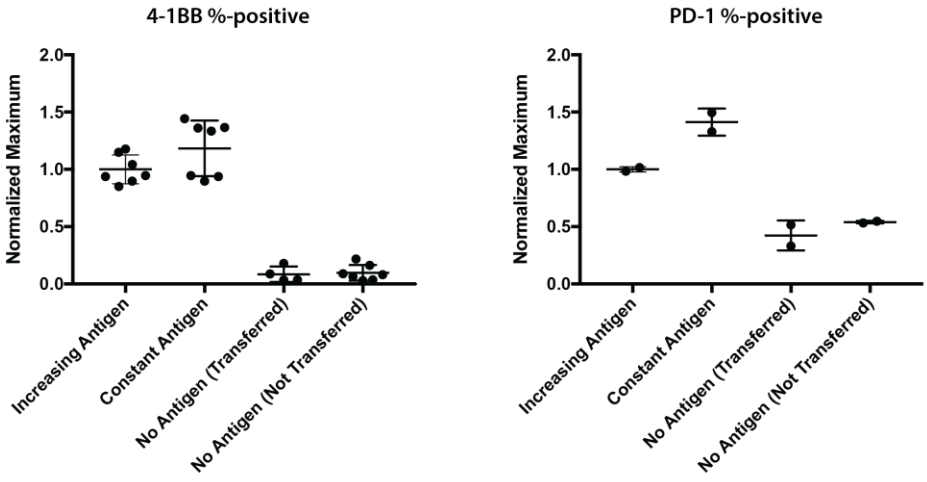


Figure 28. Phase 1: 4-1BB and PD-1 Expression. Surface expression of 4-1BB and PD-2 (%-positive) during Phase 1. Mean with SD, 4-1BB, n = 7, PD-1, n = 2. Normalization: (a) The mean of all conditions (increasing antigen, constant antigen, and no antigen) was calculated for each experimental repeat. Each repeat was normalized to its mean value. (b) The mean of the increasing antigen condition across all experiments was calculated. All values from (a) were normalized to this value. Each experiment was therefore normalized to 1 in itself before normalization to the increasing antigen condition. Statistical analysis was completed using two-way ANOVAs with multiple comparisons corrected by Tukey test. Constant antigen vs. increasing antigen for 4-1BB%-positive cells: p = 0.0478.

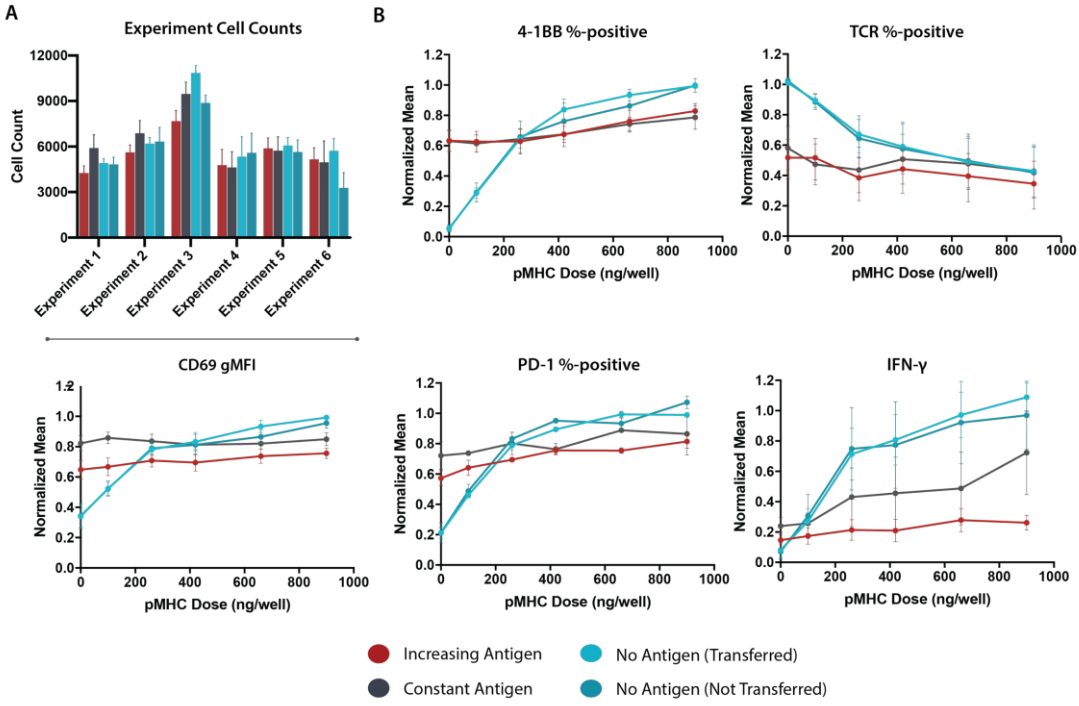
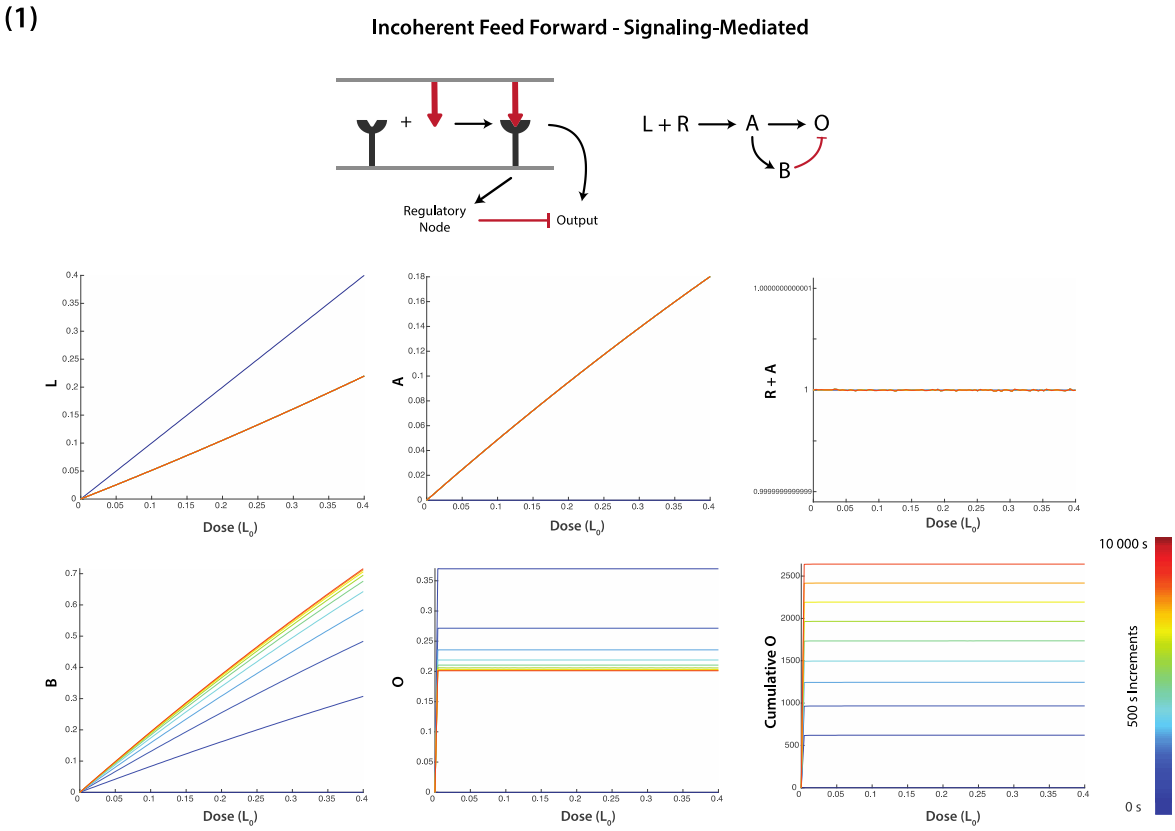
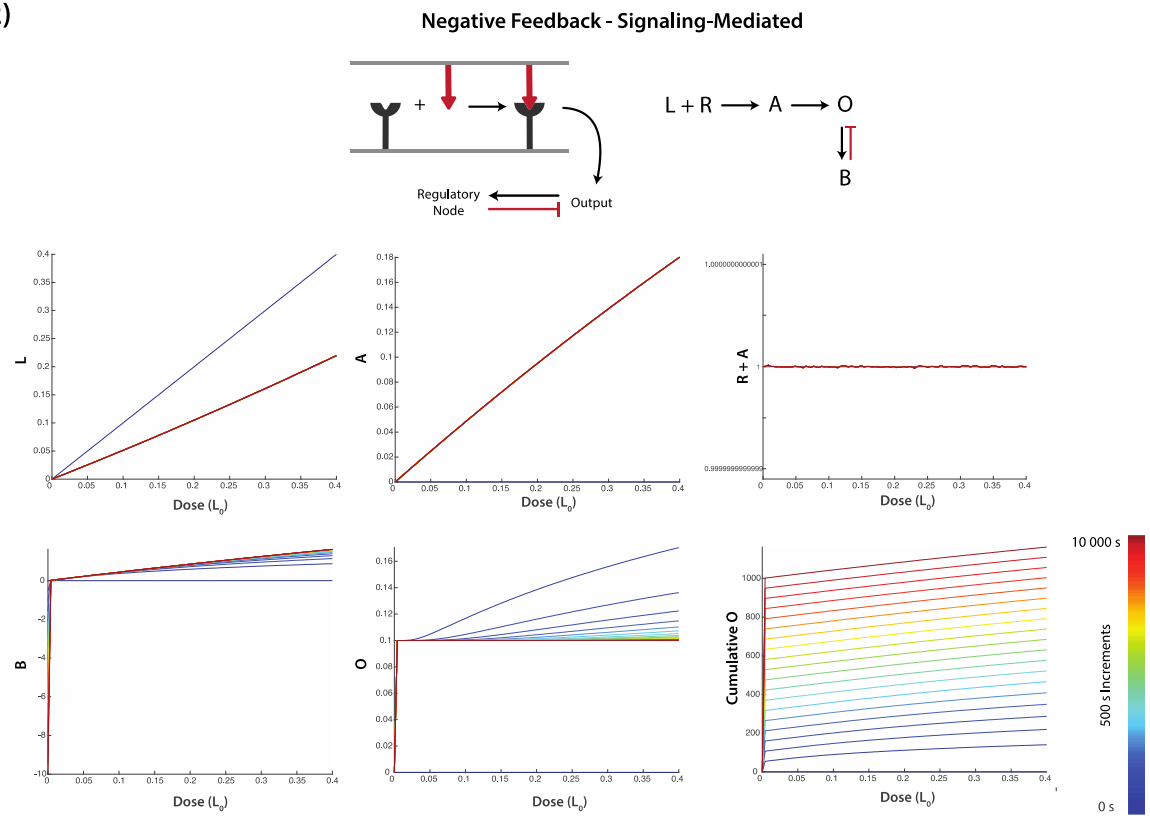


Figure 29. Phase 2: Supplementary Surface Markers, Cytokine Secretion, and Cell Counts. (A) Cell counts for six experimental repeats, indicating non-biased removal of cells from the plate surface. (B) Expanded data for Figure 18 for CD69 gMFI, 4-1BB %-positive cells, TCR %-positive cells, and IFN-γ secretion.

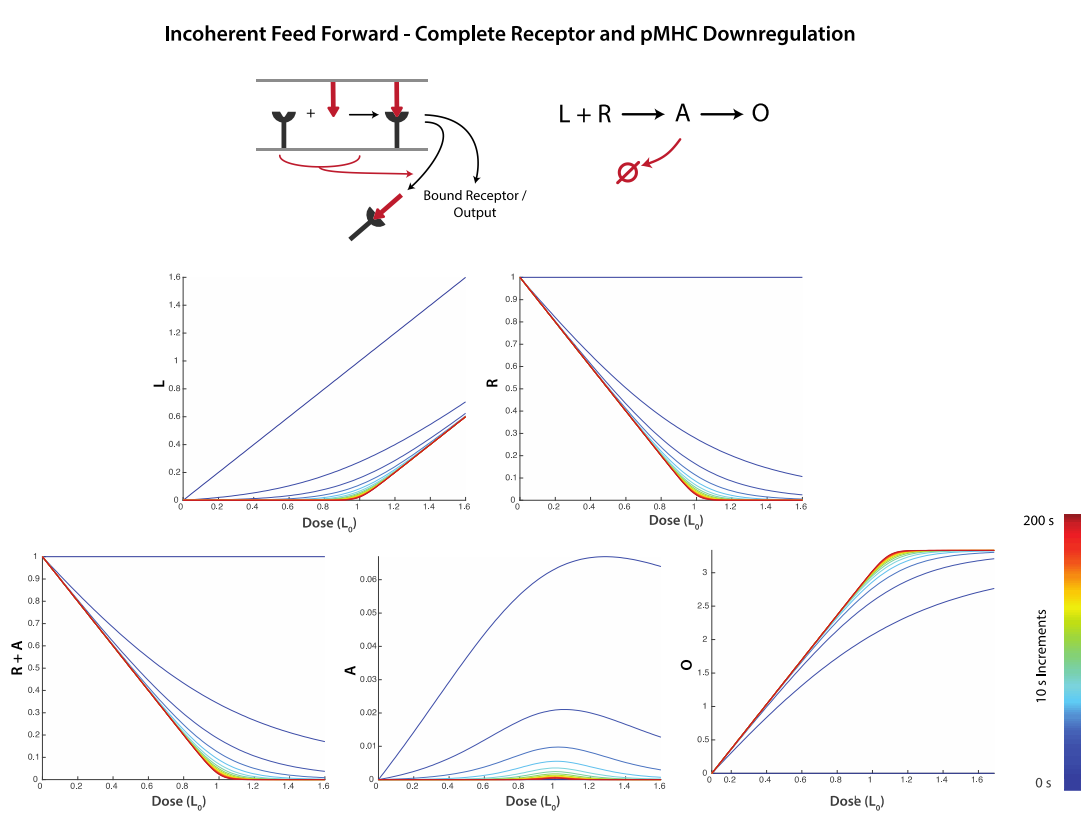
Figure 30. Model Simulations – Time- and Dose-Course Experiment (continued on following pages). Model simulations for the seven NFL- and IFFL-based models with the receptor or downstream signaling as the control mechanism for adaptation. Parameters and ODEs can be found in Supplementary Figure 23. (1) Incoherent Feed Forward – Signaling-Mediated, (2) Negative Feedback – Signaling-Mediated, (3) Incoherent Feed Forward – Complete Receptor and Ligand Downregulation, (4) Incoherent Feed Forward – Complete Receptor Downregulation, (5) Negative Feedback – Complete Receptor Downregulation, (6) Incoherent Feed Forward – Partial Receptor Downregulation, (7) Negative Feedback – Partial Receptor Downregulation



(2)

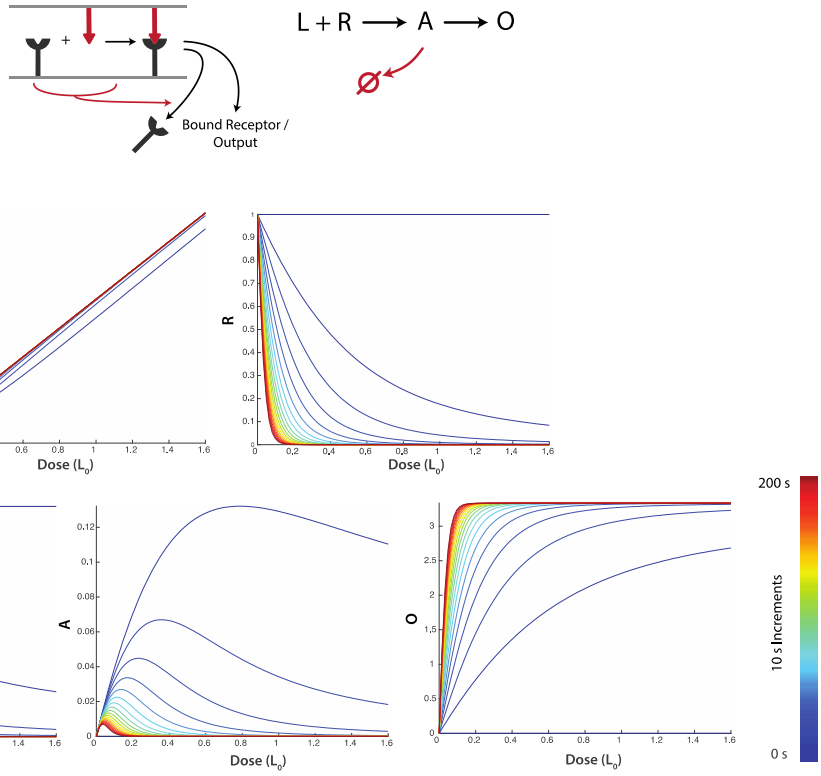

Negative Feedback - Signaling-Mediated
L + R → A → O
B
Regulatory Node
Output
L
A
R + A
B
O
Cumulative O
Dose (L0)
10 000 s
500 s Increments
0 s

(3)


Incoherent Feed Forward - Complete Receptor and pMHC Downregulation
L + R → A → O
Bound Receptor / Output
L
R
R + A
A
O
Dose (L0)
200 s
10 s Increments
0 s

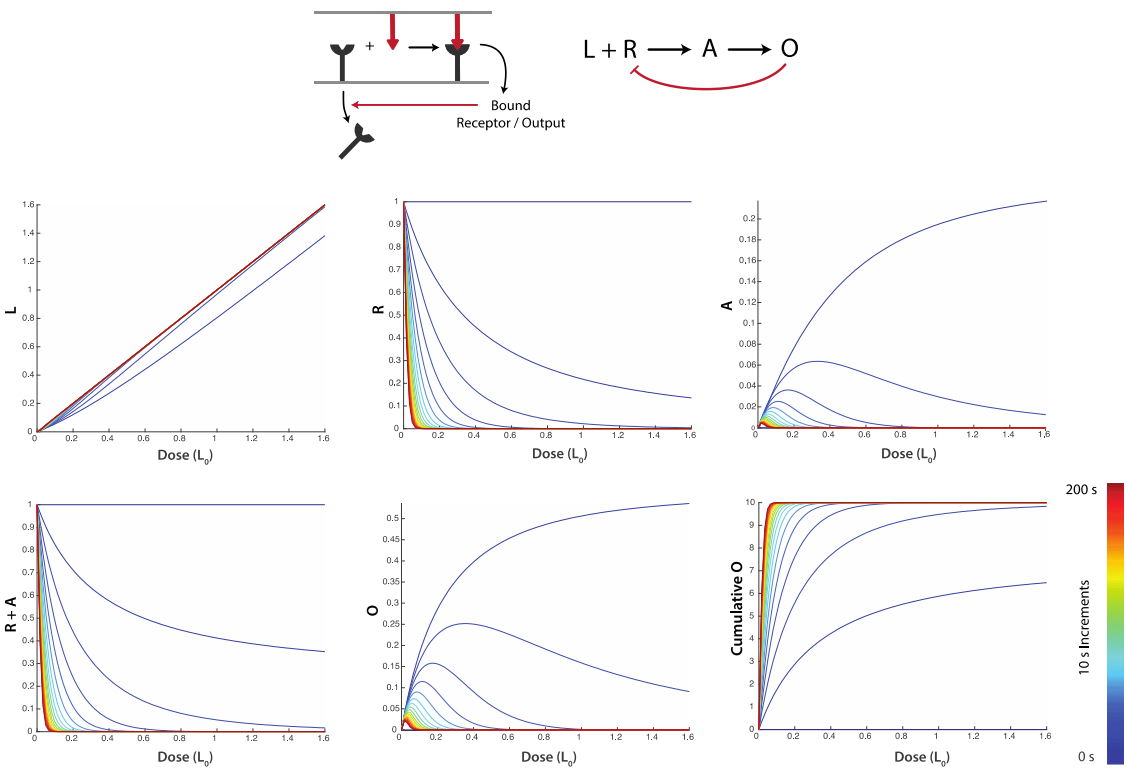
(4)

Incoherent Feed Forward - Complete Receptor Downregulation



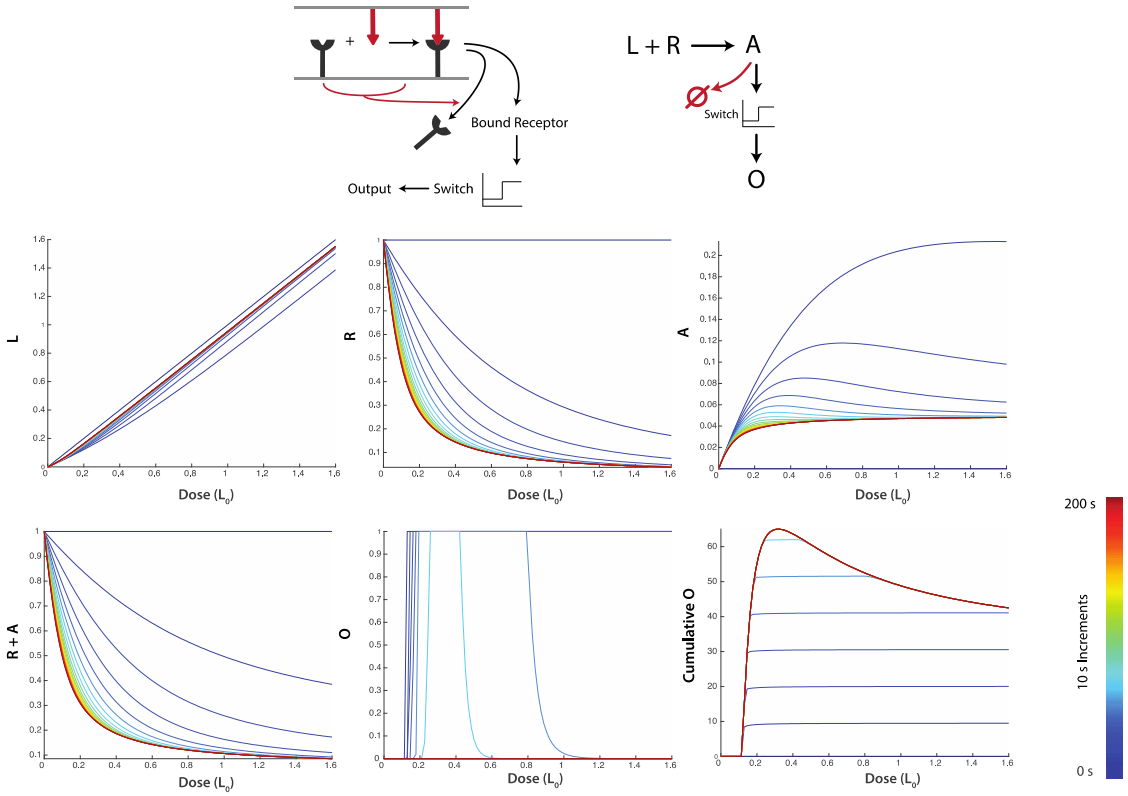
(5)

Negative Feedback - Complete Receptor Downregulation



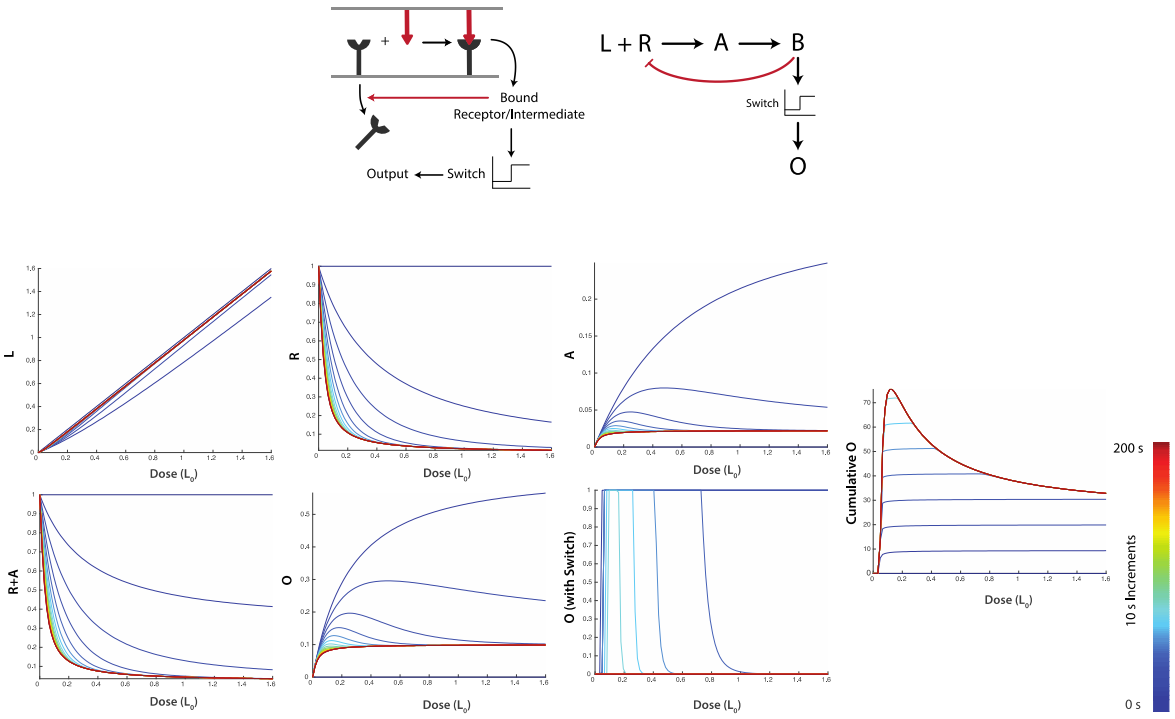
(6)

Incoherent Feed Forward - Partial Receptor Downregulation



(7)

Negative Feedback - Partial Receptor Downregulation



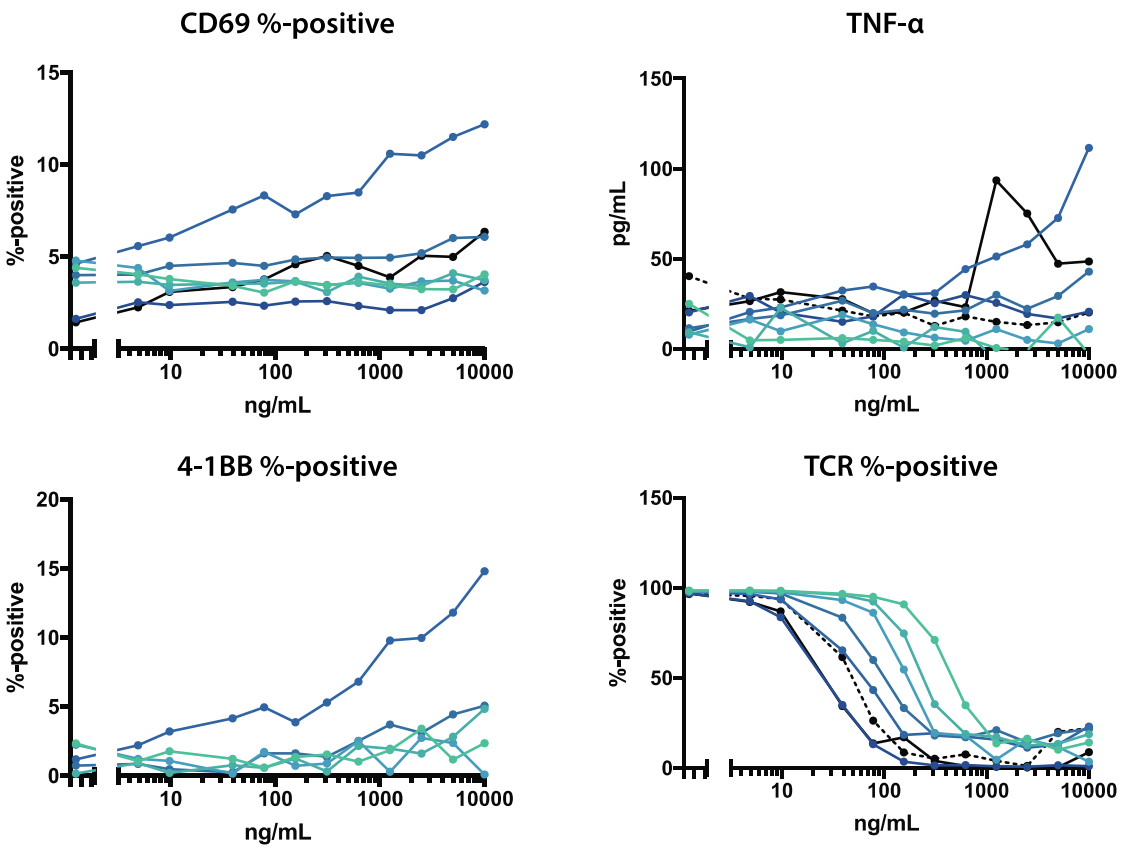


Figure 31. Otelixizumab Experiment Repeat 1: Soluble Format. Cumulative cytokine secretion (TNF-α, IFN-γ) and surface marker expression (CD69, 4-1BB, TCR %-positive) by T cells exposed to a range of otelixizumab doses in soluble form over time. 'Cold' indicates incubation at 4°C. n = 1.

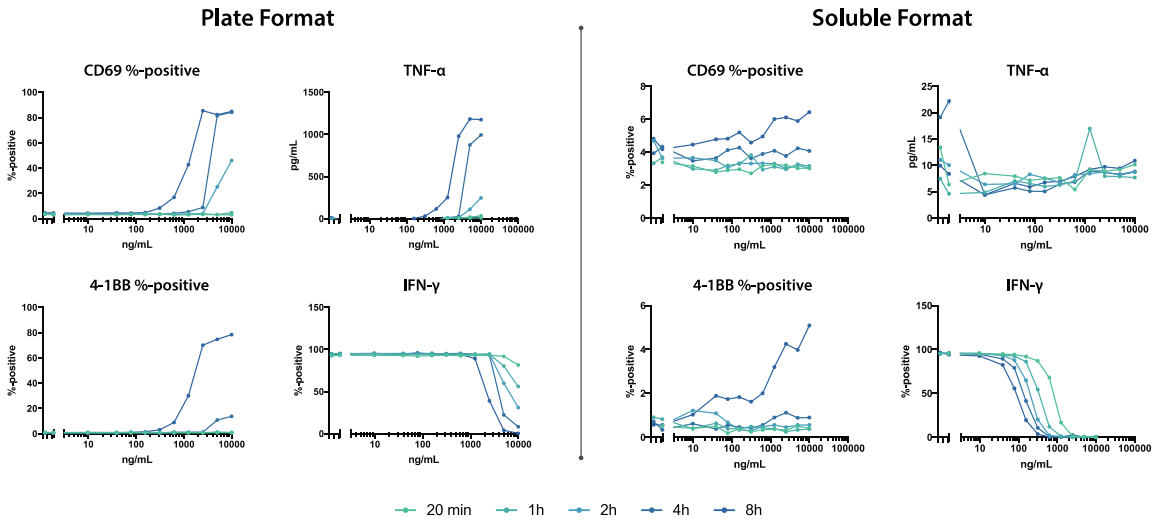


Figure 32. Otelixizumab Experiment Repeat 2: Plate-bound and Soluble Formats. Cumulative cytokine secretion (TNF-α, IFN-γ) and surface marker expression (CD69, 4-1BB, TCR %-positive) by T cells exposed to a range of otelixizumab doses over time. 'Cold' indicates incubation at 4°C. n = 1.

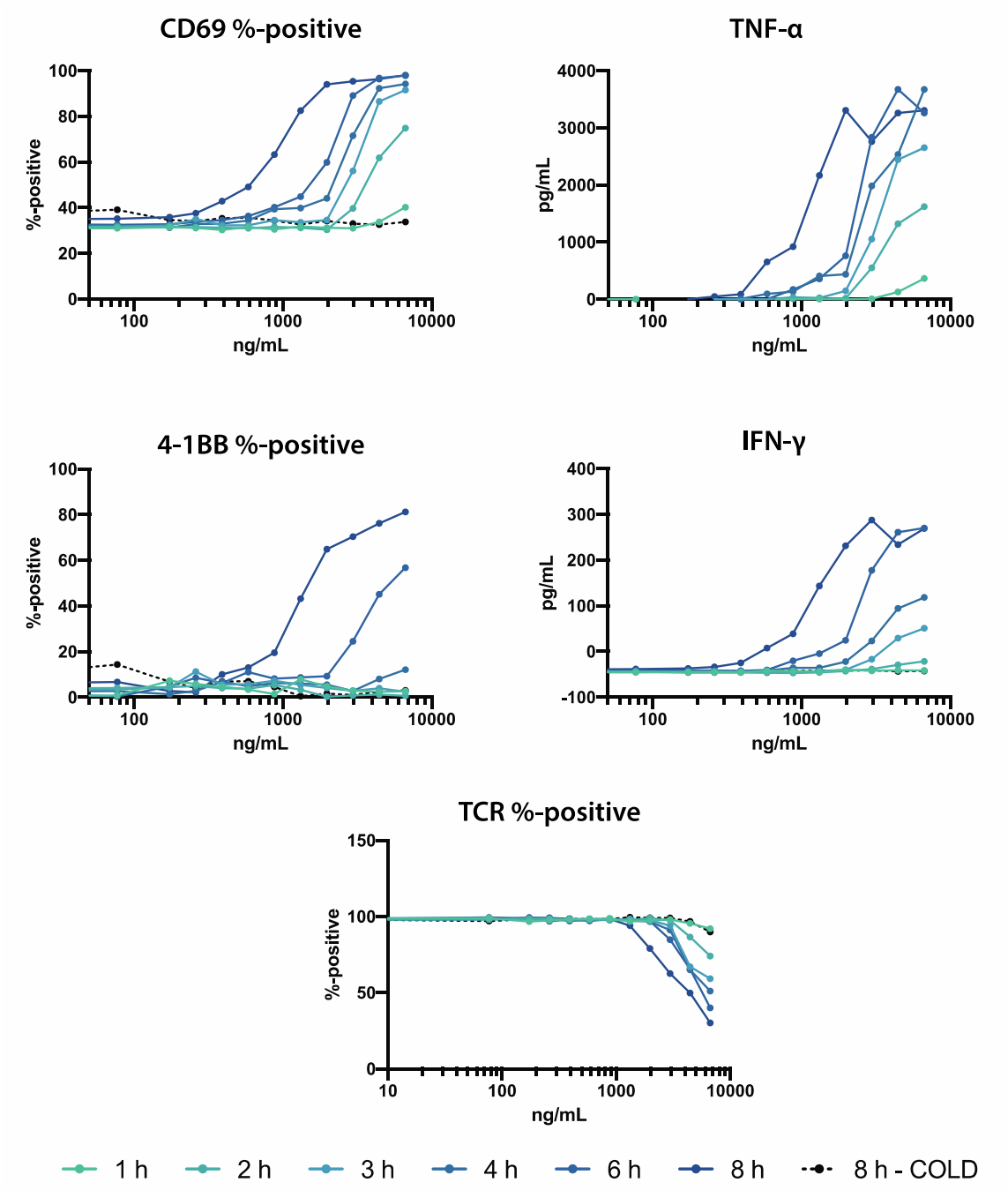


Figure 33. Otelixizumab Experiment Repeat 3: Plate-bound Format. Cumulative cytokine secretion (TNF-α, IFN-γ) and surface marker expression (CD69, 4-1BB, TCR %-positive) by T cells exposed to a range of otelixizumab doses immobilized on a plate over time. 'COLD' indicates incubation at 4°C. n = 1.

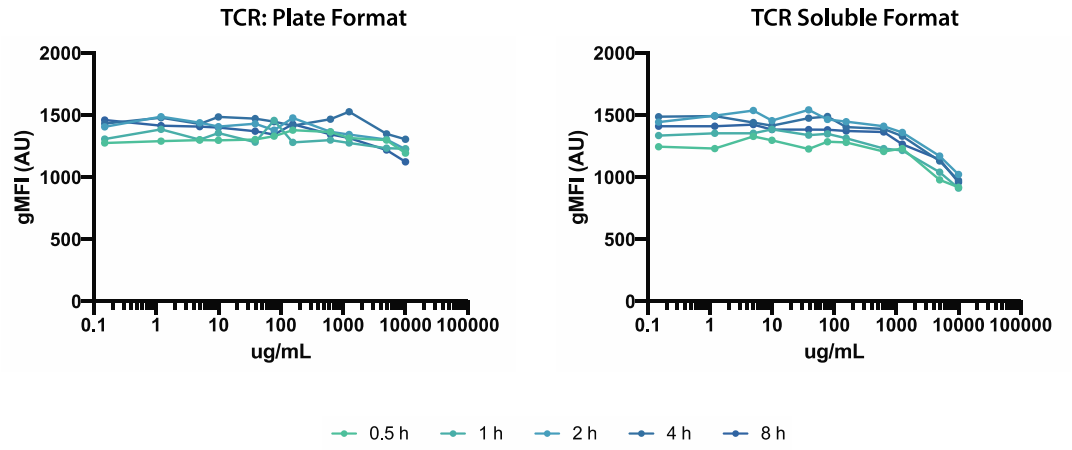


Figure 34. Alemtuzumab Experiment: Plate-bound and Soluble Formats. TCR surface expression (gMFI) by T cells exposed to a range of alemtuzumab doses in plate-bound and soluble forms over time. n = 1.

ChAgly CD3 data sheet

Issue 1: Dec 1997

Therapeutic Antibody Centre, Old Road, Headington, Oxford, OX3 7JT
Tel: 01865-744845 Fax: 01865-741291. Clinical Director: Prof Herman Waldmann. Research Director: Dr Geoffrey Hale

WARNING

This leaflet describes an experimental drug for named patient use only. Its possible clinical effects have not been fully evaluated. Full responsibility for its use rests with the consultant physician. These notes are offered for guidance, but are not necessarily complete.

ChAgly CD3 is a chimeric monoclonal antibody which recognises human T lymphocytes. The light chain is a chimeric construct of a rat variable domain and a human lambda constant domain. The heavy chain is a humanised gamma-1 which has been mutated to replace Asn^{297} with Ala in order to prevent N-linked glycosylation and so reduce or eliminate binding to Fc receptors.

Presentation

ChAgly CD3 is supplied as a frozen solution in clear glass vials containing the antibody dissolved in phosphate-buffered saline. The batch number, total amount of protein and volume of the solution are shown on the vial label.

Uses

ChAgly CD3 is intended for use as an immunosupressive agent to replace other CD3 antibodies such as OKT3. So far there are no data on the use of aglycosyl CD3 *in vivo*.

ChAgly CD3 should only be used after specific and detailed discussion with Prof H. Waldmann and Dr G Hale since special tests and precautions may be necessary.

Dose and administration

The optimum dose and number of doses have not yet been established but the dose schedule used must conform to an agreed protocol.

It is important that patients are well hydrated before antibody therapy.

ChAgly CD3 should be diluted in 10 ml of normal saline and administered by intravenous bolus, then the line should be flushed with a further 10 ml of saline.

Contra-indications, warnings etc.

Although aglycosyl CD3 is a partly humanised antibody, it might provoke hypersensitivity reactions. Intradermal testing is not recommended since this can be an effective way of provoking an immune response. Howevere, the intravenous infusions must be given with care, particularly the first. Adverse reactions to the first dose are possible although the cytokine release phenomenon which is normally seen with other CD3 antibodies should be significantly attenuated with this antibody. "First dose" reactions could include fever, chills, rigors, nausea and urticaria. These might be controlled by reducing the rate of infusion. Premedication with paracetamol (acetaminophen) is possible. Treatment with intravenous pethidine (demerol) might be helpful in severe cases.

Other more severe reactions such as bronchospasm or severe hypotension have been seen following treatment with similar antibodies and facilities to manage these complications should be available. Adverse reactions to the second and subsequent doses are less common but they might occur if an immune response were made against the antibody.

ChAgly CD3 could be immunosuppressive and may reduce T cell mediated immunity. It might cause lymphopoenia but this is considered unlikely due to the lack of effector function in vitro. Patients may become less resistant to viral infections. Reactivation of endogenous viruses, eg Herpes Zoster, has been seen in some patients treated with other immunosuppressive antibodies. Other patients have suffered from mouth ulcers and regular prophylactic care with anti-fungal and anti-bacterial mouthwashes is recommended. Careful monitoring and prompt attention to any symptoms is important.

ChAgly CD3 should not be administered to any patient with evidence of concurrent infection.

Pharmaceutical precautions

ChAgly CD3 should be stored frozen, preferably at -40°C or below. Its shelf life has not been determined, but on the basis of experience with other antibodies, we recommend storing at -70°C for up to three years or at -20°C for up to 8 weeks. It must not be stored in a freezer with automatic defrosting.

When thawed, the antibody solution should be clear and free from particles or precipitate, though it might be very slightly opalescent. Once thawed, it should not be refrozen, but may be kept for up to 48 hours at 2-8°C. Note that the solution does not contain any anti-bacterial preservative.

Legal category & Product licence information

ChAgly CD3 is an experimental drug produced in academic laboratories. It does not have a product licence and can only be administered to individual named patients according to the specific instruction of a consultant physician.

Further information

The derivation of Aglycosyl CD3 from which ChAgly CD3 was derived is described in the following publications:

Routledge, E.G., Lloyd, I., Gorman, S.D., Clark, M.R., & Waldmann, H. (1991) *Eur. J. Immunol.* 21, 2717-2725.
Bolt, S., Routledge, E., Lloyd, I., Chatenoud, L., Pope, H., Gorman, S.D., Clark, M. & Waldmann, H. (1993) *Eur. J. Immunol.* 23, 403-411.

Copies of relevant unpublished information, including a description of the manufacturing and quality control processes, can be supplied on application to Dr G Hale at the above address.

Figure 35. Otelixizumab Data Sheet

```
function [ydiff] = modelode(t,y,kon,koff,gamma)
%Complete Receptor Downregulation
%   Basic model of T cell adaptation with total receptor downregulation but
%   no ligand downregulation

%L
ydiff(1,1) = -kon*y(1)*y(2) + koff*y(3) + gamma*y(3);

%R
ydiff(2,1) = -kon*y(1)*y(2) + koff*y(3);

%A (outputput, bound complex)
ydiff(3,1) = kon*y(1)*y(2) - koff*y(3) - gamma*y(3);

%P
ydiff(4,1) = y(3);
end
```

```
clear all
close all

%%% IFFL, Receptor - COMPLETE TCR DOWNREGULATION %%%

% Notes: Adaptation only occurs when the TCR has been completely
% downregulated.

%% EXPERIMENT SIMULATION

%Step 1 Dose
dose_1 = 0.2;

%Step 2 Dose
dose_2 = 0.4;

%Step 3 Dose
dose_3 = 0.8;

%Step 4 Dose
dose_4 = 1.6;

%Duration
duration = 200;

%Parameters
kon = 1;
koff = 1;
gamma = 0.3;
```

```
kprod = 0.3;

opts = odeset('RelTol',1e-5,'AbsTol',1e-5);

%Step 1
y_init = [dose_1,1,0,0];
[t,y] = ode15s(@(t,y) modelode(t,y,kon,koff,gamma),[0 duration],y_init,opts);
L = y(:,1);
surfaceR = y(:,2);
A = y(:,3);
R = sum(y(:,2:3),2);
time = t;
dose = ones(1,length(t)).*dose_1;
peak = max(y(:,3));

%Step 2
y_init = y(end,:);y_init(1) = y_init(1) + (dose_2 - dose_1);
[t,y] = ode15s(@(t,y) modelode(t,y,kon,koff,gamma),[0 duration],y_init,opts);
L = [L ; y(:,1)];
surfaceR = [surfaceR; y(:,2)];
A = [A; y(:,3)];
R = [R; sum(y(:,2:3),2)];
time = [time;t + time(end)];
dose2 = ones(1,length(t)).*dose_2;
dose = [dose,dose2];
peak_2 = max(y(:,3));

%Step 3
y_init = y(end,:);y_init(1) = y_init(1) + (dose_3 - dose_2);
[t,y] = ode15s(@(t,y) modelode(t,y,kon,koff,gamma),[0 duration],y_init,opts);
L = [L ; y(:,1)];
surfaceR = [surfaceR; y(:,2)];
A = [A; y(:,3)];
R = [R; sum(y(:,2:3),2)];
time = [time;t + time(end)];
dose3 = ones(1,length(t)).*dose_3;
dose = [dose,dose3];
peak_3 = max(y(:,3));

%Step 4
y_init = y(end,:);y_init(1) = y_init(1) + (dose_4 - dose_3);
[t,y] = ode15s(@(t,y) modelode(t,y,kon,koff,gamma),[0 duration],y_init,opts);
L = [L ; y(:,1)];
length(L)
surfaceR = [surfaceR; y(:,2)];
A = [A; y(:,3)];
R = [R; sum(y(:,2:3),2)];
time = [time;t + time(end)];
```

```
dose4 = ones(1,length(t)).*dose_4;
dose = [dose,dose4];
peak_4 = max(y(:,3));

dose = dose';

%% EXPERIMENT SIMULATION: DOSE RESPONSE

timerange = linspace(0,200,20);
doserange = linspace(0,1.6,100);

for i = 1:length(doserange)
    y_init = [doserange(i),1,0,0];
    [t,y] = ode15s(@(t,y) modelode(t,y,kon,koff,gamma),timerange,y_init,opts);
    L_exp2(i,:) = y(:,1)';
    surfaceR_exp2(i,:) = y(:,2)';
    A_exp2(i,:) = y(:,3)';
    R_exp2(i,:) = sum(y(:,2:3),2)';
    Ctot_exp2(i,:) = y(:,4)';

end

%% Plots – Set 1

cmap = colormap(jet(length(timerange)));

%Plot Ligand
figure; hold on; grid off
for i = 1:length(timerange)
    plot(doserange,L_exp2(:,i),'linewidth',1.5,'color',cmap(i,:));
end
ax=gca; set(ax,'FontName','Arial','FontSize',10);
xlabel('Dose','FontName','Arial','FontSize',10);
ylabel('Ligand','FontName','Arial','FontSize',10);
title('Dose Escalation, IFFL, R, Ligand');
axis tight;
hold off;

%Plot Unbound Receptor
figure; hold on; grid off
for i = 1:length(timerange)
    plot(doserange,surfaceR_exp2(:,i),'linewidth',1.5,'color',cmap(i,:));
end
ax=gca; set(ax,'FontName','Arial','FontSize',10);
xlabel('Dose','FontName','Arial','FontSize',10);
ylabel('Unbound R','FontName','Arial','FontSize',10);
title('Dose Escalation, IFFL, R, Unbound Receptor');
axis tight;
```

```
hold off;

%Plot Bound Receptor
figure; hold on; grid off
for i = 1:length(timerange)
    plot(doserange,A_exp2(:,i),'linewidth',1.5,'color',cmap(i,:));
end
ax=gca; set(ax,'FontName','Arial','FontSize',10);
xlabel('Dose','FontName','Arial','FontSize',10);
ylabel('A','FontName','Arial','FontSize',10);
title('Dose Escalation, IFFL, R, Bound Receptor');
axis tight;
hold off;

%Plot Total Receptor
figure; hold on; grid off
for i = 1:length(timerange)
    plot(doserange,R_exp2(:,i),'linewidth',1.5,'color',cmap(i,:));
end
ax=gca; set(ax,'FontName','Arial','FontSize',10);
xlabel('Dose','FontName','Arial','FontSize',10);
ylabel('R','FontName','Arial','FontSize',10);
title('Dose Escalation, IFFL, No R, Total Receptor');
axis tight;
hold off;

%Plot Total Output
figure; hold on; grid off
for i = 1:length(timerange)
    plot(doserange,Ctot_exp2(:,i),'linewidth',1.5,'color',cmap(i,:));
end
ax=gca; set(ax,'FontName','Arial','FontSize',10);
xlabel('Dose','FontName','Arial','FontSize',10);
ylabel('P','FontName','Arial','FontSize',10);
title('Dose Escalation, IFFL, No R, Total Output');
axis tight;
hold off;

%% Plots – Set 2

cmap = colormap(hsv(6));

% LIGAND
figure; hold on; grid off
plot(time,L,'linewidth',1.5,'color',cmap(1,:));
ax=gca; set(ax,'FontName','Arial','FontSize',10);
xlabel('Time(s)','FontName','Arial','FontSize',10);
ylabel('Ligand','FontName','Arial','FontSize',10);
```

```
title('IFFL(III),Ligand');
axis tight;
hold off;

% UNBOUND RECEPTOR
figure; hold on; grid off
plot(time,surfaceR,'linewidth',1.5,'color',cmap(2,:));
ax=gca; set(ax,'FontName','Arial','FontSize',10);
xlabel('Time(s)','FontName','Arial','FontSize',10);
ylabel('Unbound Receptor','FontName','Arial','FontSize',10);
title('R Downregulation, Unbound Receptor');
axis tight;
hold off;

% BOUND RECEPTOR
figure; hold on; grid off
plot(time,A,'linewidth',1.5,'color',cmap(3,:));
ax=gca; set(ax,'FontName','Arial','FontSize',10);
xlabel('Time(s)','FontName','Arial','FontSize',10);
ylabel('Bound Receptor','FontName','Arial','FontSize',10);
title('R Downregulation, Bound Receptor');
axis tight;
hold off;

% TOTAL RECEPTOR
figure; hold on; grid off
plot(time,R,'linewidth',1.5,'color',cmap(4,:));
ax=gca; set(ax,'FontName','Arial','FontSize',10);
xlabel('Time(s)','FontName','Arial','FontSize',10);
ylabel('Total Receptor','FontName','Arial','FontSize',10);
title('R Downregulation,Total Receptor');
axis tight;
hold off;
```